Correlating scored daily anatomical changes to in-vivo EPID dosimetry and cone beam CT based dose calculations

A retrospective study

Vineet Mohan

TU Delft

Correlating scored daily anatomical changes to in-vivo EPID dosimetry and cone beam CT based dose calculations

A retrospective study

by

Vineet Mohan

to obtain the degree of Master of Science
at the Delft University of Technology,
to be defended publicly on Friday, September 29, 2017 at 1:00 PM.

Student number:	4478622	
Project duration:	February 1, 2017 – September 29, 2017	
Thesis committee:	Dr. ir. D. R. Schaart,	TU Delft, supervisor
	Dr. A. Mans,	NKI-AvL, supervisor
	I. Olaciregui-Ruiz,	NKI-AvL, supervisor
	Dr. F. M. Vos	TU Delft
	Dr. Z. Perko	TU Delft

TU Delft

Abstract

At the Antoni van Leeuwenhoek Hospital/Dutch Cancer Institute (NKI-AvL) in Amsterdam, inter-fractional anatomical changes during the course of radiotherapy are monitored using cone beam CT scans, taken prior to irradiation. These scans are assessed visually, and the fractions are scored according to a 'traffic light protocol'. Based on the magnitude of change, a green, yellow, orange or red colour, in increasing order of severity, is assigned to the fraction.

The goal of this work was to ascertain if the colour of the traffic lights, which were assumed to be indicators of anatomical change, correlate to changes in dosimetry for H&N VMAT treatments, as well as lung IMRT treatments.

The in-vivo EPID dose was reconstructed in the patient for each fraction, using a back-projection algorithm that is used clinically at the NKI. Calibrated CBCTs of each fraction were obtained using DIR or anti-scatter grid methods researched at the NKI, which were then imported to a TPS to obtain the fraction dose. These two modes of dosimetry were compared against each other, as well as against the traffic light colours for H&N treatments. For lung treatments, due to unavailability of CBCT based dose data, only EPID dosimetry was used; two different models of the back-projection algorithm were compared in this case. γ index and DVH metrics were used to express deviation in the dose distributions.

Deviations over successive fractions for 18 H&N treatments were studied. The traffic light protocol correlated poorly with CBCT based dose and EPID reconstructed dose ($\rho = 0.33$ and 0.35 respectively). The CBCT and EPID dose correlated with each other quite strongly ($\rho = 0.72$), however the EPID dose was more sensitive in its fluctuations.

Deviations for 98 IMRT lung fractions were studied. The traffic light protocol correlated even more poorly with the EPID reconstructed dose than in the H&N study ($\rho = 0.18$). The calculated transmission model of the EPID was found to exaggerate the deviations in comparison to the measured transmission model. Since VMAT innately uses the calculated transmission model, this explains the sensitivity of the EPID results seen in the H&N study.

We have shown that the traffic light protocol does not correlate with dosimetric changes, due to differences in assessment criteria. 15 out of 18 H&N treatments showed moderate ($\rho \geq 0.4$), if not strong, correlations between deviations of EPID reconstructed dose and CBCT based dose, strengthening the EPID's applicability for in-vivo dosimetry.

Acknowledgements

I would like to thank Dr. Dennis R. Schaart, Dr. Anton Mans and Igor Olaciregui-Ruiz for their supervision, advice and input regarding my thesis. I would like to thank Simon van Kranen and Lukas Schroder for their input and help with cone beam CT data. I would also like to thank everyone in the EPID dosimetry group for their approachability, friendship and help, which made the time spent on this project an absolute joy. I'd like to thank my parents, without whose support I would have never been given the opportunity to study in Delft. Lastly, I'd also like to thank all my friends, especially Donna de Weijer, who have made my time away from home seem so much more enjoyable.

Vineet Mohan
Delft, September 2017

Contents

1 Introduction

Over the last few decades, advances in medicine have resulted in an increase in the average lifespan of the population. However, an ever-ageing population translates to a higher incidence of cancer. Radiotherapy has become an increasingly popular mode of cancer/tumour treatment due to its non-invasive nature. Engineering advancements have also increased the capability for precise dose delivery. The evolution of complicated treatment techniques like intensity modulated radiotherapy (IMRT) and volumetric modulated arc therapy (VMAT) have helped reduce dose delivery to normal tissue while maintaining conformal dose within the tumour. VMAT simultaneously manipulates beam angles, dose rates and gantry rotation speeds dynamically to deliver the treatment plan. With such complexity, quality assurance has become an important tool to assess treatment planning and dose delivery. At the NKI-Avl, over 4000 patients are treated annually [1] with IMRT or VMAT on linear accelerators (linacs), Figure 1.1. With the addition of the Gamma-knife and the MR-linac, the quality of treatments carried out at the NKI will only increase in the forthcoming years.

1.1. Quality Assurance in Radiotherapy Treatments

Before a treatment plan is made, a computed tomography (CT) scan of the patient is taken. Often, a positron emission tomography (PET) scan is also taken and overlaid over the CT scan to help delineate the active tumour regions. A physician delineates on the scan, the target volumes and the organs at risk. A dose prescription is prepared based on constraints and limits for the different delineations. The treatment plan is calculated based on simulations of patient geometry, machine characteristics and physical interactions. Beam angles, dose rates and multileaf collimator (MLC) positions at different control points, are just some of the parameters that are exported by the treatment planning system (TPS) software. The dose distribution of the plan is calculated on the CT geometry of the patient (Figure 1.2). In most cases, the plan is fractionated, and is thus carried out over the span of several days or weeks. Fractionation is carried out due to its effect of allowing normal tissue to recover from damage caused by radiation to DNA, while tumour tissue stays damaged.

The goal of radiotherapy from a quality assurance perspective, is to make sure that the dose distribution that is delivered, is as close to that which was planned. However, the situation that is simulated by the TPS, and the situation when a patient is set up at a linac are quite different. There are a number of uncertainties that are introduced, such as positional errors regarding the set up of the patient, patient geometry errors, plan exporting errors, linac or machine based errors etc. Linacs undergo frequent maintenance checks to ensure from a hardware quality assurance (QA) perspective, it functions normally. The output of the linac is carefully monitored day to day and deviations are taken into account. In this work we focus only on patient related errors i.e. deviations introduced due to changes in the patient anatomy.

At the NKI, head and neck (H&N), as well as lung patients, are set up using as online imaging protocol. This means that before every fraction, a cone beam CT (CBCT) is taken

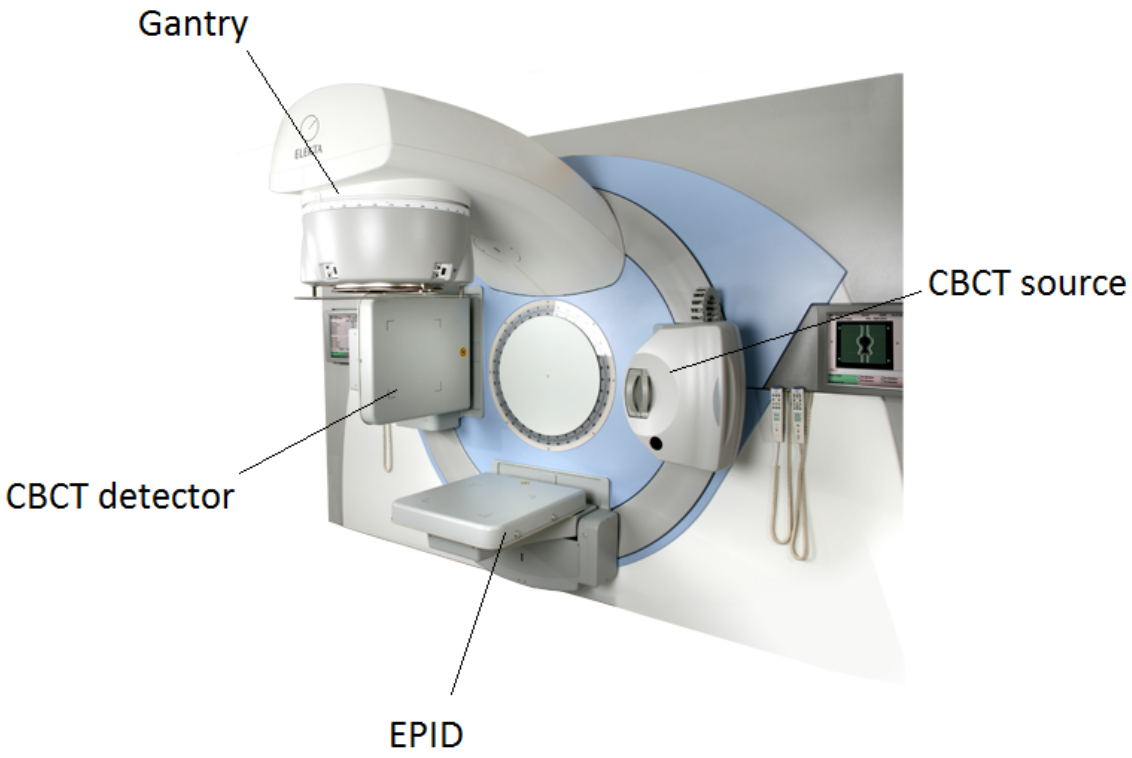

Figure 1.1: A typical linear accelerator at the NKI (image retrieved from Elekta website). The Elekta Synergy (Elekta, Crawley, UK.) comes equipped with two imaging panels, the EPID and the cone beam CT.

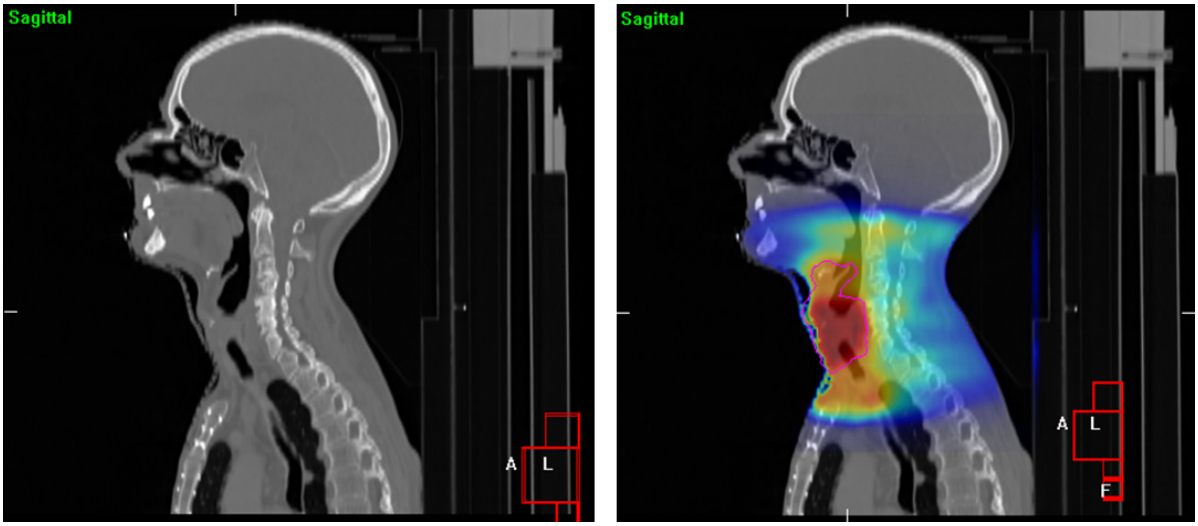

Figure 1.2: The planning CT of a patient, as seen on the left, as the base of treatment planning. On the right the planning target volume (PTV), which encompasses the tumour, is delineated and the dose distribution is evaluated on the anatomy by the TPS.

to help position the patient such that the tumour mass is in the same position as in the planning CT (pCT), or is covered adequately by the PTV from the pCT. For the purpose of this work, we assume that the patients were positioned in every fraction with a negligible amount of rigid set-up error, and thus any patient-related uncertainties are purely due to anatomical changes.

Common inter-fractional anatomical changes that can occur involve weight loss, tumour growth or shrinkage and tumour shifts. Depending on the site of the tumour, other types of

changes may also occur such as atelactasis and pleural effusion in the lungs. These changes can have an effect on the distribution of the dose in the patient, and may result in under-dosage in the tumour or overdosage in an organ at risk. To mitigate this risk, the CBCT is compared to the pCT, just prior to irradiation, while the patient is still laying on the treatment couch. A radiotherapy technician (RTT) looks for tumour coverage within the PTV, differences in important delineations, as well as the magnitude of these changes (in centimetres), and makes a quick decision regarding the treatment. The decisions and their resulting workflow fall under the guidelines of the 'traffic light' protocol of the NKI. The inspection of the CBCT is purely visual, and no evaluation of the dose to be delivered on the current anatomy is carried out.

The CBCT is used to ensure that everything prior to irradiation is in order. However, the only tool that exists to ensure that the fraction went ahead as planned, is a device known as the electronic portal imaging device (EPID). During the irradiation of a fraction, the EPID is extended and records the in-vivo data i.e. the radiation passing through the patient which is then incident on the EPID panel. This is known as transit EPID dosimetry. This data can then be used to back-project and reconstruct the dose which was deposited in the patient, using a simple algorithm. This delivered dose distribution can then be compared with the planned dose distribution of the TPS, to evaluate how well the fraction was carried out. EPID dosimetry is however primarily still a tool used to detect large deviations from the plan and not used to accurately determine dose delivered to different structures. Reasons for a deviation can be anatomical changes, acquisition errors, reconstruction errors, errors in patient set-up, the use of immobilization devices, errors in data transfer etc. In case of large deviations, the plan is carried out on a polystyrene phantom, and the EPID dose on the phantom is reconstructed to check for the source of the error.

The EPID dose however, is at best an indicator. A more accurate method of calculating the fraction dose or the 'dose of the day' is by using the CBCT with the TPS, to calculate the dose plan on the patient anatomy of the day. This however, assumes that there are no machine errors or TPS errors. There are also several other problems with this approach. CBCT scans have very low image quality and are not calibrated to Hounsfield Units (HU), unlike normal CT scans. There exist some methods to overcome these obstacles, and research is being done at the NKI to pursue these. They will be discussed later and be used in this project as an additional approach to dose calculation.

The goal of this project is to relate daily anatomical changes scored by the traffic light protocol, to in-vivo EPID reconstructed dose, as well as CBCT based dose calculations. The motivation for this, is to know if the traffic light protocol is representative of the severity of dosimetric changes. This would strengthen it's use as a tool in determining the necessity of re-planning a treatment. For this project, head and neck cancer patients were the focus. A follow up study on lung patients was also done since this patient group sees some of the largest anatomical deviations.

2

Literature Study

2.1. Methods

The aim of the project is to correlate the colours of the traffic light protocol, the EPID reconstructed dose, and the dose calculated from the CBCT scan. The imaging and positioning protocols as well as the traffic light protocol were researched on the NKI's internal online documentation website, iProva. All images in this section were also retrieved from iProva. Articles and publications regarding EPID dosimetry and the algorithms used at the NKI were provided by the EPID dosimetry group. Articles about different CBCT based dose calculation approaches were found using Google Scholar using the keywords 'cone beam CT', 'dose calculation' and 'deformable image registration'.

2.2. Effect of Inter-fractional Anatomical Changes

When an anatomical change occurs during the course of a photon therapy treatment, it affects the depth-dose curve of the incoming photons [2]. Thus the radiological path traced by the photons in the treatment beam is altered and the dose distribution in the patient is changed. This may result in an overdosage or underdosage to the organs at risk (OARs) or tumour.

A study by Height [3] showed that tumour regression can cause as much as a 50% reduction in volume of the gross tumour volume (GTV)and 70% volume reduction in lymph nodes in head and neck patients. Even a 20% volume reduction in parotid gland, which is an OAR, was reported. Anatomical changes directly affect the depth-dose curve of the incoming photons. Some studies have shown that these changes can alter the median dose to the PTV by as much as 2% in head and neck tumours and up to 5% in lung tumours [4, 5], when compared to the planned dose. Whereas, a recent study [6] showed that photon therapies are rather robust to anatomical changes, on average 0.5% dose deviation in pancreatic tumours, especially when compared to other particle therapies which are much more sensitive to changes in tissue density.

To minimise the effect of these inter-fractional anatomical changes and allow for accurate treatment procedures, there are protocols which are followed at the NKI [7].

2.3. Protocols at the NKI

2.3.1. Patient Set-up and Positioning

Depending on the site, an offline or online imaging protocol is used to set up patients. In the offline case, a shrinking action level with an initial action threshold that differs per site is used. However, since this project will focus on H&N and lung patients, the online imaging protocol is used. In the online imaging protocol, a CBCT scan is taken before each fraction is irradiated.

In the online protocol, the patient is first set up on the treatment couch using the lasers in the treatment bunker. The patients are given skin tattoos/markers, and each fraction the

goal is to align the patient's tattoos with the path of the lasers. This is done with rudimentary table shifts. At this point a CBCT of the patient is acquired. The CBCT is then compared to the coordinates of the pCT, and the PTV (planning target volume) is usually selected as the correction reference point. The scans are rigidly 'matched' using bony anatomy or grey values, and the correction to be carried out in the form of table shifts is calculated. The table is then shifted finely to the position required and a repeat CBCT scan is made to ensure that the patient is in the correct position.

2.3.2. Traffic Light Protocol

At this point the patient is properly positioned as accurately as possible to the reference pCT position. However, daily anatomical changes of the patient may still be present and these cannot be further corrected for. They are instead, visually evaluated by the radiotherapy technician (RTT), and scored according to a traffic light protocol. The traffic light protocol, as the name suggests, is based on the different traffic light colours. The colours, green, yellow, orange and red, indicate the degree or magnitude of the anatomical deviations in increasing order of severity. The criteria that determines the traffic colour code of the scan/fraction depends on the site of the tumour. However, the work-flow that follows each colour code is the same for all sites [8, 9].

If a green colour code, or no colour code, is assigned to a CBCT scan, it indicates that there are no aberrations and the anatomy of the day matches that of the pCT within certain margins. In this case, no action is taken by the RTT.

If a yellow colour code is assigned to a CBCT scan, the RTT notifies the radiation oncologist (RO) of this via e-mail, but the RO's response is not required in order for the current and next fraction to be carried out.

If an orange colour code is assigned to a CBCT scan, the RTT notifies the RO of this via e-mail, and the RO must respond to this before the next fraction. The current fraction is still carried out however, since it is more vital to continue treating the tumour, than it is to prevent possible adverse effects from the anatomical changes.

If a red colour code is assigned to a CBCT scan, the RTT must immediately call the RO. The current fraction may only be carried out after permission from the RO.

Typical responses from the RO can range from decisions to continue treatment as planned, stop the treatment, alter the treatment plan, schedule a new CT scan etc.

2.3.3. Traffic Light Protocol Criteria - Head and Neck

For the positioning and set up of H&N patients, a multiple region of interest (ROI) registration method is used [10]. Several ROIs are selected using clipboxes, which are semi-automatically placed on bony structures and are used as the reference for the registration. Once the CBCT is rigidly matched to the pCT, the set-up error as calculated from the registration is measured in translations and rotations shifts. Since the couch cannot be tilted, using the PTV as the correction reference point, the correction to be applied, only in translations, is calculated in the form of table shifts. After the table shift is performed, the traffic light protocol is followed. The following criteria must be assessed and filled into the XVI logbook by the RTT.

First, contour changes in the patient are evaluated. Contour changes are variations in the 'outline' of the patient, when the pCT and the CBCT plan are compared (Figure 2.1). A very common cause of contour changes is weight loss. Usually a change of 2cm or more is classified as an orange.

Second, changes in build-up are assessed (Figure 2.2). In patients with superficial tumours, tumours that are close to the upper layers of the skin, additional build-up material is placed on the patient's skin, to ensure electron equilibrium and deposition of dose in the target volume. However, in the case of tumour shrinkage or even weight loss, an air gap between the build-up material and the skin can be present, which will influence the electron equilibrium, and thus the dose distribution. An air gap of 1cm or less is classified as green, whereas an air gap of 1-1.5cm, 1.5-2cm and more than 2cm are classified as yellow, orange and red respectively.

Third, the changes in the size of the clinical target volume (CTV) is assessed. In the case of an increase in the size of the CTV (Figure 2.3a), a green colour code is assigned if the CTV

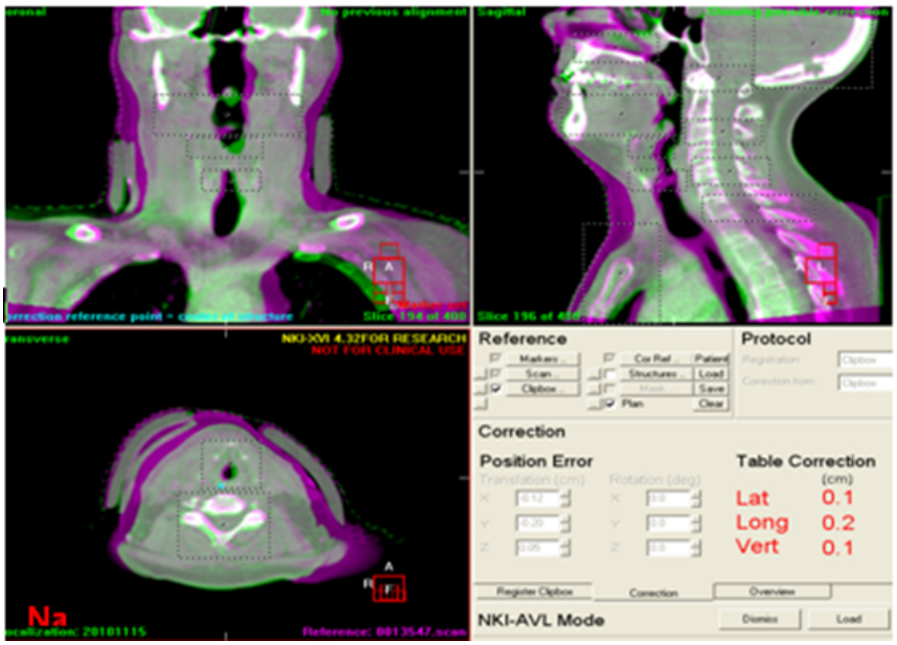

Figure 2.1: The traffic light protocol is evaluated based on an overlay image of the pCT, in purple, and the CBCT in green. In this patient, weight loss is apparent from the purple boundary. This results in a contour change, as well as an air gap between the bolus and the skin in the bottom left image.

Figure 2.2: On the left of the image we see an earlier fraction of a patient, and on the right we see the current fraction. A reduction in the tumour size is noticeable, and an air gap is present between the bolus and the skin.

is still well within the PTV, a yellow colour code is assigned if the CTV just fits closely inside the PTV, and an orange colour code is assigned if the CTV exceeds the boundary of the PTV.

In the case of a shrinkage of tumour size (Figure 2.3b), an orange colour code is assigned if the CTV shrinks by more than 2cm.

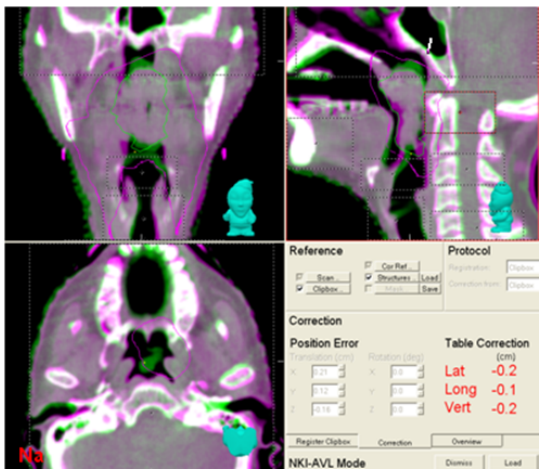

(a) The tumour progression, visible in green, has grown outside the margin of the PTV.

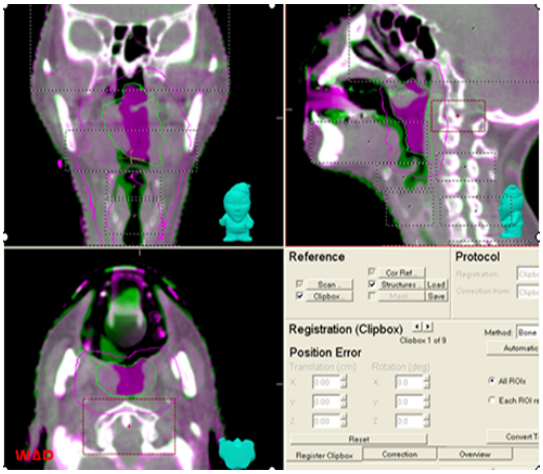

(b) The tumour has shrunk in size, which is why we see a large purple mass inside the PTV, where the tumour used to be.

Figure 2.3: Changes in the CTV volume

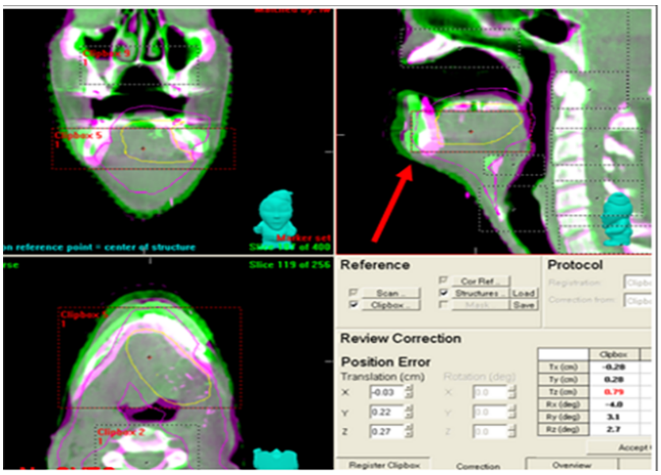

Figure 2.4: The mandible has largely shifted from its original position. This patient would now be irradiated on the tongue.

Next, a shift of the target volume is assessed (Figure 2.4). If the target volume just fits closely inside the PTV, a yellow colour code is assigned. If the volume lies outside the PTV, an orange colour code is assigned for the first fraction where this occurs.

Sometimes H&N patients can have obstructions in their airway which can result in difficulty during breathing (Figure 2.5). If the patient has obstructions but does not have any complaints regarding discomfort, a yellow colour code is assigned. If a patient has mild complaints, an orange colour code is assigned, and if a patient has severe complaints, a red colour code is assigned.

In some cases, due to changes in the placement of certain tools with respect to their position on the pCT (Figure 2.6), but not necessarily due to their misuse, an orange colour code is assigned.

According to Conijn[9], from a retrospective analysis done on 168 patients in 2013, in 46% of patients, relevant anatomical changes were found during the course of treatment. Of all fractions, 54% were found to be green, 25% yellow, 21% orange and 0% red. 6% of patients required a replanning via adaptive radiotherapy.

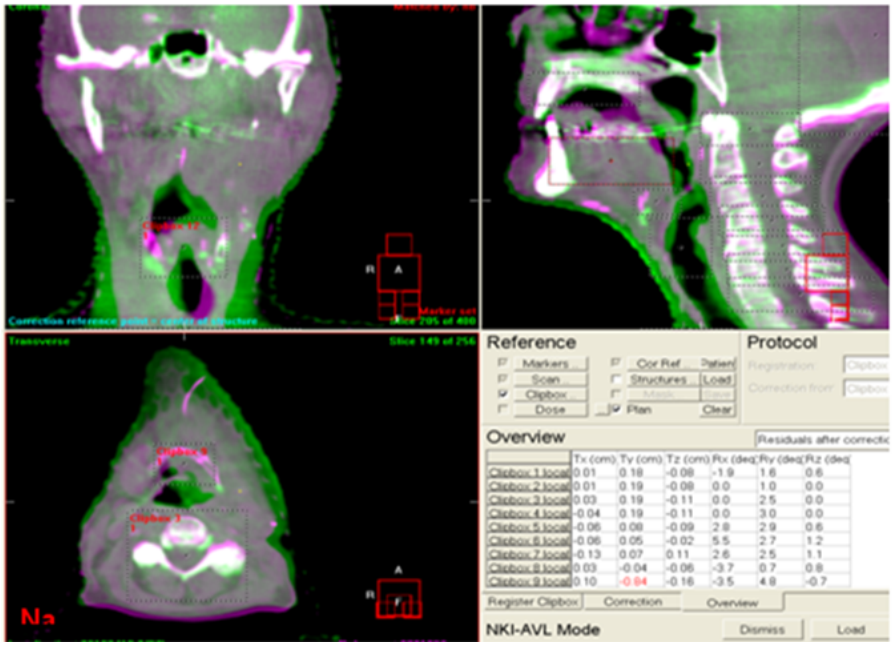

Figure 2.5: A lot of swelling and narrowing of the airways can be seen in green. In this situation, the RTT must ask the patient if he/she is experiencing difficulty breathing.

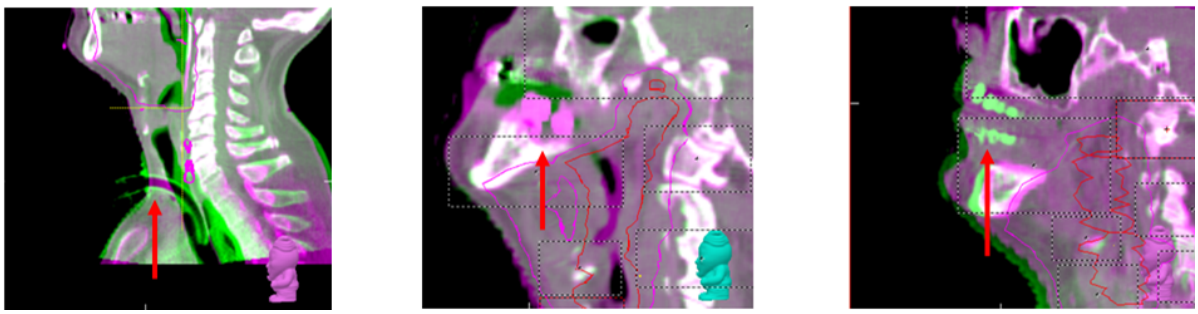

Figure 2.6: In the left image, the patient has received a tracheostoma after the pCT was made. In the image in the middle, the patient's teeth have been pulled out after the pCT. In the right image, the pCT was made without dentures, but the patient has dentures at the time of the fraction.

2.3.4. Traffic Light Protocol Criteria - Lung

Similar to the H&N online protocol, a CBCT scan is taken every fraction for patient set up as well as for evaluating anatomical variations. The carina (bottommost part of the trachea) is automatically selected and matched, and the table shift is calculated. Once the alignment is as accurate as possible, the traffic light protocol is assessed by the RTT.

The changes in the GTV are first assessed. In the case of tumour growth (Figure 2.7a), a green colour is assigned if there is local GTV growth within the PTV, a yellow colour if there is general GTV grown within the PTV, an orange if the GTV is tight-fitting within the PTV (or also in the case of doubt), and a red if the GTV lies outside the PTV. A shrinkage (Figure 2.7b) of the GTV of more than 0.5cm is assigned a yellow colour code.

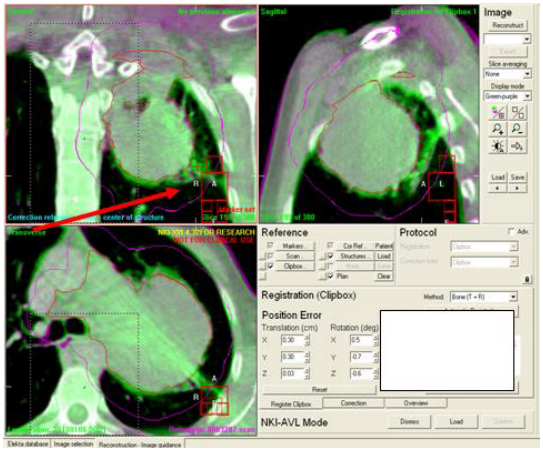

(a) The tumour has progressed, visible in green, beyond the boundary of the PTV.

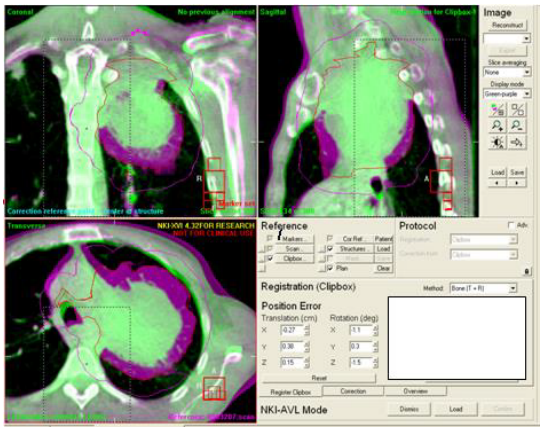

(b) The tumour has shrunk significantly, visible by the purple shell around the tumour.

Figure 2.7: Changes in the tumour volume.

A shift of the target volume is assessed next (Figure 2.8). A shift which results in the GTV fitting tightly within the PTV is assigned an orange colour code, and a red is assigned if the GTV lies outside the PTV.

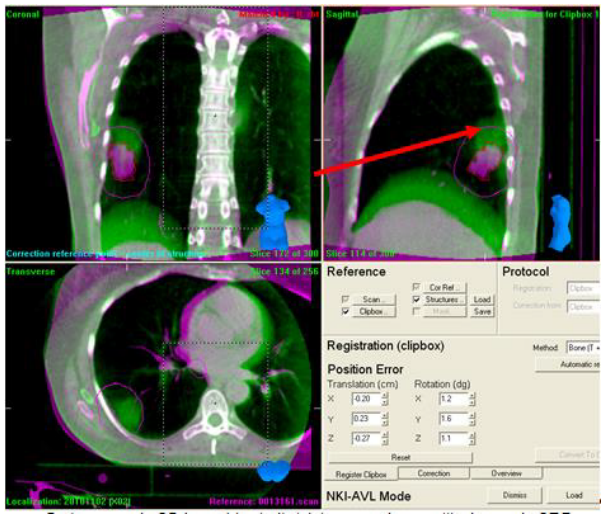

Figure 2.8: The tumour in the CBCT, visible in green and also by the red arrow, has shifted from its original position on the pCT, in purple.

Next, the changes in the condition of atelectasis in the patient are assessed (Figure 2.9). Atelectasis is the collapse of one or more lobes of a lung. Lung tumour patients can be presented with atelectasis before treatment, or during the course of treatment. Its condition

may improve or worsen as well, during the course of the treatment. If there are minimal changes, a green colour code is assigned. If there is a sudden origin, disappearance, growth or shrinkage of atelactasis, without a mediastinal shift, then a yellow colour code is assigned. However if this occurs in combination with a mediastinal shift, and the GTV is tightly fit within the PTV, then an orange colour code is assigned. A red colour is assigned if the aforementioned conditions occur in combination with the GTV lying outside the PTV.

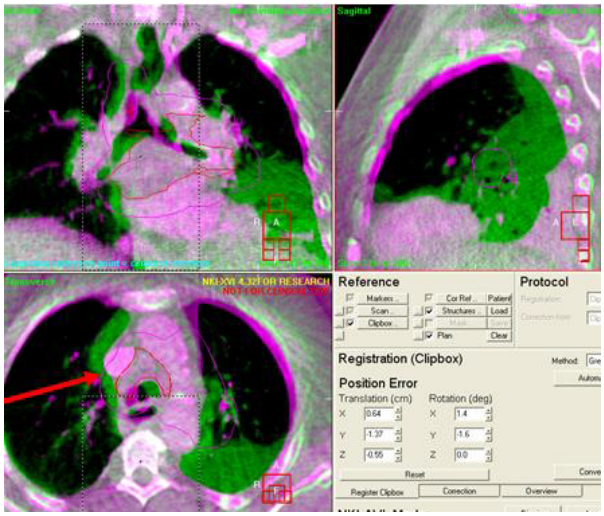

Figure 2.9: Severe increase in atelectasis has caused a shift of the mediastinum, visible from the red arrow. It's possible that the lymph nodes may now lie outside the PTV.

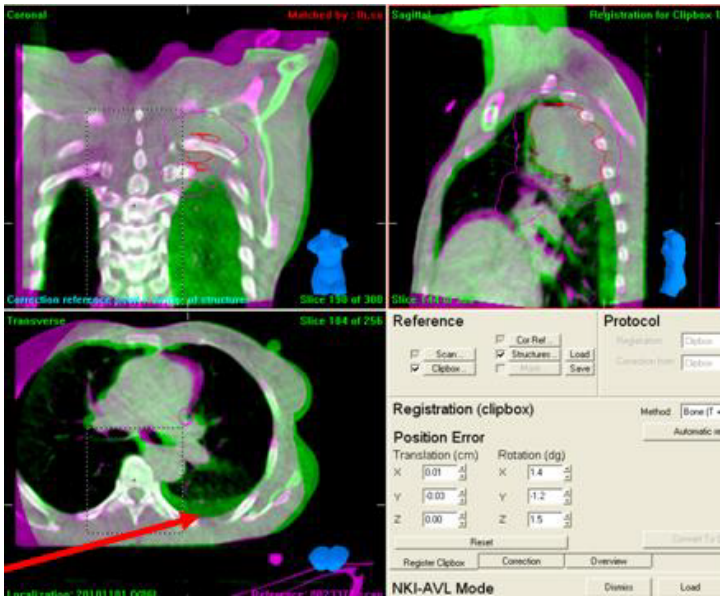

Figure 2.10: Pleural effusion is visible as a green layer. Due to the patient laying on his/her back, the effusion is to be seen on the dorsal side, and if the patient lays on his stomach it can be seen on the ventral side.

Another pulmonary condition which is investigated on the CBCT is that of pleural effusion, excess fluid in the pleural cavity around the lungs (Figure 2.10). Decrease or disappearance of pleural effusion is assigned a yellow colour code, and origin or increase of pleural effusion is assigned an orange colour code.

If there is inflammation present in the lungs (Figure 2.11), and the patient has no complaints, an orange colour code is assigned. If there is inflammation present and the patient has a fever and is coughing, a red colour is assigned.

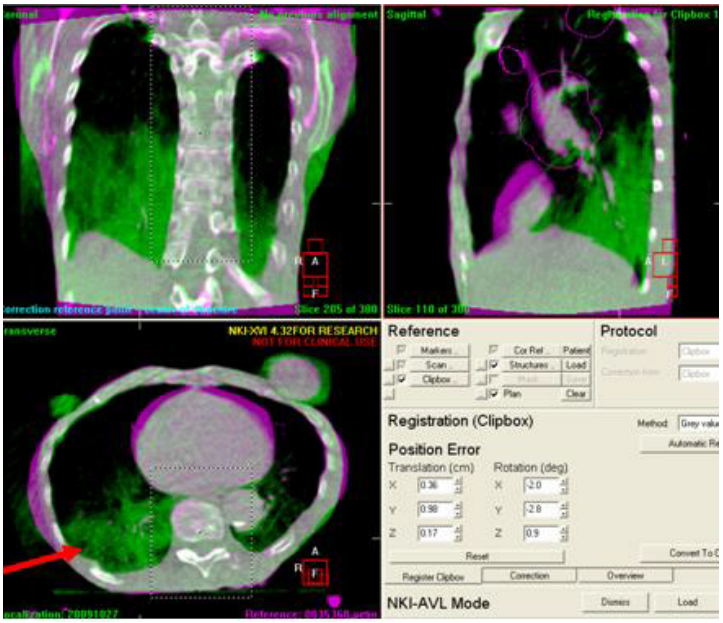

Figure 2.11: The lung image is more erratic than in the case of atelectasis or pleural effusion. In this case, the patient has pneumonia, and the air sacs in the lung are inflamed.

Kwint[8] analysed 177 patients and found that 128 (72%) had treatments with at least one fraction with a traffic colour of yellow or higher and only 28% of treatments had only green fractions. However in this study, only 7 CBCT scans per taken per treatment. About 210 fractions of intra-thoracic changes were observed. Tumour regression accounted for the most changes (37%), followed by tumour baseline shifts (27%), changes in atelectasis (19%), tumour progression (10%), pleural effusion (6%) and infiltrative changes (3%). 9% of patients required replanning via adaptive radiotherapy.

Møller[11] also found that 23% of changes in lung density were caused due to atelectasis, pleural effusion and infiltrative changes.

2.4. EPID Dosimetry

2.4.1. History

Dose verification in radiotherapy was, and often still is, usually done using ionization chambers, diodes, arrays of the same, radiographic film and other types of dosimeters in a pretreatment setting, using a phantom. However these pretreatment methods don't reflect the actual situation inside the patient, during irradiation.

In-vivo dose verification has also been done using point detectors placed on the skin, but yet again, these don't reflect the dose inside the patient [12]. An simple and non-invasive method of reconstructing the dose in the patient is by making use of an EPID.

Electronic Portal Imaging Devices or EPIDs were originally designed in order to verify patient position during set up (Figure 2.12), prior to irradiation, by imaging bony anatomy or fiducial markers, relative to the pCT. However, over the last two decades, improvements in the properties and construction of the EPID detector have enabled it to also be used as an important dosimetric tool. At the NKI, the installed linacs are manufactured by Elekta and have two energy modes, 6MV and 10MV, as well as the option to use the beams without the flattening filter. Each linac comes with an EPID attached, opposite the head at a source-detector distance of 160cm and the distance cannot be adjusted. The EPID itself can be lowered into position and folded back up, and can also be displaced a few centimetres, once fully lowered, horizontally (Left-Right) and vertically (Gun-Target).

The modern EPIDs, as used by the NKI, have pixel arrays made from amorphous silicon [13, 14]. A photodiode and field effect transistor form a pixel, and the pixels detect direct and indirect radiation. In direct detection, the photon deposits its energy directly to the photo-

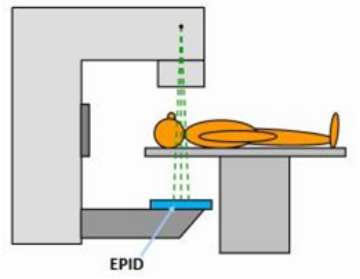

Figure 2.12: The EPID records the radiation incident on the panel, after it has passed through the patient.

diode. In indirect detection, a scintillating screen is used to convert the incoming radiation into optical photons, which are then detected by the photodiode. A thin 1mm copper plate is also placed before the scintillator, in order to reduce low energy scattered photons from the patient, as well as to convert incident photons into electrons that can deposit dose in the scintillator. Photomultiplier tubes increase the gain of the optical photons detected. Some EPIDs may also have additional build-up before the detector to ensure electron equilibrium. The role of the EPID in the NKI is no longer for positional verification, but exclusively for quality assurance in the form of in-vivo and pre-treatment dosimetry, as well as monitoring the beam that emerges through the multileaf collimator. Instead, all the linacs at the NKI are equipped with an on-board CBCT for patient set-up and positioning.

The basic idea behind EPID dosimetry, is that the the EPID measures the radiation that passes through the patient or phantom and is incident on the detector. Pre-treatment dose verification on a phantom with EPID images, while useful, doesn't reflect the patient anatomy accurately. Instead, transit dosimetry, where the EPID images are acquired when the patient is irradiated during a fraction, is performed. From this point there are two approaches which are taken. In the forward-projection approach, the treatment planning system predicts the dose that is delivered to the EPID, and a 2D predicted portal dose image is generated. This is then compared to the actual 2D portal dose image measured by the EPID. This method is simple, and can be used to detect errors, however the dose distribution within the patient remains unknown and the location of a deviation may also remain unknown. In the back-projection approach, which is used at the NKI, the EPID dose is used to reconstruct the in-vivo dose in the patient after taking into account various parameters such as scatter, transmission, pixel sensitivity etc. The intensity values of the pixels measured by the flat panel after attenuation through the patient, can be converted to dose, which are then projected back into a plane inside the patient that is parallel to the EPID. When successive planes are back-projected, a dose distribution in 3D is obtained. The 3D distribution can then be compared to that of the TPS, to assess how well the treatment was carried out. This assessment is usually done using the gamma (γ) index or using dose-volume histogram (DVH) parameters. Later fractions can be re-planned to compensate for any errors made. One of the biggest advantages of using EPID dosimetry is that it can be automated, doesn't require any additional hardware, can be repeated immediately, doesn't need additional time to be digitized (unlike with films), and the data can be archived and stored relatively easily.

2.4.2. Algorithm Development

When the algorithm was initially proposed in 2006 [12], the measured EPID signal for each IMRT field was used to reconstruct the 2D dose in the patient in a plane parallel to the EPID position. The signal measured by the EPID was first converted to dose at the EPID level using a dose response function, kernels to correct for lateral scatter within the EPID, and a sensitivity matrix to restore the shape of the beam profile.

Once the total dose at the EPID level is known, the scatter from the patient to the EPID is eliminated from this total dose by use of a constant EPID-patient scatter kernel. Once this scatter is subtracted, we now have the primary portal dose incident on the EPID. The primary portal dose consists of the radiation that is incident on the panel, which originated from the head of the linac, and not from within the patient.

The next step is to back-project the dose into the plane of the patient. In order to do this, not only is the portal image of the patient under the linac needed, but also an open image of the same treatment field. This is needed in order to estimate the transmission or attenuation of the beam through the patient. The attenuation through the patient material as well as the intensity loss due to the inverse square law is taken into account, to find the primary dose in the patient. The transmission is also used to estimate the scatter to primary ratio. The scatter to primary ratio, and an in-patient scatter kernel is used with the primary dose in the patient to find the in-patient scatter dose. The scatter dose and the primary dose is added to find the total dose in the patient.

In 2009 the algorithm was updated [15] to include an extension to 3D reconstruction. The algorithm till the primary portal dose stayed the same but the back-projection thereafter was improved, with the introduction of a beam hardening parameter as well as a build-up correction and a depth dependency for the mid plane scatter estimation.

In 2010 the algorithm was expanded to include VMAT treatments [16]. Accurate determination of transmission using open and portal arcs is not possible due to the lack of synchronization between the changes in dose rates and the acquisition of images. This leads to a lot of artefacts in the images. Instead a new concept, called calculated transmission was introduced to enable VMAT EPID dosimetry, whereby the pCT was used to calculate the radiological path length. However this meant that the same transmission was used for all fractions.

In 2011, the algorithm for IMRT was updated to include calculated transmission as well [17], by using the pCT. It eliminated the need to measure open field images, thus eliminating the labour and time intensive process. Yet again, this meant that the same transmission would be used in all fractions. Since the patient anatomy changes between fractions, it is logical to assume that the the transmission would also change. Measured transmission uses the real transmission value of the fraction, whereas calculated transmission uses the value from the pCT. Therefore calculated transmission based reconstructions would be relatively less accurate, and more sensitive to anatomical changes.

It is important to state that the algorithm used at the NKI is a 'water-based' algorithm. While it may use the body contours from the pCT, it assumes that the patient body is homogeneous inside. For most sites the quality of the reconstruction is not affected, however in some sites with large and frequent inhomogeneities, such as lung, an additional correction is required due to large deviations in the reconstructions [18].

One of the biggest advantages of the EPID dosimetry work-flow at the NKI, is that it is fully automated. As soon as a fraction is irradiated, the dose distribution is reconstructed and compared to that of the planned dose. The fraction flags an alert if certain criteria are exceeded. The criteria used by the EPID dosimetry group are based on γ indices as well as the deviation of the median dose to the PTV (ΔPTV D50), and the dose difference at the dose reconstruction point, which is usually the isocenter. There are three levels of alerts however it is important to state that these alerts are not related to the traffic light protocol alerts. In the case of an alert, the reason for the deviation is investigated by a radiotherapy technician or medical physicist.

In a 3 year study from 2012-2014 [1] it was found that 31% of plans generated alerts, out of a total of more than 15,000 plans. More specifically, 35% of plans for lung and 42% of plans for H&N generated EPID alerts. 55% of alerted lung fractions were due to patient-related anatomical changes and 37% were due to limitations of the dose reconstruction algorithm. 31% of alerted H&N fractions were due to patient-related anatomical changes, and 53% of alerts were due to errors in image acquisition and improper use of bolus material. However only a very small fraction of these alerts result in clinical action.

For H&N fractions, the data for all fractions is recorded on the EPID, but the data beyond the third fraction is not analysed. For lung treatments however, only EPID the data for the first three fractions are recorded and analysed.

2.4.3. Shortcomings and Future Work

There are some limitations to the back-projection algorithm used at the NKI, such as uncertainties in the results for all clinical field sizes and depths, and the use of a pencil-beam type

dose calculation algorithm [1]. However in this work, one of the major limitations is that for the VMAT treatments, the pCT is used to obtain the patient contour, and is also used to calculate the transmission. If the patient anatomy differs from the pCT, an error is propagated into the dose reconstruction model. One possible way of overcoming this is by using the daily CBCT scan instead of the pCT scan. This was investigated for H&N treatments [4] and it was shown that the EPID results were improved. It was found that using the pCT caused deviations to be more sensitive, in the case of volume changes in the PTV. However the actual change in dose between the pCT and CBCT based EPID reconstructions were very small, and the reduction in alert rate was not too significant. The fraction dose from the CBCT, i.e. the dose calculated by the TPS using the CBCT scan of that fraction, also showed the same small changes with respect to the planned dose.

EPID dosimetry is used to find deviations in general, but if we wish to find specifically patient-geometry or anatomical related changes a new QA technique has been developed. A 'virtual' dose reconstruction uses open arcs or fields (treamtent arcs or fields without any material in the beam path) recorded on an EPID in conjunction with pCT data of the patient, to predict the primary portal dose on the EPID. This dose is then reconstructed using the back-projection algorithm in the 'virtual patient', which has the anatomy of the pCT [19]. This virtual reconstruction gives us a dose reconstruction assuming the patient's anatomy is identical to the pCT. It includes machine and plan related errors, as well as errors in the reconstruction algorithm. Thus, if this virtual dose distribution is used as a reference, instead of the TPS plan dose distribution, deviations in in-vivo fractions will be solely due to patient geometry, since the other systematic errors are cancelled out.

Since the purpose of this work is to correlate the colours of the traffic light protocol, which are indicators of anatomical changes, it would be beneficial to use the virtual reconstruction technique for EPID dosimetry, as well as the fraction dose from the CBCT since they provide this information.

2.5. Cone Beam CT

2.5.1. Introduction

With the advent of the on-board cone beam CT, image guided radiotherapy can now ensure the position of the target in 3D with accuracy unlike ever before [20]. Nowadays not only are the acquisition times fast, but also the reconstruction times. In combination with the low dose to the patient, these are just some of the many advantages of using a CBCT machine. In some cases, several CBCT scans are taken before a fraction is irradiated.

The NKI uses Elekta-Synergy (Elekta, Crawley, UK) linacs, which are capable of advanced image guidance. The on-board CBCT scanner allows for 2D, 3D as well as 4D imaging using a kV beam. The CBCT system for Elekta is known as XVI (X-ray volume imaging) and it is accompanied with software for acquisition and reconstruction. The flat panel used by XVI is the same model as that of the EPID.

2.5.2. Protocol

When the CBCT scan is acquired there are a number of parameters than can be adjusted, such as the gantry angle range of rotation, the speed of rotation, tube voltage and current, detector position (which affects the field of view), type of filter and collimation. These parameters are usually pre-set for different sites. Usually in the case of imaging bony anatomy a gantry speed of 1 rpm is used. However in the case of imaging 4D scans, a speed of 0.125 rpm is used to ensure sufficient number of breathing cycles. The detector position, displaced along its horizontal axis, affects the field of view of the reconstruction. For no displacement, a small FOV, a cylinder of 25cm height and 25cm base diameter, is reconstructed. In the case of a medium FOV, the reconstructed cylinder has a base width of 40cm, however the gantry must always rotate 360 degrees in this case. H&N scans are usually medium FOV and lung scans are small FOV, with the first lung fraction acquired in 4D. Different tube voltage and current are used to optimise image quality in different sites depending on the soft tissue (like prostate) or bone content (head and neck). The filter used in most cases is an F1 bow-tie shaped filter that reduces scatter and skin dose to the patient, however the

insert can be changed.

Once the above scan parameters are set and the scan is completed, it is reconstructed using the FDK method [21]. A software scatter correction is then applied to improve the quality of the scan. However, to display the scan in a useful manner, it first needs to be registered or matched to the pCT, as discussed in the above section. The correction reference point (usually the PTV) and the match method (usually bony anatomy with translations and rotations) is set. The structures to be displayed are also selected (usually GTV or PTV). After the match, the reference scan (which is usually the pCT) is displayed alongside the CBCT. They can also be overlaid using a purple-green colour wash. The purple colour indicates local structures present on the reference scan that are not present in the CBCT. The green colour indicates local structures present in the CBCT that are not present in the reference scan. The delineation of the selected structures are overlaid on the scans as well so that the adequacy of the coverage can be judged by the RTT. It is at this point the traffic light protocol is evaluated. The shift calculated by the match is translated into table translational shifts, and performed on the couch. After this point the fraction may be irradiated.

2.5.3. CBCT Based Dose Calculation

The daily CBCT scans are typically used for patient positioning and for observing anatomical changes. However there has been growing interest to use these scans to evaluate changes in dose distribution that would occur in altered patient geometry. The CBCT scan reflects the ground truth i.e. the anatomy of the day, the basis on which the colour of the traffic light protocol is determined. The TPS calculated dose on the CBCT would then be as close as possible to the ground truth dose. However there are several problems with using CBCT scans for dosimetric purposes.

CBCT scans suffer from poor image quality and are not in calibrated HU (Figure 2.13). This is because of beam hardening artefacts, as well as excessive photon scatter detected, caused by the the large area of the detector and beam size [22]. The quality also suffers due to delay in the acquisition as well as temporal effects of organ motion in certain sites. In normal CT scanners, the CT numbers are calibrated in HU. The HU are used to convert to electron density, which allows the TPS to then calculate dose distribution on the anatomy. There exist some methods nevertheless, to use these CBCT scans to calculate dose.

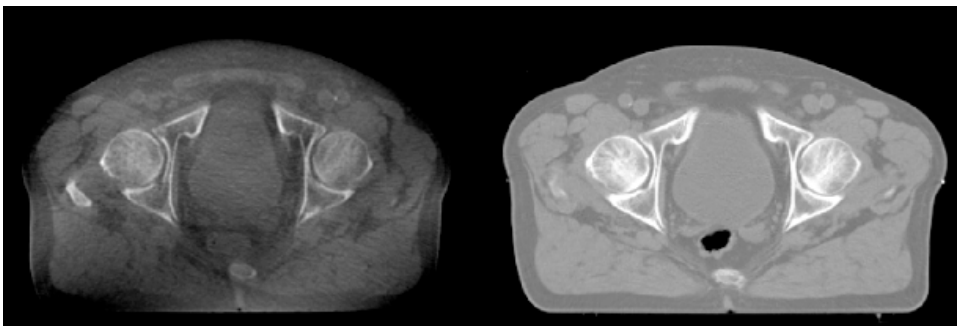

Figure 2.13: The image quality of the reconstruction for a CBCT (left) and a pCT (right).

One approach, which was also used in the paper discussed in the previous section [4, 23], uses deformable image registration (DIR). A deformation vector field is generated using a b-spline method, and applied to the pCT such that it matches the anatomy of the CBCT. Thus the structure of the pCT is adjusted to the CBCT, but the HU of the original pCT are retained. This scan then can be fed into the TPS for dose calculation. This method is used in research conducted at the NKI for H&N CBCT scans. The same method could be used in lung scans as well however, it has been observed that DIR artefacts often occur in lung scans due to change, presence or absence of atelectasis [24].

Some techniques have been investigated for lung and other sites as well such as CT number to electron density calibrations using phantoms, replacing CBCT numbers with bulk averaged CT numbers for the same site, selectively replacing the CT number of certain voxels more likely to produce artefacts and using standard HU look-up tables[5, 25].

In one study, a region on the CBCT with atelectasis or pleural effusion was delineated and then transferred to the same location on the pCT using rigid registration [11]. This region was then set to the CT number of lung tissue or water, and the dose was recalculated, and then compared to the original pCT. A visual estimation of the change in dose was also done depending on the thickness of the delineation that the field passed through. While this method was found to be suitable to determine if a treatment needed to be re-planned or not, the method was found to be unreliable for accurate dose determination, due to uncertainties in the delineation, registration, unaccounted deformations as well as fixed HU for the effected regions.

Another study also looked at the DIR technique using the pCT to match the CBCT as mentioned before, as well as a population-based look up table to convert CBCT numbers to HU [26]. While the DIR method was rather successful, the look-up table method suffered from intrinsic artefacts in the CBCT scan such as shadowing effects, and variance in CBCT numbers in different areas of the field of view.

Recently, research at the NKI has also been shown that the quality of the CBCT reconstruction can be greatly improved by combining hardware and software improvements. By using a highly specific anti-scatter grid in combination with an iterative scatter correction algorithm, significantly higher quality images are reconstructed without additional dose to the patient [22]. The grey values of the scans are then calibrated to HU using an image quality phantom. The DIR technique and the anti-scatter grid in combination with the iterative scatter correction are relevant to this study since they are researched and used at the NKI. The workflow for both these methods is described in section 3.4.2.

Both these methods require additional hardware or software, and are currently not part of the routine clinical workflow. Thus it is also beneficial to know if the EPID reconstructed dose can substitute the CBCT calculated dose.

2.6. Conclusions

The criteria for the traffic light protocol for the sites of H&N and lung were studied. It was found that the protocol was quite rudimentary and highly visual in nature. For some types of anatomical deviations, only one colour could be assigned, no matter how large the deviation (tumour shrinkage for example). The imaging protocols for patient positioning and set up were also reviewed. A brief history of the development of the EPID dosimetry algorithm used at the NKI was accounted and its shortcomings were discussed. The idea of a 'virtual' EPID dose reconstruction is key in identifying anatomical changes using the EPID. Some methods of CBCT based dose calculation used in research around the world were discussed. Two of these methods, which are also researched at the NKI, the DIR method and the anti-scatter grid method, were available to be used in this work and thus will be discussed further in Section 3.4.2.

3

Methods

Two main studies are performed in this chapter. The first study will deal with the research and analysis of H&N patients. The second section will deal with lung patients. Due to the time constraints involved in collecting new patient data, the following studies are retrospective in nature.

3.1. Patient Database

The NKI has a vast database of its patients that is accessible via an SQL server. It contains patient information as well as information about the diagnosis, treatment and fractions. The databases relevant to this study were the EPID database, and the XVI-logbook database.

The EPID database contains patient IDs, treatment IDs, treatment type, sites, dates of fractions, linac number, EPID alert codes and many other parameters. The XVI-logbook database contains the information regarding the traffic light protocol, i.e. colour codes for each fraction, as well as the entered condition for each criteria in the protocol by the RTT.

3.2. Metrics for Dose Distribution Comparisons

The following studies deal with dose distributions from multiple sources. The planned dose distribution from the TPS, the dose distribution as calculated on the CBCT by the TPS, the in-vivo EPID dose distribution reconstructed for a given fraction, and the EPID dose distribution reconstructed for a virtual patient. In order to analyse the dosimetric effects of anatomical changes, we have to be able compare dose distributions. To do so we make use of the following metrics.

The metrics used in the following studies are a combination of γ indices and DVH parameters. γ is an index that is evaluated using a distance formula. It contains a dose distance criterion as well as a distance-to-agreement criterion, and is evaluated on two dose distributions, where one is the reference dose distribution [27, 28]. The general Γ formula is computed as follows:

$$\Gamma(\vec{r_e}, \vec{r_r}) = \sqrt{\frac{(D_e(\vec{r_e}) - D_r(\vec{r_r}))^2}{\Delta D^2} + \frac{|\vec{r_e} - \vec{r_r}|^2}{\Delta d^2}}$$

Where $\vec{r_e}$ is the position of a grid point in the evaluated dose distribution, and $\vec{r_e}$ is the same in the reference dose distribution. $D_e(\vec{r_e})$ and $D_r(\vec{r_r})$ are the evaluated and reference doses at the points $\vec{r_e}$ and $\vec{r_r}$ respectively. Δd is the distance-to-agreement criterion, which in this thesis is selected to be 3mm and ΔD is the dose criterion, which in this thesis is selected to be 3% of the maximum dose. The first term under the square root is the dose difference term, and the second is the distance term. After this, the γ- index function is evaluated on the result of the above equation.

$$\gamma(\vec{r_r}) = min\{\Gamma(\vec{r_e}, \vec{r_r})\} \forall \{\vec{r_e}\}$$

The γ-index function for every reference grid point, is a minimised and generalised version of the original function, on the set of the evaluated grid points. γ in the following studies are calculated in 3D [28], and the in-house tool used to do so is known as DoseCompare. The γ is evaluated with the aforementioned criteria, and is calculated only within inside the 50% isodose region.

The mean of the γ-index for all points in the 3D reference grid is known as γ mean, and is used throughout this study. In addition to γ mean, γ pass rates are used in regular EPID dosimetry, and were also evaluated for the following studies but have been excluded. The passrates typically used are γ-1%, which is the percentage of points with a γ of less than 1, and the γ-99, which is the value below which 99% of points lie.

In addition to γ indices, dose volume histogram (DVH) parameters are also used. The only structure we will deal with in this thesis is the PTV (planning target volume). The D50 or median dose, is defined as the dose delivered to 50% of the volume of a structure, as derived from a DVH graph.

An important point to mention, is that γ mean is an unsigned value. It gives an indication of deviation but does not indicate if there was an overdose or an underdose. Relative differences in the PTV D50 however, do indicate this.

3.3. Correlating in-vivo EPID Alerts and the Traffic Light Protocol

An initial study was performed to see if the EPID alert codes and the traffic light protocol had any correlation. The secondary objective of this study was to become familiarised with the SQL environment since the rest of this project involved data mining and analysis.

The site chosen was lung, with all treatment plans having a prescribed dose of above 44 Gray. As mentioned before, only the first 3 fractions of a lung treatment are recorded with the EPID and analysed. However, it was found in the database that, it is quite common for an extra fraction to be recorded or for the data of a fraction to be missing. In the case of replanning due to adaptive radiotherapy, 3 more fractions are recorded. It is also quite common for patients to have had multiple treatments.

The goal was to match the EPID alert code of a fraction, which is in the EPID database, to the traffic light code of a fraction which is in the XVI-logbook database. A total of 852 fractions or 284 treatments were analysed, and the results were plotted in a bar graph.

3.4. Correlating the Dosimetric Effects of Anatomical Changes with the Traffic Light Protocol for H&N VMAT Treatments

3.4.1. Patient Selection

For the head and neck study, the selection of patients was dependent on CBCT dose data that was already available. The method used was the DIR technique as described in Section 2.5.3, and the dose distributions had been calculated for every fraction for about 100 treatments, starting from 2010. However, since the traffic light protocol was only implemented in 2012, this narrowed the selection of patients for which there was already available data. 17 head and neck patients were selected, each with 35 fractions for which both, the CBCT dose using the DIR method, and the EPID dose data were available.

One additional H&N patient was selected, for which the CBCT dose would be calculated using the anti-scatter grid method (Section 2.5.3). The anti-scatter grid was only installed on one linac for a few months since December 2016, hence the number of available patients was very limited. Thus, in total 18 treatments were selected (17 using the DIR CBCT dose method and 1 using the anti-scatter grid method), which had a total of 630 fractions.

3.4.2. Calculating the Fraction Dose Using CBCT Data

The CBCT scans were reconstructed using the clinical model, which implements uniform scatter correction. For 17 treatments, the CBCT dose distribution was calculated using the DIR technique, using the in-house registration software Match42 and the treatment planning system software Pinnacle (V9.10, Philips Medical Systems, Eindhoven, The Netherlands). The CBCT scan was rigidly registered to the pCT using a chamfer-matching algorithm and

defining the tumour as well as other bony anatomical structures for the registration. After this, using a cubic b-spline method, the pCT was deformably registered to match the CBCT. This modified CT scan was then imported into the Pinnacle software, where the treatment plan was re-calculated on it. The dose distribution obtained was then exported and the median dose to the PTV was also calculated. The PTV is defined in room coordinates and thus remains unchanged, even in the CBCT scan. However in some cases, the PTV lies outside the body or in the build up region, thus the PTV in the CBCT scans are defined as the intersection of the PTV and the patient body, minus a 4mm margin [4].

For the anti-scatter grid technique, the CBCT scans of one patient were reconstructed with the appropriate filter parameter, and the iterative scatter correction approach using the XVI software [22]. The resulting CBCT scans were then imported to pinnacle, where the treatment plan was calculated on them. The resulting dose distribution was exported, and the D50 dose to the PTV was also calculated.

3.4.3. Calculating the Fraction Dose Using EPID Dosimetry

The VMAT EPID data recorded for each of the fractions was reconstructed in 3D using the in-house EPID dose verification software, Divas. The same machine parameters and calibration settings (EPID sensitivity and EPID calibration model), at the time of recording of the data, were used to reconstruct the dose. The dose distribution for every fraction was exported, and the D50 dose to the PTV was logged.

Quite often, a few fractions are missing EPID data. This can occur due to misplaced data or failure to record data on the EPID during irradiation. Some fractions occasionally also have misplaced CBCT data. These fractions were removed from the study.

3.4.4. Reference Dose

The goal of the study is to measure the deviation of the dose distribution in each fraction, in both forms, the CBCT dose as well as EPID dose, and see how they correlate to the traffic light colours. However in order to measure deviation, a reference with which the deviation is measured, has to be determined. The reference dose distribution should be one where no anatomical changes have yet played a role. Logically, one would assume that dose calculated on the pCT by the TPS would be the best choice.

However, by using the TPS dose as a reference for the EPID, we measure deviations that may not be related to anatomy at all, such as machine, plan exporting, set-up and reconstruction related errors. While these errors are clinically relevant, for the purpose of this study, they are unnecessary.

A virtual reconstruction uses EPID data from open fields (treatment fields without any material in the beam path), and reconstructs the dose in the virtual anatomy of the patient, i.e. the pCT of the patient. It is a more realistic version of the planned dose, after being delivered and reconstructed by the EPID. A virtual dose distribution would be the best reference, since measuring the deviation with respect to it would eliminate systematic non-patient related uncertainties, and any deviations measured are purely due to changes in anatomy. Since these fractions were irradiated in 2012, these linacs have been equipped with new EPIDs and the concept of using a virtual fraction would be rendered moot. A new virtual fraction on a different EPID would not take into account the same degree of uncertainties than 4 years ago.

Thus, the choice of the reference was the reconstructed dose of the first fraction. This way, similar to comparing with a virtual, non-patient related uncertainties mentioned above are accounted for, and logically, one would expect the minimum deviation of patient anatomy from the pCT on the first fraction. In all the H&N treatments, the first fraction was also seen to be assigned a green traffic light colour code. There is however, always the risk that the reconstructed dose of the first fraction encountered some error, which would not normally be present, such as an acquisition or large set-up error.

The choice of using the first fraction as the reference dose has also been applied before. In a study that involved using the EPID to monitor anatomical changes during the course of the treatment, difference images were used, where the first fraction was used as the reference [29].

The choice of the reference for the CBCT was also chosen to be the calculated dose of the first fraction, in order to keep consistency. However, in the case where a virtual fraction for the EPID would be possible, using the TPS dose as a reference would be logical.

Usually a treatment is designated to one linac, but a few fractions can be carried out in another linac (and thus another EPID), due to changes in schedule or unavailability of the the linac. Fractions which were recorded on other linacs/EPIDs were removed from the study.

For each treatment, the first fraction was taken as the reference, and the relative changes in the dose distribution of successive fractions were calculated using γ mean, using the DoseCompare tool. The relative change in the D50 to the PTV was also calculated using the first fraction as reference.

Thus for each fraction, there were 6 parameters. The fraction number, the EPID γ mean, the EPID ΔPTV D50, the CBCT γ mean, the CBCT ΔPTV D50 and the traffic light colour code for the fraction. Plots were made between these parameters and correlations were investigated.

3.5. Correlating the Dosimetric Effects of Anatomical Changes with the Traffic Light Protocol for Lung IMRT Treatments

The lung study was in fact, a follow up study after the results of the H&N study were analysed. Lung patients display more anatomical deviations than other sites, and are thus good candidates for evaluating the traffic light protocol [1, 8]

From the literature study performed, as well as from discussions with colleagues, it was understood that the DIR approach to CBCT calculation would not work well for lung patients. Artefacts during the DIR occur due to atelectasis and anatomical changes in the lung, which require density overrides in certain regions to correct [24]. These overrides however are very general and can propagate uncertainties into the dose calculation step. Already in lung CBCT scans, the quality of the reconstruction is poor due to motion from respiration. Moreover, the first fraction of a lung CBCT is always recorded in 4D, further complicating the dose calculation process.

The anti-scatter grid approach could not be used due to the lack of patients, and the quality of reconstruction was also low compared to other sites. In addition to this, the FOV of the scan is small, which means that the reconstruction is not of the whole thorax, but only one side of it, which contains the diseased lung. It requires to be merged with the missing data from a pCT, before it can be fed into the TPS for dose calculation. Thus for the lung study it was decided not to use the CBCT calculated dose, and only use EPID reconstructed dose.

3.5.1. Patient Selection

Since in-vivo EPID dosimetry is performed for all treatments, the available number of patients/treatments was very large. However with only 3 fractions recorded per treatment, a large number of patients would be required to gather sufficient data. Patients with at least one alert in their treatment were preferred (at least one fraction yellow or orange). 34 treatments were chosen, using the SQL database, with a total of 100 fractions between them. The patients selected were across different linacs, but had all been treated relatively recently. The treatments had been recent enough, that the same calibration models and EPIDs were still in use, allowing us to make us of the virtual reconstruction.

3.5.2. EPID Dose

The EPID data for each IMRT field was recorded for the first 3 fractions and was reconstructed in 3D with Divas. The rest of the procedure is the same as in section 3.4.3. The fractions with missing data, or which were recorded on a different linac, were removed. The dose distribution was exported, and the PTV dose was logged.

The procedure was done twice, once using calculated transmission, i.e. transmission calculated from the planning CT, and once using measured transmission i.e. transmission measured using the data from the open field image. The open field images used for the virtual reconstruction were used for this.

3.5.3. Reference Dose

In this study, as mentioned before, virtual reconstruction was possible (Figure 3.1). In order to do this, an open fraction needed to be recorded. Open treatment fields were recorded on the EPID, at the respective linac where the treatment was recorded. This was done for all 33 treatments, and the dose distribution of the virtual reconstruction was exported, and the PTV dose was logged.

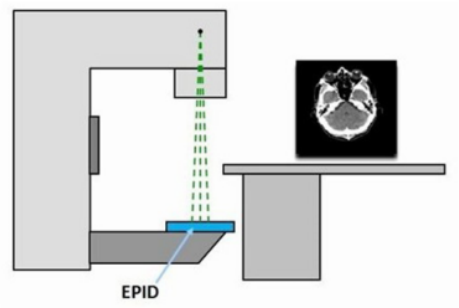

Figure 3.1: An open arc or field is recorded and then back-projected to reconstruct the dose in a virtual patient, which has the anatomy of the planning CT.

For each treatment, the virtual reconstruction was used as the reference, and the relative changes in the dose distribution of successive fractions were calculated using γ mean, using the DoseCompare tool. The relative change in the D50 to the PTV was also calculated, using the virtual D50 dose to the PTV as reference.

4

Results

4.1. Correlating in-vivo EPID Alerts and the Traffic Light Protocol

852 fractions of different conventional lung treatments were analysed for their EPID alerts and traffic light colours. Only the first 3 fractions were counted, since no EPID data is recorded for the successive fractions. Of these fractions, 603 had been assigned a green traffic light code, 93 had been assigned yellow, 143 had been assigned orange and 13 had been assigned red.

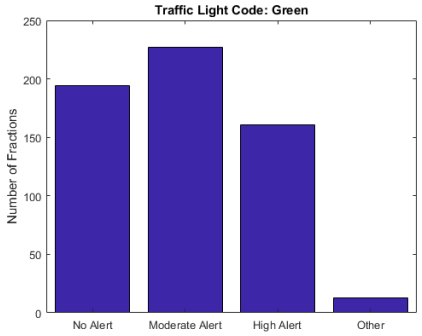

(a) EPID alerts generated for green traffic light fractions.

(b) EPID alerts generated for yellow traffic light fractions.

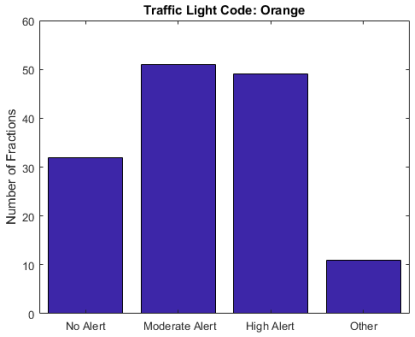

(c) EPID alerts generated for orange traffic light fractions.

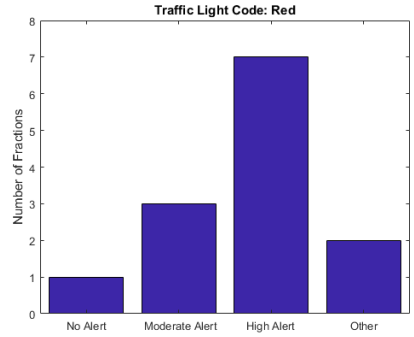

(d) EPID alerts generated for red traffic light fractions.

Figure 4.1: Bar graph plots for EPID alerts vs traffic light protocol colours for lung fractions.

For each traffic light colour, the break-up of the EPID alerts that were assigned to these fractions is plotted as a bar graph (Figure 4.1). A separate bar graph was made for each traffic light colour. EPID alerts have three levels of severity, high, moderate and no alert, which are

dependent on γ criteria, as well as mean dose to the PTV and the isocenter dose. Another miscellaneous alert category is used to indicate an error that occurred in the analysis of the fraction, due to missing data, error in reconstruction etc.

The correlation between the EPID alerts and the traffic light colours is ρ = 0.1294, p-value = 0.0002. For the sake of accuracy, the 'other' EPID alerts were removed from consideration. An interesting point to note was that there were more orange fractions than yellow.

4.2. Correlating the Dosimetric Effects of Anatomical Changes with the Traffic Light Protocol for H&N VMAT Treatments

Of the 630 fractions from the 18 treatments, after removal of fractions with missing data, discarding fractions with acquisition errors, and not counting the first fraction due to them being references, 509 fractions were left in total.

In order to facilitate plotting, the traffic light colour codes were assigned numbers from 1-4. Since the traffic colours are determined after assessing the CBCT, we would expect to see something like Figure 4.2, where the deviation between the fraction dose and the reference dose, as measured by γ mean on the x-axis, correlates well with the traffic light colours, on the y-axis. One would expect higher γ mean values as the severity of the traffic light colours increased. What was found however, is plotted in Figure 4.3. The distribution of the green, yellow and orange alerts are overlapping and show a large spread.

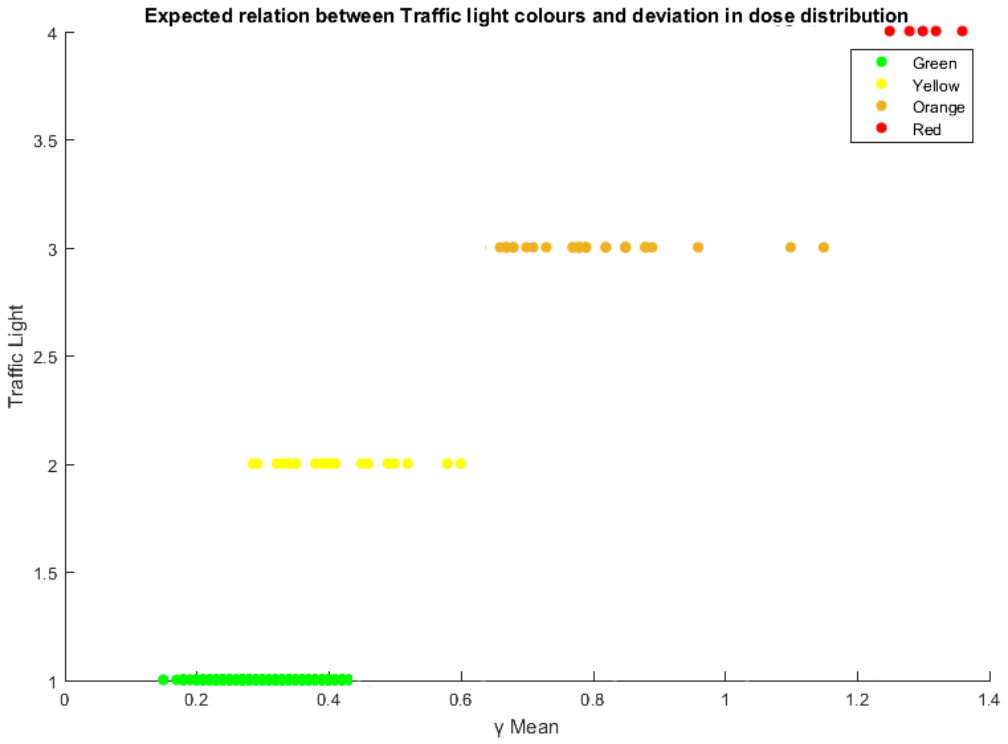

Figure 4.2: The behaviour we *expect* when we compare traffic light colours and a measure of dose deviation. With increasing dose deviation, the traffic light colours also increase in severity. Each fraction is plotted as a point with its traffic light colour for simplicity.

Similar behaviour is seen in Figure 4.4, where the EPID γ mean is plotted versus the colour codes. While the correlation in these graphs is clearly not strong or obvious, the number of green fractions reduce as we move right on the x-axis, and all the red fractions appear to be on the far side on the x-axis. The average γ mean values and standard deviations for the EPID and CBCT dose distributions given in Table 4.1.

The average CBCT and EPID γ mean increases with increasing severity, with yellow and

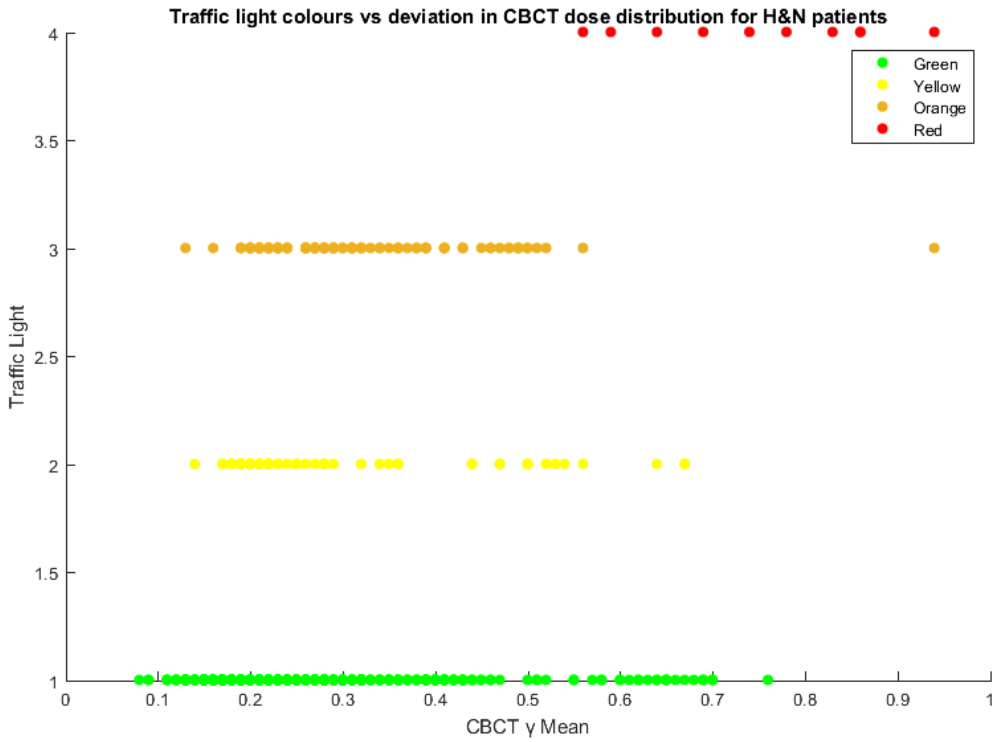

Figure 4.3: All H&N fractions and their associated traffic colours plotted against the γ mean of the CBCT dose distributions. ρ = 0.3229

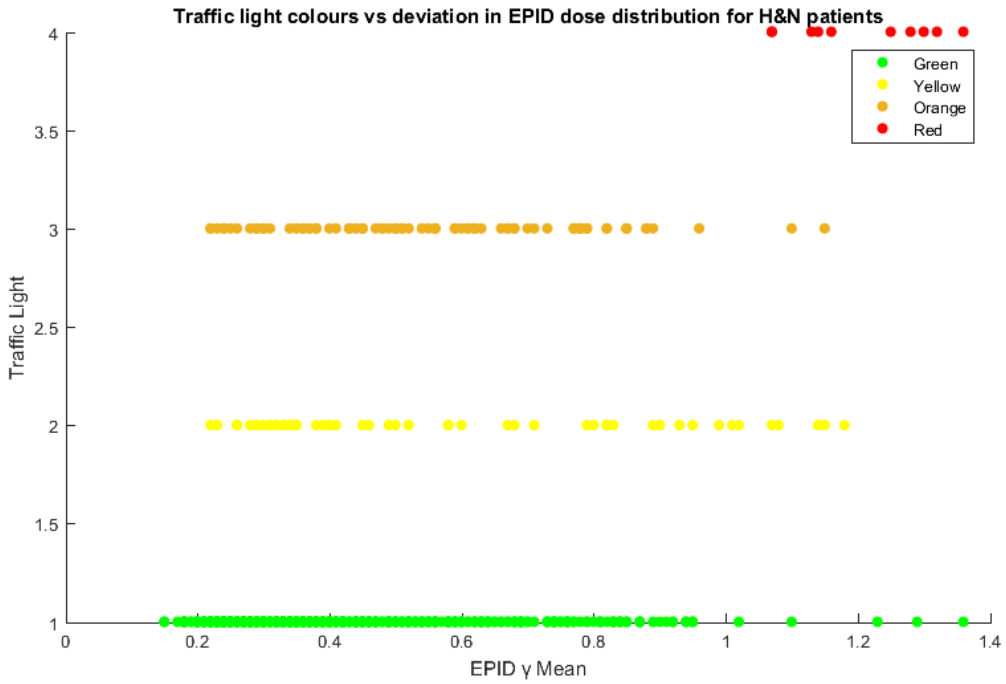

Figure 4.4: All H&N fractions and their associated traffic colours plotted against the γ mean of the EPID dose reconstructions. ρ = 0.3510

Table 4.1: The average γ mean values and their standard deviations for the different traffic light colour assigned fractions for H&N patients.

Traffic Light Colour	Average CBCT γ Mean (SD)	Average EPID γ Mean (SD)
Green	0.27 (0.13)	0.45 (0.21)
Yellow	0.31 (0.15)	0.59 (0.3)
Orange	0.33 (0.12)	0.56 (0.21)
Red	0.75 (0.13)	1.21 (0.11)

Table 4.2: Correlation coefficients and classification of treatment for each H&N patient.

Patient Number	CBCT & EPID γ-mean	CBCT & EPID ΔPTV Dose	Class
1	0.8596	0.6557	Strong
2	0.3149	0.2124	Weak
3	-0.4734	0.1662	Weak
4	0.4228	0.6985	Moderate
5	0.9388	0.9228	Strong
6	0.758	0.6463	Strong
7	0.7453	N/A	Strong
8	0.5865	-0.1265	Moderate
9	0.5256	0.8235	Strong
10	0.9415	N/A	Strong
11	0.042	N/A	Weak
12	0.0514	0.9112	Strong
13	0.0099	N/A	Weak
14	0.4112	0.1343	Moderate
15	0.4459	0.1321	Moderate
16	0.4342	0.8546	Strong
17	0.6182	0.7092	Strong
18	0.9148	0.9204	Strong

orange colours having very similar values. The number of reds is low due to the rarity of such a severe classification, and thus has a very small sample size. The average EPID γ mean is around 0.2 higher than the CBCT γ mean, and standard deviation values are much higher, with the exception of reds.

In order to better visualise the relationship between EPID and CBCT deviations, the following analyses were done on a treatment-specific basis. Since the deviation is measured based on the first fraction of each treatment, the subsequent plots (Figure 4.5 - 4.8) are more meaningful than plots containing fractions of all treatments.

For each treatment, the EPID γ and the CBCT γ mean were plotted over successive fractions. The correlation between the two was also calculated. The same was also done with the EPID PTV dose and the CBCT ΔPTV D50. One would expect that the shape or curve of these lines would overlap each other.

The 18 treatments were classified based on their degree of correlation into 'strong correlation' (Figure 4.5 and 4.6), 'moderate correlation' (Figure 4.7) and 'weak correlation' (Figure 4.8). Displaying graphs for every treatment is not feasible (however these can be seen in the Appendix, Figure B.1 - B.18), so the table of the correlation between the CBCT and EPID γ as well as PTV dose are given in Table 4.2. Patient 18 is the patient for which the anti-scatter grid technique was used to calculate the CBCT dose. Treatments for which the CBCT or EPID PTV dose was unavailable are flagged as 'N/A'.

A treatment was classified with a strong correlation if either the D50 correlation coefficient

or the γ mean correlation coefficient was above 0.7, a moderate correlation if it was between 0.4 and 0.7, and a weak correlation if it was below 0.4. Negative correlations were treated as weak correlations.

Interestingly, patient 17 and 18 that once displayed poor correlation, showed strong correlation if the second fraction was used as the reference instead of the first. The implications will be discussed later (Section 5.2.2).

An additional table (Table B.1) with the number of non-green fractions per treatment as well as the slopes of the γ mean regression lines from the plots below, can be seen in the Appendix.

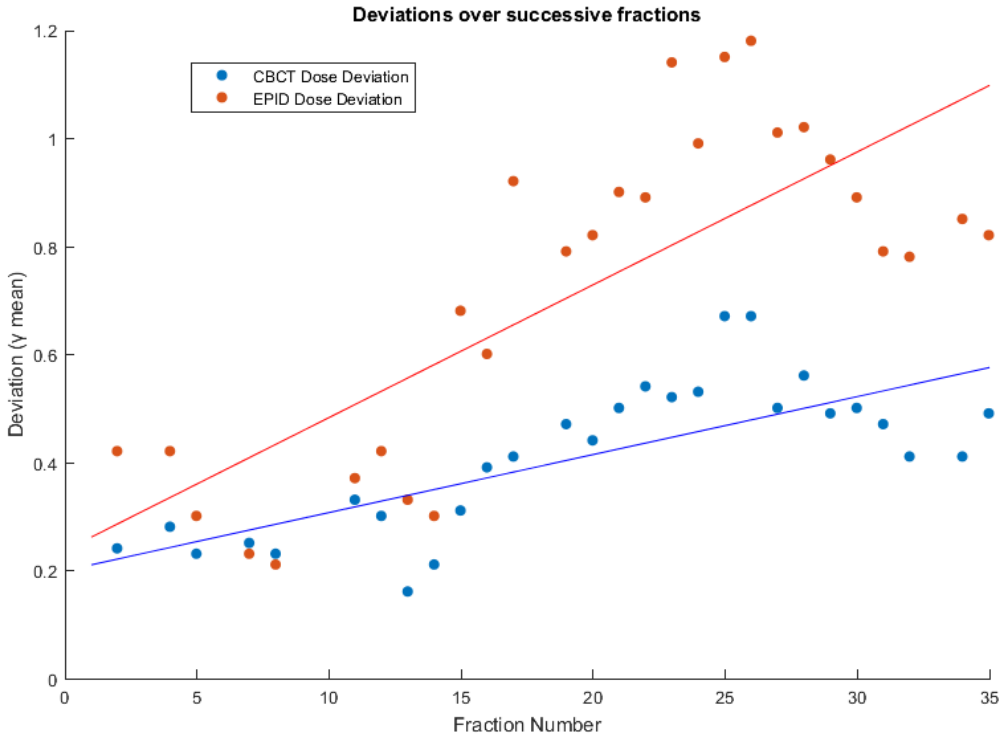

(a) Patient 5: CBCT and EPID γ mean over successive fractions. The two curves display the same shape, even in the dips and peaks. The EPID slope is steeper, however.

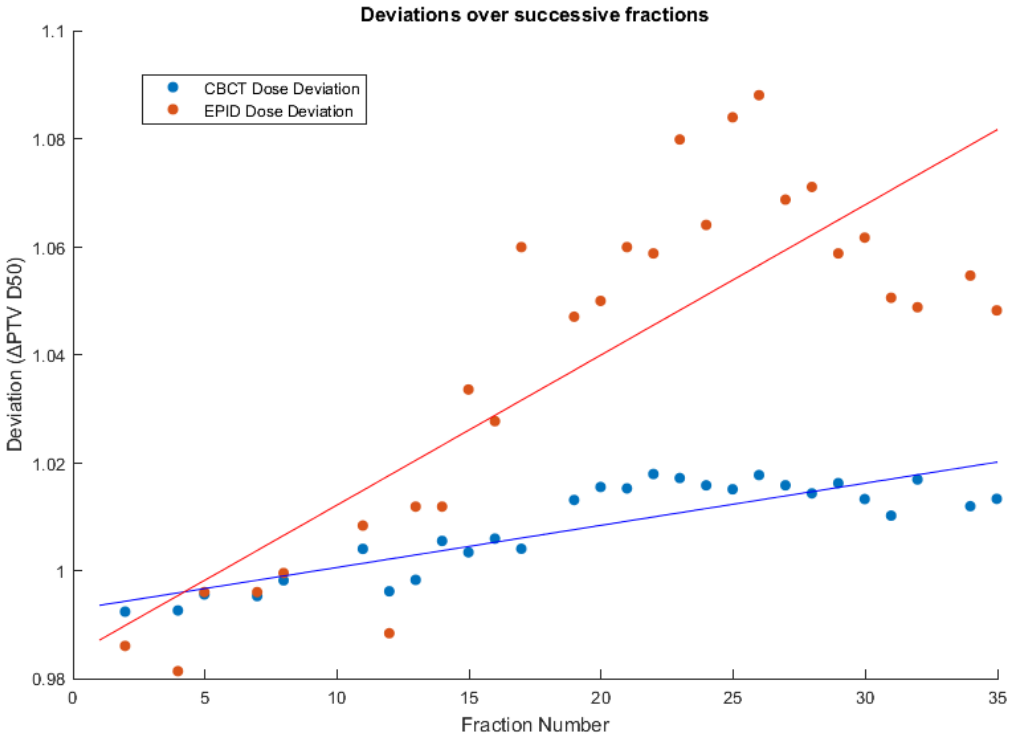

(b) Patient 5: CBCT and EPID ΔPTV D50 over successive fractions. The tiny fluctuations above and below the regression line of the CBCT are amplified in the EPID plot.

Figure 4.5: Examples of patients/treatments that displayed a strong correlation between CBCT and EPID dose metrics.

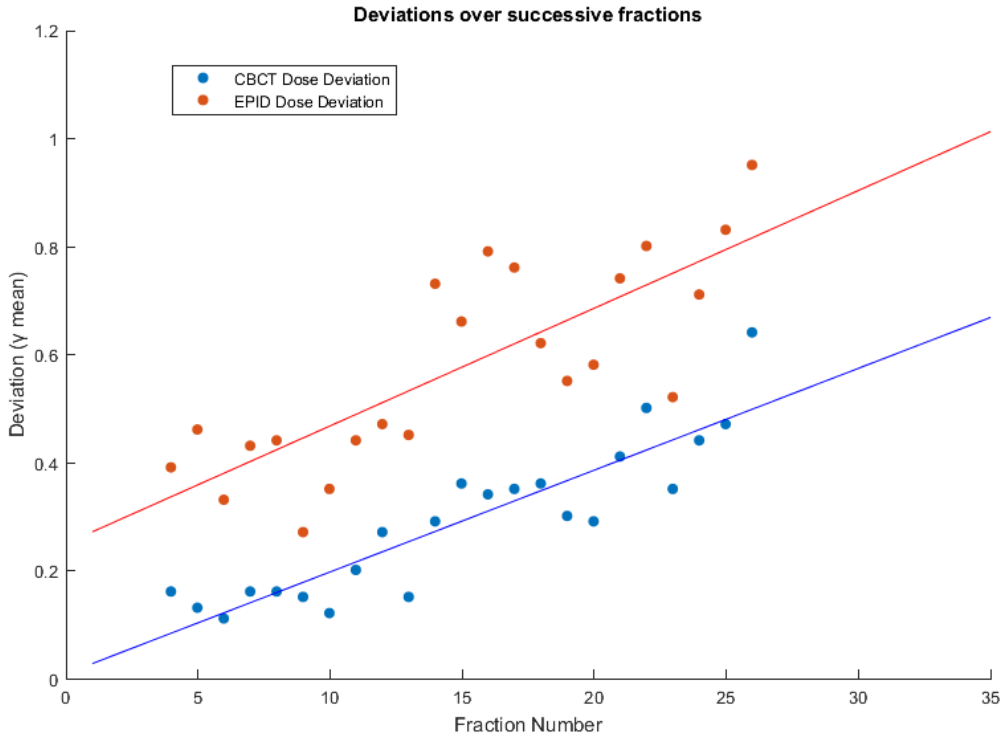

(a) Patient 18: CBCT and EPID ΔPTV D50 over successive fractions. Similar behaviour to patient 5 yet again. In this case however the regression lines are parallel.

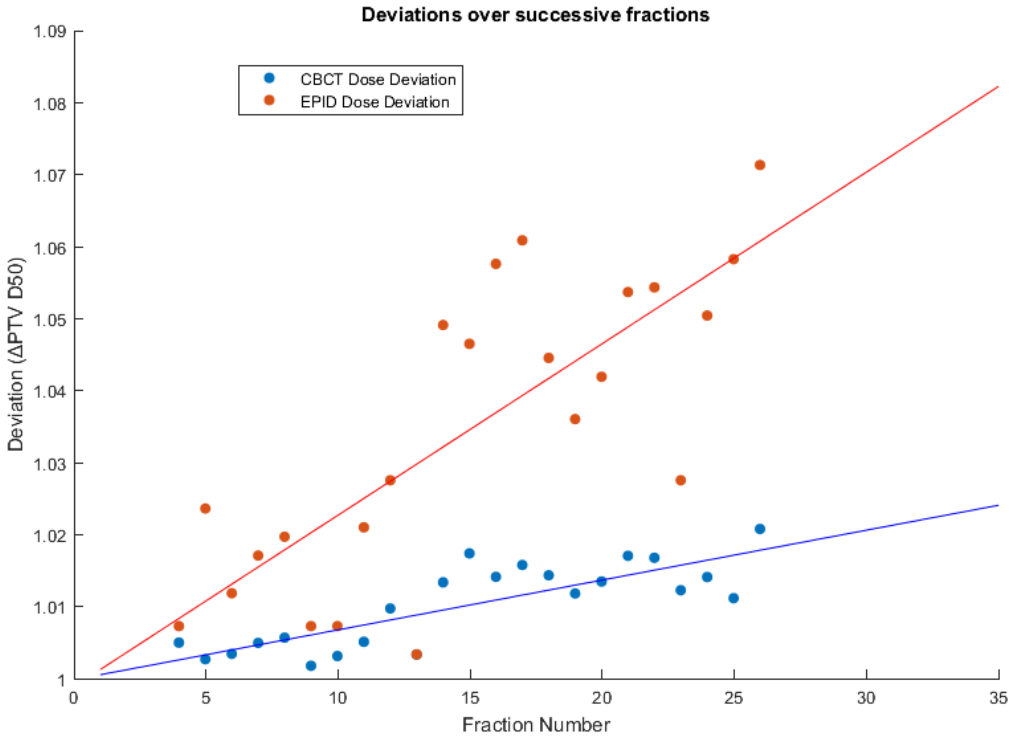

(b) Patient 18: CBCT and EPID ΔPTV D50 over successive fractions. Similar behaviour to patient 5 yet again, with similar slopes as well.

Figure 4.6: Examples of patients/treatments that displayed a strong correlation between CBCT and EPID dose metrics.

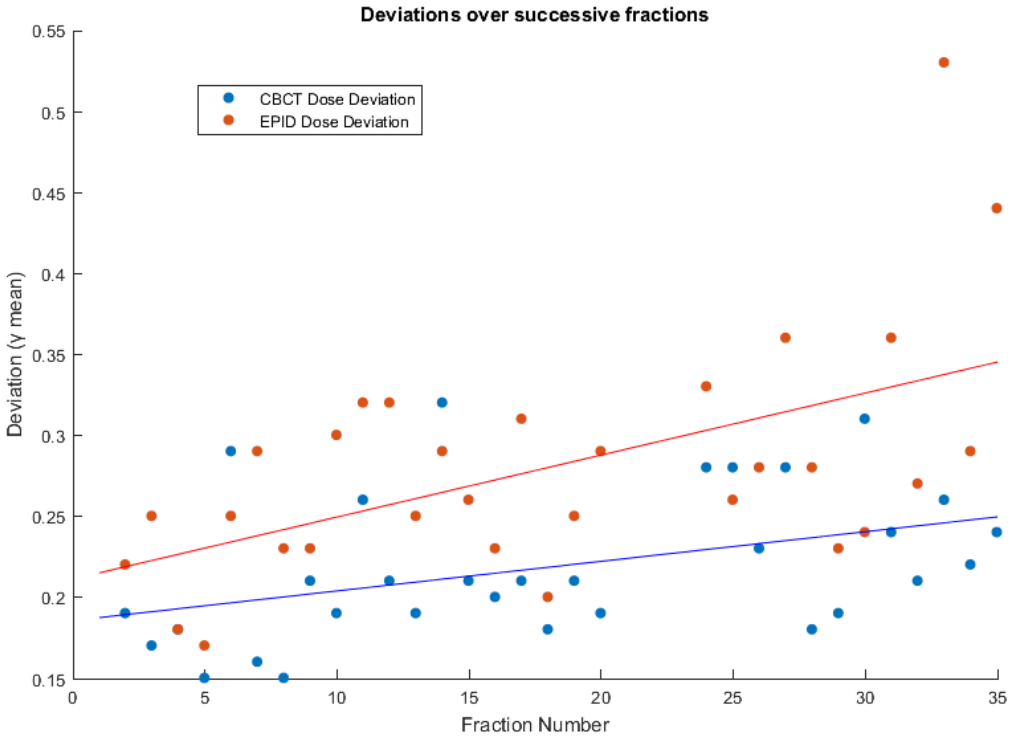

(a) Patient 4: CBCT and EPID γ mean over successive fractions. The regression lines show similar trends, however the correlation between the points seems to disappear halfway through the treatment.

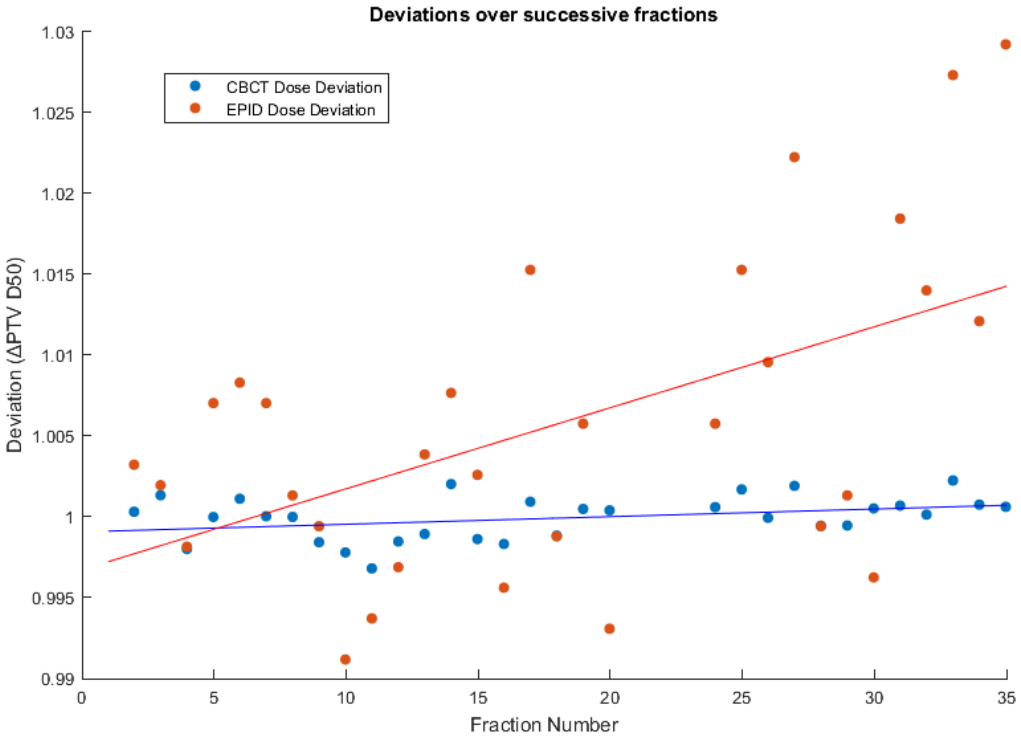

(b) Patient 4: CBCT and EPID ΔPTV D50 over successive fractions. The correlation here is much stronger than the γ mean graph. Yet again, the deviations are amplified in the EPID curve.

Figure 4.7: Examples of patients/treatments that displayed a moderate correlation between CBCT and EPID dose metrics.

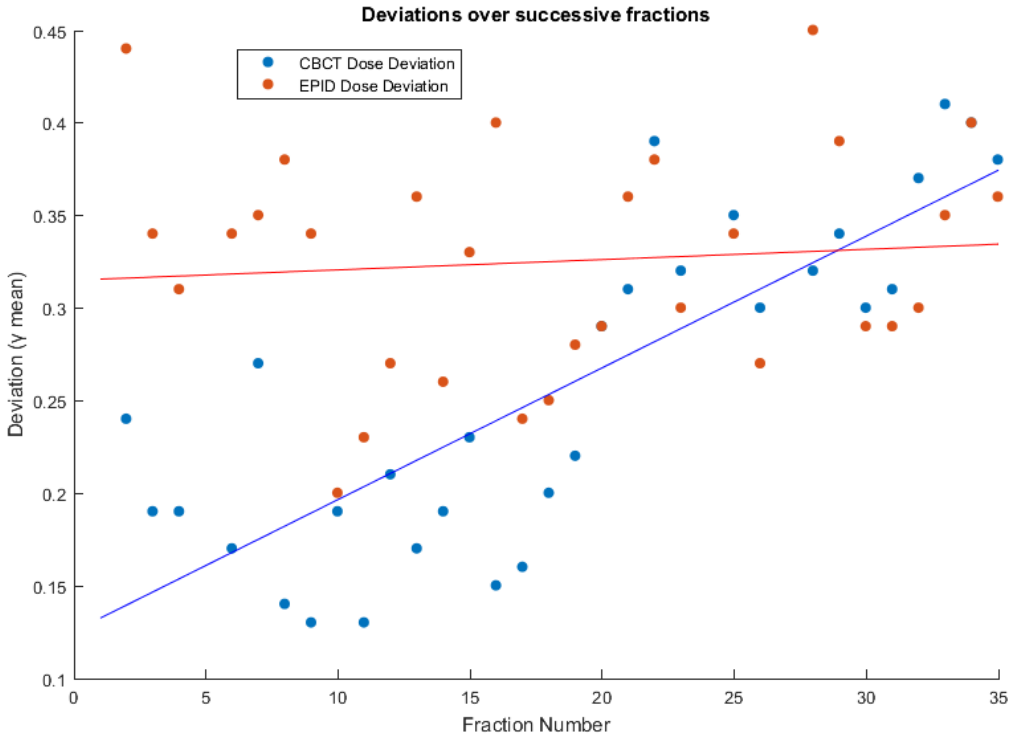

(a) Patient 2: CBCT and EPID γ mean over successive fractions. The CBCT shows the deviation increasing during the course of the treatment, however the EPID regression line is almost flat, with the points scattered around it randomly.

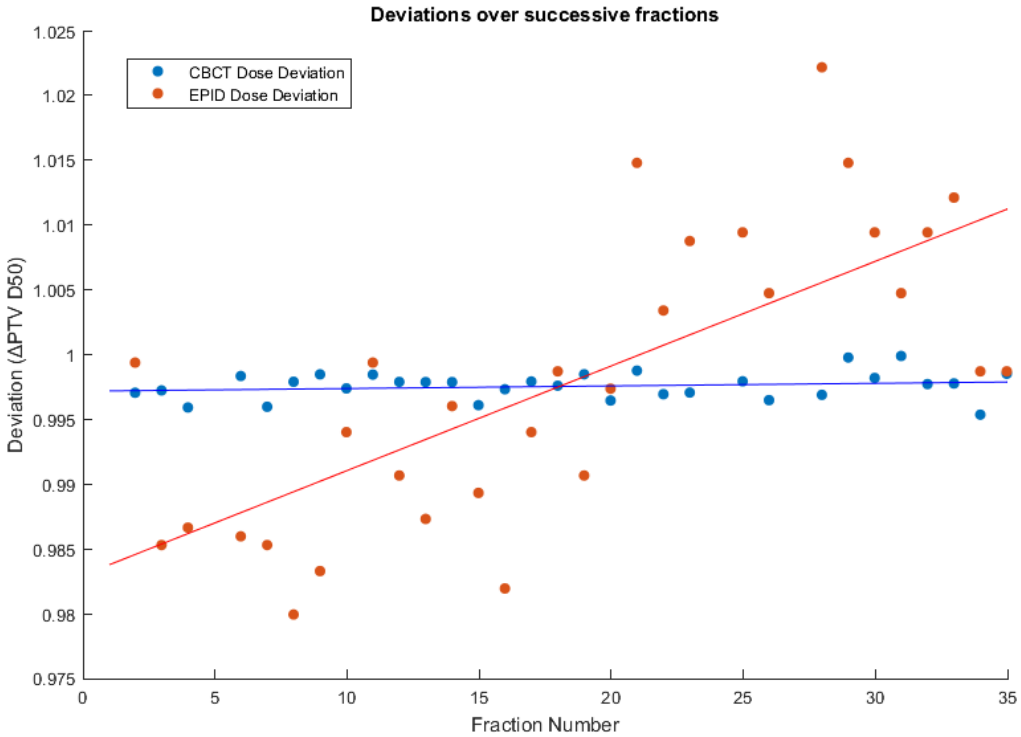

(b) Patient 2: CBCT and EPID %ΔPTV D50 over successive fractions. The regression lines is flat for the CBCT but shows an increase for the EPID.

Figure 4.8: Examples of patients/treatments that displayed a weak correlation between CBCT and EPID dose metrics.

4.3. Correlating the Dosimetric Effects of Anatomical Changes with the Traffic Light Protocol for Lung IMRT Treatments

For the lung study, the EPID dose was reconstructed using the calculated transmission and then with measured transmission. Each treatment used the virtual reconstruction as reference. The γ mean for the EPID measured and calculated was plotted for all fractions of all treatments (Figure 4.9). The same was done for the Δ%PTV D50 (the percent deviation in the D50 to the PTV) of the EPID measured and calculated reconstructions (Figure 4.10). The γ mean of the measured transmission reconstruction was seen to be always lower than the calculated transmission, however the correlation between the two curves was strong ($\rho = 0.8238$, p-value ≈ 0). The Δ%PTV D50 curve followed roughly the same shape ($\rho = 0.7574$, p-value ≈ 0). In the plots, groups of 3 fractions can be seen together locally around the same deviation. These are from the same treatment. The x-axis has no preferential direction, as the fractions could have been presented in any order. What matters is that the same fractions are used for the same x-point in both, the measured and calculated curves. The correlation we seek is in the similar shape of the two curves, however the overall shape does not matter. The average of the γ mean and Δ%PTV D50 and their respective standard deviation values are given in Table 4.3. The average difference in γ mean is around 0.4, and the average Δ%PTV D50 difference is about 2% between the two models. Standard deviation in the calculated transmission model is much higher.

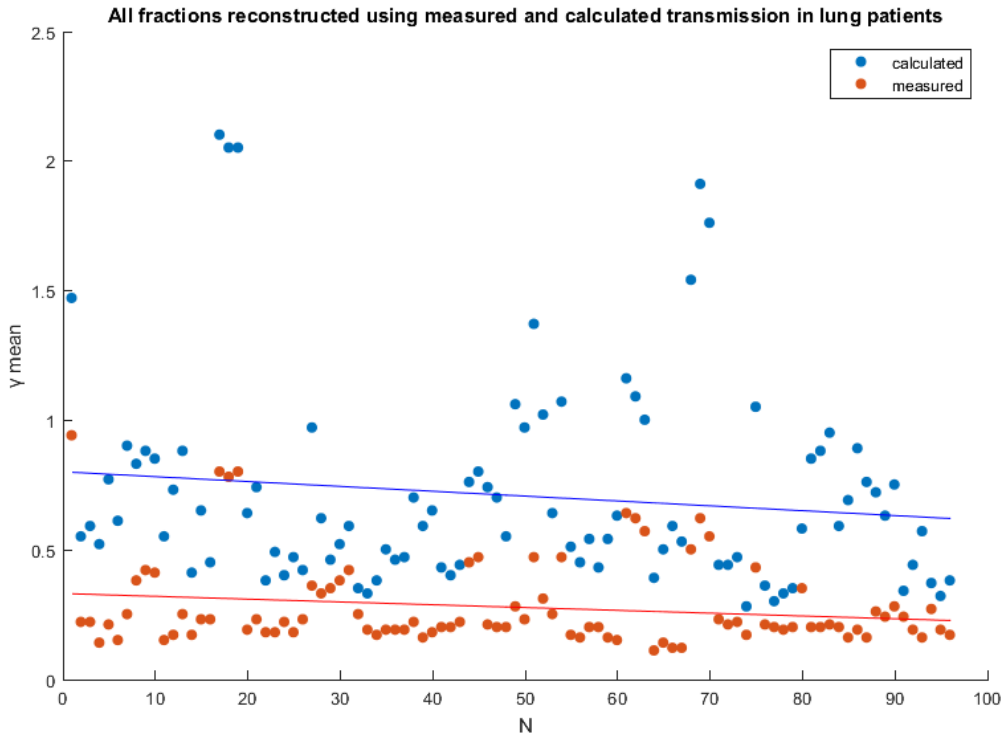

Figure 4.9: γ mean of the EPID reconstructions, using measured and calculated transmission. $\rho = 0.8238$

Theoretically the γ mean of a fraction, using the virtual as a reference, should show us dose deviations only due to the anatomical changes. Thus a comparison of the γ mean against the traffic colour codes is needed. We only plot the measured transmission γ mean and not the calculated transmission γ mean, because the measured transmission is more accurate, while the calculated transmission assumes that the patient geometry is the same as in the pCT, which makes it overly sensitive to daily anatomical deviations. This was discussed briefly in the literature study in Section 2.4.2, and is clearly seen in (Figure 4.9 and 4.10). The measured transmission γ mean was plotted, and colours were used as indicators for the

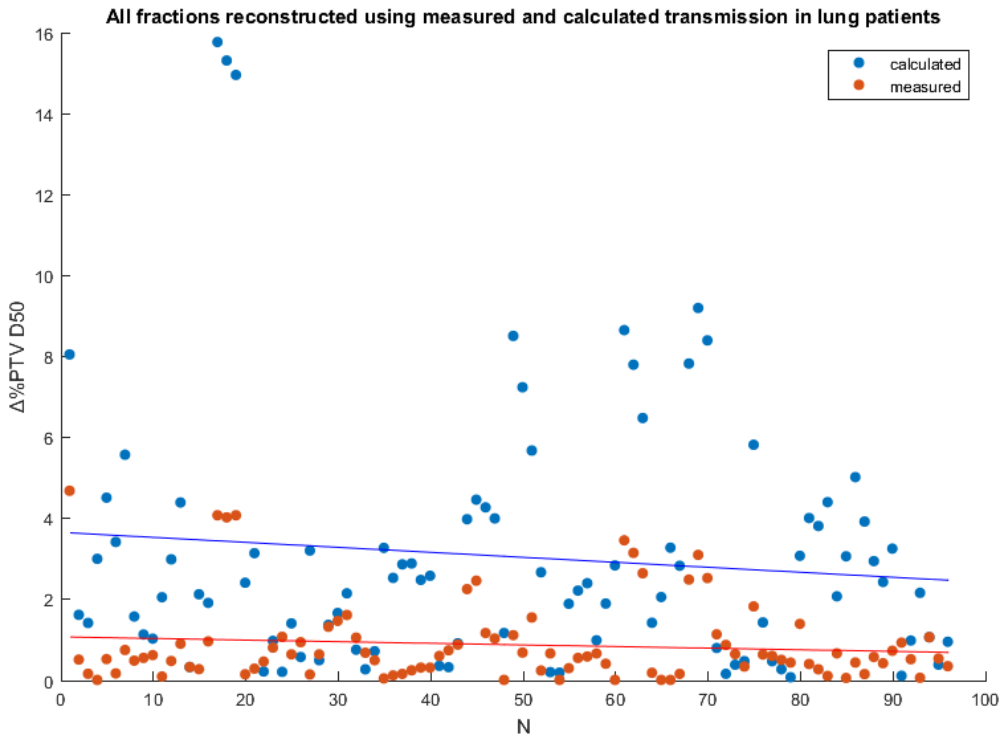

Figure 4.10: ΔPTV D50 of the EPID reconstructions using measured and calculated transmission. ρ = 0.7574

Table 4.3: The average γ mean and Δ%PTV D50 and their standard deviations, when reconstructed using different transmission models.

Transmission Model	Average EPID γ Mean (SD)	Average EPID Δ%PTV D50 (SD)
Measured	0.28 (0.17)	0.89 (1.01)
Calculated	0.71 (0.4)	3.06 (3.14)

traffic colour codes (Figure 4.11).

Once again the x-axis is merely used to show the number of fractions and has little other meaning. The correlation is calculated between the traffic light colours and the γ mean. For this plot, any fraction with a yellow or more severe traffic light colour was flagged as having an alert. A green fraction was flagged as a non-alert. It was found that there was no significant correlation (ρ = 0.1757, p-value = 0.0868). The average γ mean and Δ%PTV D50 for an alert and non alert are given in Table 4.4.

The average γ mean and Δ%PTV D50 values are higher for higher alert types, however the increase is minimal between non-alerts and alerts when compared with the values from the H&N table, Table 4.1.

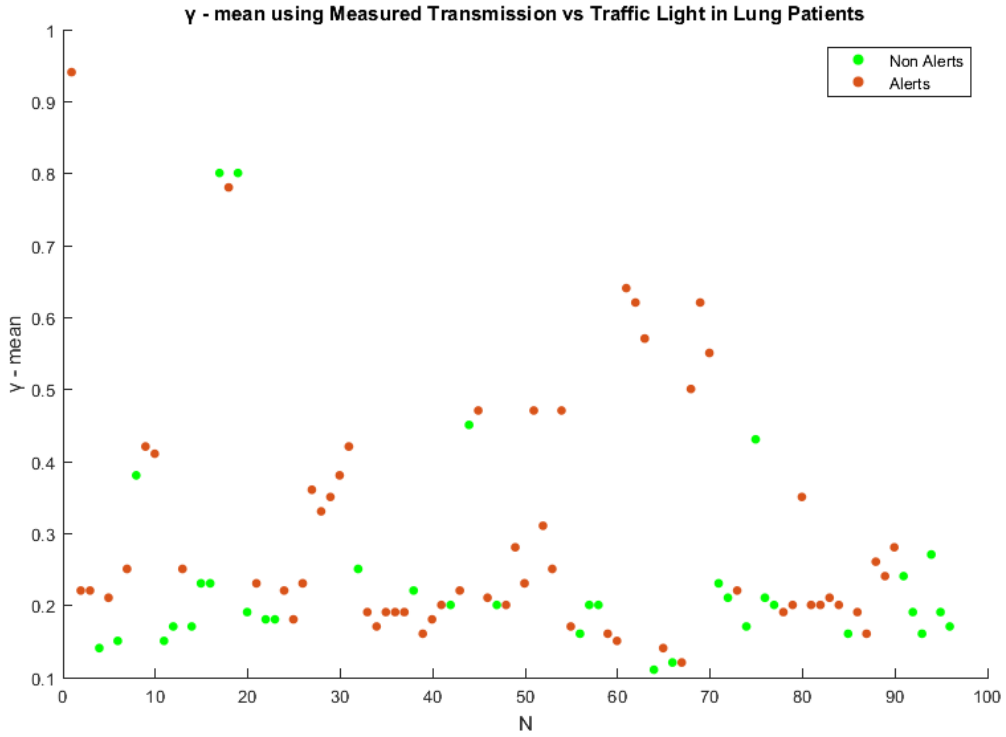

Figure 4.11: γ mean of the measured reconstruction labelled with the type of traffic light alert. Poor correlation was found. ρ = 0.1757, p-value = 0.0868

Table 4.4: The average γ mean values and their standard deviations for the different traffic light colour assigned fractions for Lung patients, using measured transmission.

Traffic Light Colour	**Average EPID γ Mean (SD)**	**Average EPID Δ%PTV D50 (SD)**
Non-Alert (Green)	0.24 (0.16)	0.79 (0.94)
Alert (Yellow, Orange, Red)	0.30 (0.17)	0.95 (1.05)

5

Discussion

5.1. Correlating in-vivo EPID Alerts and the Traffic Light Protocol

From the initial study it was observed that the EPID alerts did not correlate very well with the scored results of the traffic light protocol ($\rho = 0.1294$). Over 65% of the green traffic light fractions were flagged by the automated EPID dosimetry software as fractions which need to be reviewed. At the same time, 29% of yellow and 24% of orange fractions were cleared by the EPID dosimetry software as non alerting fractions. 57% of all lung fractions were alerted, which is more than the 36% reported by Mijnheer [1].

The reason for this lack of correlation is likely due to the fact that the two protocols rely on different criteria for their severity levels. The traffic light protocol is based on a visual analysis of a CBCT scan, while the EPID alerts are based on metrics evaluated on a reconstruction of the dose distribution. For instance, some traffic light alerts may not have a dosimetric basis, and may relate only to changes outside the 50% isodose region, where the EPID dosimetry criteria is not evaluated, or even just to the well-being of the patient (Section 2.3.3 and 2.3.4). In these cases we wouldn't expect an EPID alert at all.

Another important point to state is that the EPID alert is raised on dose reconstructed in the anatomy of the patient, based on data acquired by the EPID. Limitations of the EPID algorithm cause inaccurate dose reconstructions, which also raise EPID alerts. Thus many times they may false positives with respect to the traffic light colour. According to Mijnheer [1], 35% of alerted lung fractions are due to model limitations.

Thus the EPID and traffic light alerts are based on different criteria that are not necessarily related. However, we do see a diminishing percent of EPID non-alerts and increasing percent of more severe EPID alerts, as the traffic light code increases in severity, which would imply a slight correlation, fuelling the need for the further studies discussed below. The most severe traffic light colours in this site are due to changes in tumour volume changes and atelectasis [8], which are changes in the transmission parameter. These are usually detected by the EPID.

5.2. Correlating the Dosimetric Effects of Anatomical Changes with the Traffic Light Protocol for H&N VMAT Treatments

5.2.1. Traffic Light Protocol vs EPID/CBCT Dose

From the H&N study we observed that the dose metrics from the CBCT and the EPID dose distribution correlated with the traffic light colours on a treatment-wide scale with a correlation coefficient of 0.33 and 0.35 respectively. This may not be strong correlation, but it can account for the very slight correlation seen in the first study between EPID alerts and traffic light protocol colours, as well as the increase in the average γ mean as the severity of the traffic light increases as seen in table 4.1.

The reason for a lack of strong correlation however, can be accounted for using the same reasoning as the previous subsection. This is due to the visual analytical nature of the traffic

light protocol. The RTTs simply follow a protocol to ensure that the treatment is carried out as planned, and any deviations before irradiation occurs should be prevented or documented, in case action needs to be taken later, such as replanning. The dose actually calculated by the EPID and the CBCT need not agree with the protocol. As also discussed above, there are situations where a dosimetric effect would not be expected at all.

Another point of view to be discussed is the accuracy of the traffic light protocol itself. The protocol is performed within a couple of minutes of visual analysis, and can be subject to biases from the RTT. It is quite likely that an anatomical change may not be accounted for in the protocol, or may not be noticed by the RTT. These changes could alter the dose, but would be present as a false negative in the XVI-logbook database.

Attention was then turned to the CBCT and EPID dose distributions for each individual treatment. Validation of in-vivo EPID dose versus CBCT dose is still invaluable for the EPID dosimetry group at the NKI, since the CBCT dose is assumed to be the ground truth of the fraction.

5.2.2. EPID Reconstructed Dose vs CBCT Calculated Dose

General Observations

If all fractions are taken into account regardless of the classification made earlier, then the correlation coefficient between the CBCT γ mean and the EPID γ mean is $\rho = 0.7156$. However doing so for more than 500 fractions from different treatments doesn't allow in depth analysis, which is why classification was done for further analysing. This enabled us to find that for certain treatments the EPID was in excellent agreement with the CBCT, but in some treatments there was absolutely no agreement.

Each treatment was analysed and classified based on the correlation between the EPID and CBCT dose distributions. Out of the 17 treatments calculated using the DIR method, 9 were found to have a strong correlation, 4 a moderate correlation, and 3 a weak correlation. For patient 18, the CBCT dose was calculated using the anti-scatter grid method. Here too a strong correlation between the CBCT and EPID dose was seen. Patient number 5, as seen in the result section, showed a strong correlation in both the γ mean as well as the PTV plot. The shape of both the curves fit each other closely in the γ plot, with almost each point above/below the regression lines behaving the same.

Sensitivity to Deviations

For patients of all correlation strengths, the deviation in EPID γ was much more sensitive than the CBCT γ. The γ for each EPID point was significantly higher than the same CBCT point. This implies that for the same anatomical deviation, the change in the dose distribution calculated by the EPID is more than that of the CBCT. The deviation in the CBCT PTV dose was also seen to be very small over successive fractions. The reason for this is that the PTV in the CBCT has a smaller margin than the original PTV (4mm smaller), thus the dose coverage is more consistent within this region, however the EPID PTV margin is still the same, and sees more sensitive fluctuations, just like the EPID γ.

The reason for this sensitivity is attributed to use of calculated transmission. Since H&N treatments are VMAT arcs, there is no choice but to use calculated transmission [16]. However, in the paper from Rozendaal [4], where the DIR method was used to calculate the CBCT dose, the CBCT scan was also used in the EPID algorithm, to calculate the transmission. In this scenario, the calculated transmission would bring the reconstructed dose closer to the ground truth, since the contours used are from the anatomy of the day. He showed that deviations were more sensitive when using the pCT for calculated transmission, about a 0.3-0.5% change in dose per percent change in volume, and in fact the EPID was 5 times more sensitive to volume deviations than the TPS. Pecharroman-Gallego [17] showed that the difference in γ mean between calculated transmission and measured transmission was on average 0.2. We see the same order of difference in Table 4.1. In order to investigate this deviation further, the lung study was approached using the two different transmissions.

Reference Fraction Choice

For all patients, the first fraction was taken as reference. While this does not pose a problem

for the CBCT dose distributions, it may for the EPID reconstructed dose distributions. If an acquisition error or set-up error occurs in the first fraction, using it as a reference results in a bad γ mean curve, because the whole distribution is affected. The ΔPTV D50 curve is not affected however, since the difference in relative dose is plotted and thus it is only scaled and shifted by a constant.

Initially, patient 17 and 18 showed good ΔPTV D50 agreement between the EPID and CBCT but the γ mean agreement was very weak ($\rho = 0.1551$, p-value = 0.4218 and $\rho = -0.3517$, p-value = 0.0919 respectively). The initial γ mean curve is plotted in Figure 5.1. Upon closer investigation it was found that the EPID reconstruction for the first fraction for both treatments had a significant overdose. Upon changing the reference fraction to the second fraction, the γ mean curve improved dramatically, and this was shown in the plot in the result section (Figure 4.6) for patient 18, as well as in the result table (Table 4.2).

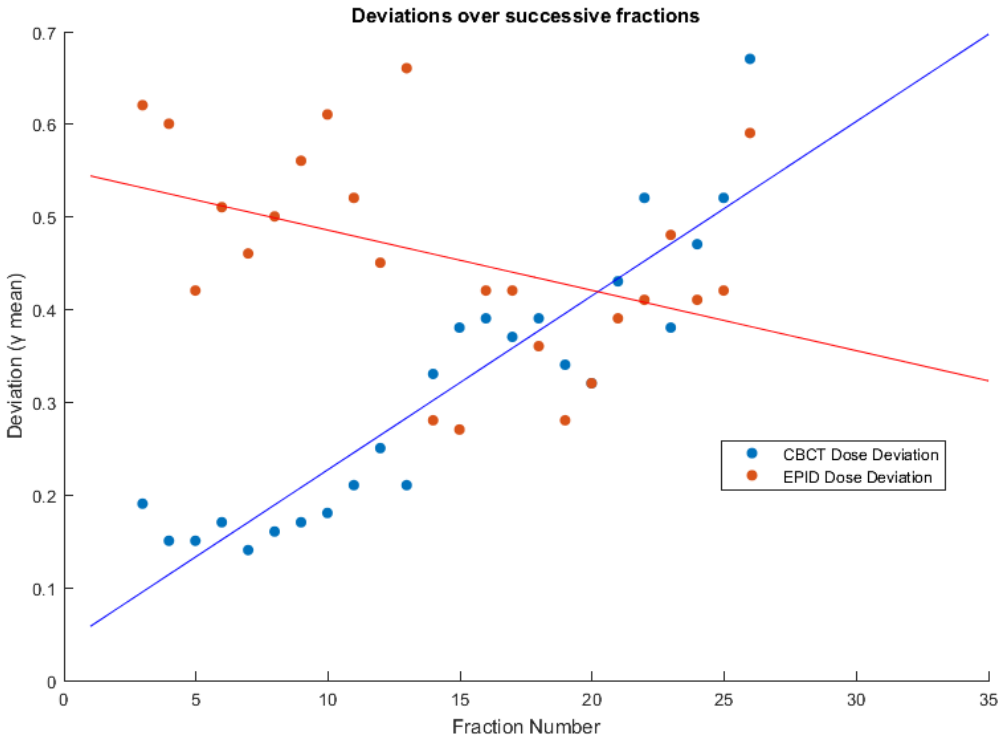

Figure 5.1: Patient 18: CBCT and EPID γ mean over successive fractions, using the *first* fraction as reference. The correlation is very poor. The figure in the result section uses the second fraction as reference.

Patient 12 also displays strong correlations between the EPID and CBCT ΔPTV D50, but weak correlations between the γ curves. A change in the reference to the second or third fraction did not help, as the results of these fractions showed the same behaviour as the first. Using a reference of a later fraction runs the risk of ignoring anatomical deviations that would have occurred in that time. The reference fraction should have no effect of anatomical changes in it, and since the amount of anatomical change increases during the course of treatment, the risk of it being a poor reference increases. From the curve shown in the result section for patient 12, the dose to the PTV appears to change dramatically from fraction to fraction, making the use of a 4th fraction as a reference a bad choice since deviations may have already occurred.

Ideally, the virtual fraction should be used as reference, however as mentioned before, this was not possible due to the fact that these were not recent patients.

5.3. Correlating the Dosimetric Effects of Anatomical Changes with the Traffic Light Protocol for Lung IMRT Treatments

The lung study served as an extension to the H&N study, to evaluate the traffic light protocol. But it also served to study the sensitivity to deviations arising from using the pCT to calculate transmission. Since open fields were recorded for the virtual reconstructions, they could also be as open images to acquire the real 'measured' transmission.

5.3.1. Measured vs Calculated Transmission

For all fractions and their corresponding reference fraction (virtual), the γ mean and the Δ%PTV D50 was evaluated and plotted. It was found that the γ mean was higher for every fraction using the calculated transmission reconstruction. On average the difference in γ mean of the calculated and measured fractions, was found to be 0.4 (4.3), which is higher than that reported by the Rozendaal [4] as well as that seen in Table 4.1. The Δ%PTV D50 was also higher in most fractions. This clearly shows that using calculated transmission overestimates the change in the dose distribution due to the anatomical changes that occur, but is much larger than the value reported in H&N. This is logical since the magnitude of changes in the lung site are much larger than that of H&N.

5.3.2. Traffic Light Protocol vs EPID Dose with Measured Transmission

Using measured transmission gives us a more accurately reconstructed EPID dose distribution. This should in theory, reduce the gap between sensitivity to deviations that we saw in the H&N study between the CBCT and EPID dose distribution. Assuming so, the γ mean of the measured transmission reconstructed fractions, colour coded for the traffic light protocol, was plotted, and the correlation was calculated. The colours of yellow and above were counted as 'alerts' since only 3 fractions per treatment were available and the total number of fractions were not enough to do a thorough enough correlation study, as was done in the H&N study. Besides, this would only strengthen any correlation that exists.

A weaker correlation coefficient of 0.18 was found between the traffic light protocol and the EPID γ mean than compared to the H&N study (Figure 4.11 and Table 4.4). Lung treatments are highly susceptible to intra-fractional motion as well, which may cause unforeseeable dose deviations. Also, given the large number of fractions that receive severe traffic colour codes, and the higher number of oranges than yellows, it is possible that RTT bias may play a role.

6

Conclusions and Recommendations

6.1. Traffic Light Protocol

It is clear from the H&N and the lung study that the scored colours of the traffic light protocol, are not a good indicator of deviations in dose distribution, as reconstructed by EPID dosimetry and calculated from CBCT scans. This can be attributed to the difference in criteria as discussed in the previous section. Despite the purely visual nature of the traffic light protocol, it is still a useful clinical tool to ensure that treatments and fractions are monitored regularly and plays an important role for replanning in adaptive radiotherapy [8, 9].

It is also clear from the study that the traffic light protocol for lung has a weaker correlation to the dose deviation than that of H&N. In addition, the larger number of orange fractions than yellow may point to the need for a review of the criteria that classifies severity of the traffic light colours in lung.

6.2. EPID Dosimetry

The results of this work imply that the EPID dosimetry algorithm at the NKI is able to reconstruct dose distributions in 3D for H&N VMAT treatments with good agreement compared to the 'ground truth',i.e. the dose calculated on the CBCT scan by the TPS. However, the results are still noisy in comparison with those of the CBCT methods, showing a wider spread of deviation values (Table 4.1), and larger magnitudes of deviation than that seen by the CBCT dose. This is due to the fact that calculated transmission is used for VMAT treatments, and using measured transmission is impossible. A few modifications however, can still be made to the current algorithm to improve its dose calculation capability.

Making use of the CBCT instead of the pCT for calculating transmission is invaluable, since it will reduce the overestimation of geometrical errors, and also since measuring open fields is a time consuming process. The DIR method is fairly successful, but using the anti-scatter grid and iterative scatter correction CBCT approach is more promising, since the registration process is site-specific and may induce artefacts. If successful, this method can be used on all linacs, and clinical reconstructions of the CBCT can be used directly by the EPID software for dose reconstruction.

Cumulative deviation tracking of treatments, as was done in this study, could also be useful in determining if a treatment needs to be replanned. Since CBCT based dose calculations are not routine clinical workflow, but EPID dosimetry is, and there is a strong correlation between them, EPID dosismetry could be used to evaluate the deviation over successive fractions. This could be automated, and additional labour wouldn't be required since EPID data for all fractions of H&N patients are recorded.

Lastly, EPID alert criteria should be modified depending on whether measured or calculated transmission is used. In the lung study, the values of gamma mean were calculated using the virtual reconstruction as reference. However, the EPID automated system calculates gamma using the TPS as references, thus bigger deviations are expected, and these deviations will be amplified by the calculated transmission model.

A

Nomenclature and Abbreviations

Abbreviation/Term	**Definition/Expansion**
CBCT	Cone Beam Computed Tomography
CBCT Dose	Dose calculated by the TPS on a calibrated CBCT scan
CT	Computed Tomography
CTV	Clinical Target Volume
D50	Median Dose
DVH	Dose Volume Histogram
EPID	Electronic Portal Imaging Device
EPID Alerts	Alerts raised by the automated EPID analysing software, based on γ and DVH criteria
EPID Dose	Dose reconstructed using EPID data for a given fraction
GTV	Gross Tumour Volume
Ground Truth	The assumed real value of what we wish to measure. The CBCT dose is assumed to be the ground truth
HU	Hounsfield Unit
H&N	Head and Neck
IMRT	Intensity Modulated Radiotherapy
Linac	Linear Accelerator
MLC	Multileaf Collimator
OAR	Organs at Risk
Open Arc/Field	A treatment arc or field recorded without a patient or attenuating material in the path of the beam
pCT	Planning CT
PET	Positron Emission Tomography
PTV	Planning Target Volume
QA	Quality Assurance
RO	Radiation Oncologist
RTT	Radiation Therapy Technician
TPS	Treatment Planning System
TPS Dose	The dose calculated by the TPS software on the planning CT
Traffic Light Colours	Colours assigned to fractions based on a visual analysis of the anatomical changes seen in a CBCT scan
Transmission	An input parameter to the EPID reconstruction algorithm, which accounts for attenuation through the patient
Virtual Dose	The dose reconstructed by the EPID after using the pCT to predict the portal image from an open arc/field

VMAT	Volumetric Modulated Arc Therapy
ΔPTV D50	Relative change in the median dose to the PTV
γ Mean	The mean of γ evaluated for all points in the reference dose distribution w.r.t. the evaluated dose distribution

B

Additional Tables and Graphs

It was found that in some H&N treatments (Patient 4,11,13,14 and 16 which are plotted below), the slope of the CBCT γ mean curve was near zero (Table B.1). The slope of the EPID γ mean curve was much larger for these treatments. Since we assume the CBCT dose to be the ground truth, we attribute the deviation measured by the EPID to be noise. These treatments with near 0 CBCT slope, also had very few non-green traffic light colours. In fact if we only consider treatments that have more than 5 non-green traffic light colours, the correlation between the slopes of the curves increases.

Table B.1: Slope of the γ mean regression lines from the plots of each H&N treatment. Correlation coefficient between the EPID and CBCT slopes is ρ = 0.7 and p-value = 0.0013. If we disregard treatments with less than 5 non-green fractions, ρ = 0.81 and p-value = 0.0046.

Patient Number	EPID γ-mean Slope $\times 10^{-2}$	CBCT γ-mean slope $\times 10^{-2}$	#Non-Green Fractions
1	0.8	1.25	15
2	0.71	0.006	9
3	0.19	0.008	14
4	0.18	0.38	2
5	1.08	2.5	16
6	1.05	1.2	16
7	0.73	0.83	0
8	0.3	0.99	11
9	0.44	1.46	16
10	2.1	3.01	11
11	0.13	0.75	0
12	0.006	0.001	0
13	0.008	0.62	1
14	0.001	0.36	1
15	0.44	0.6	6
16	0.26	2.65	4
17	0.34	0.47	17
18	1.89	2.18	5

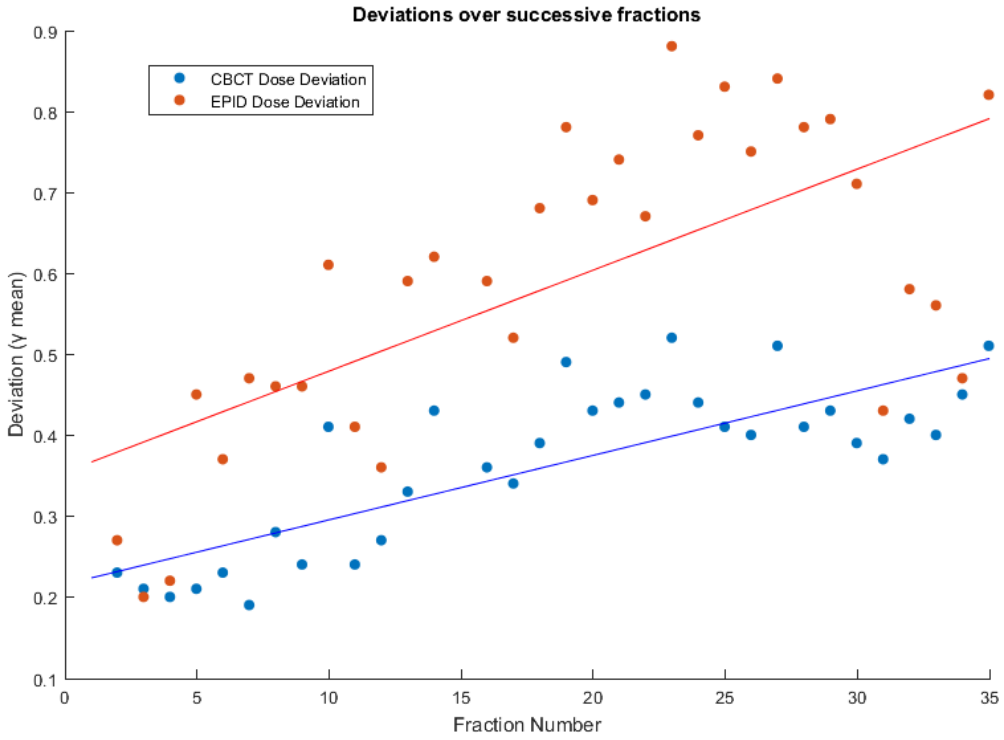

(a) Patient 1: CBCT and EPID γ mean over successive fractions.

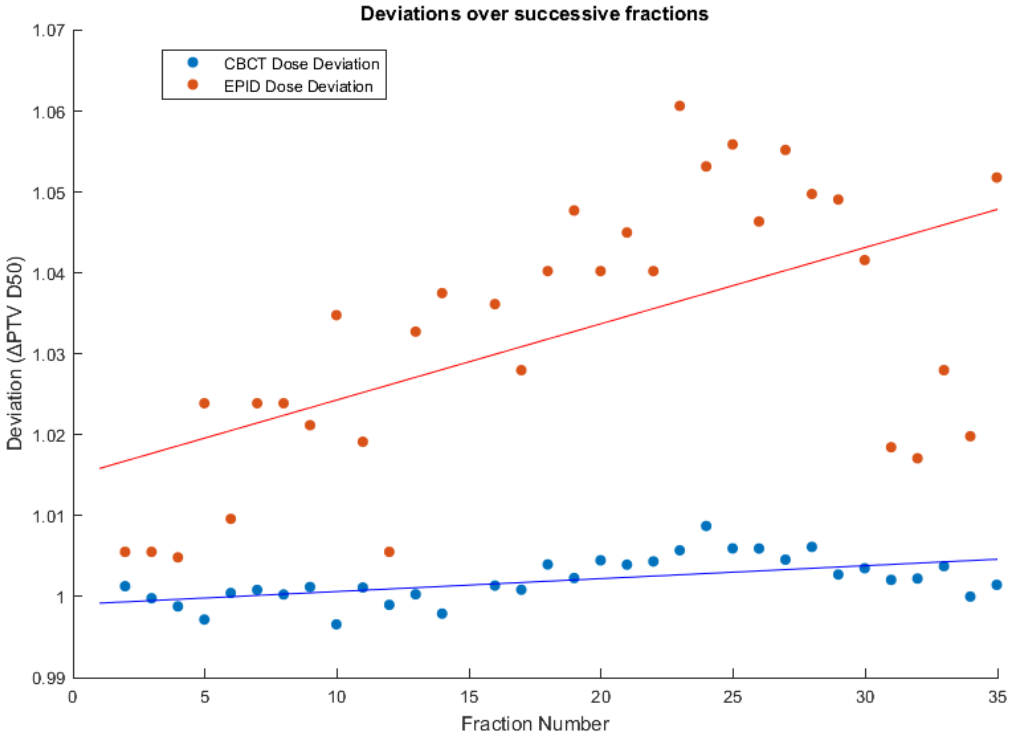

(b) Patient 1: CBCT and EPID ΔPTV D50 over successive fractions.

Figure B.1: Patient 1

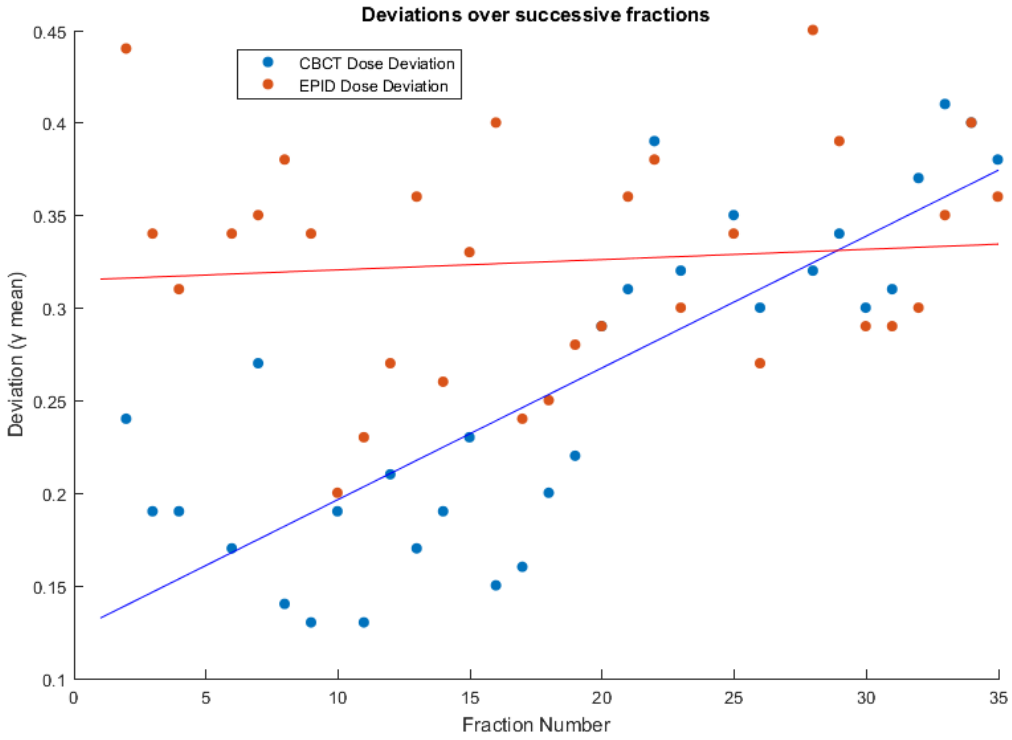

(a) Patient 2: CBCT and EPID γ mean over successive fractions.

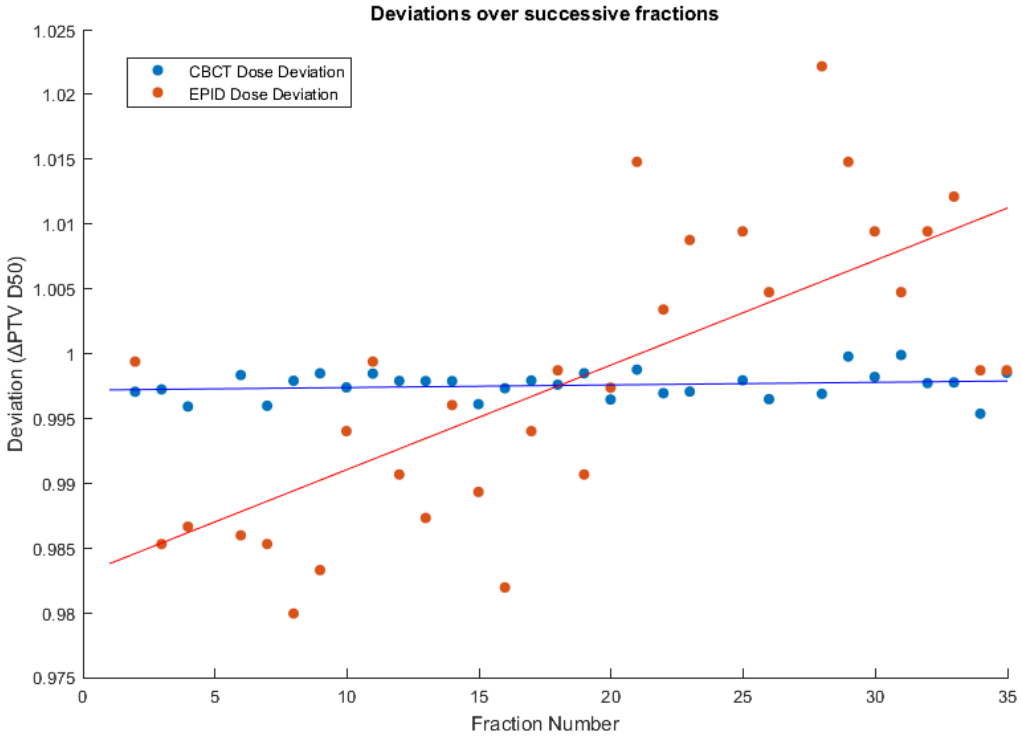

(b) Patient 2: CBCT and EPID ΔPTV D50 over successive fractions.

Figure B.2: Patient 2

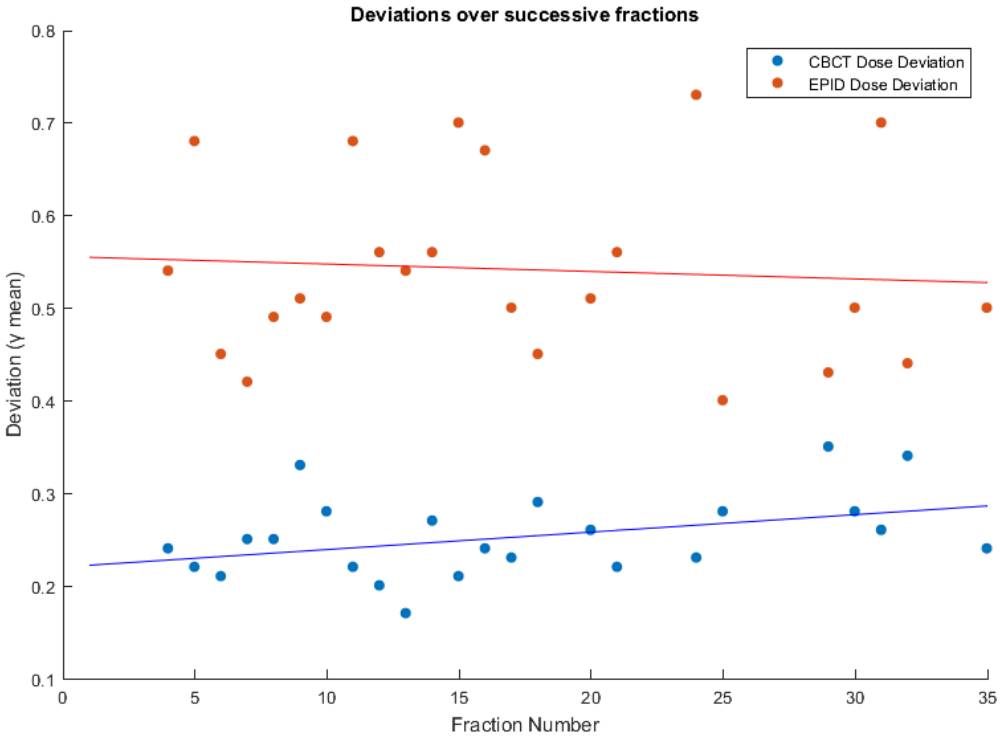

(a) Patient 3: CBCT and EPID γ mean over successive fractions.

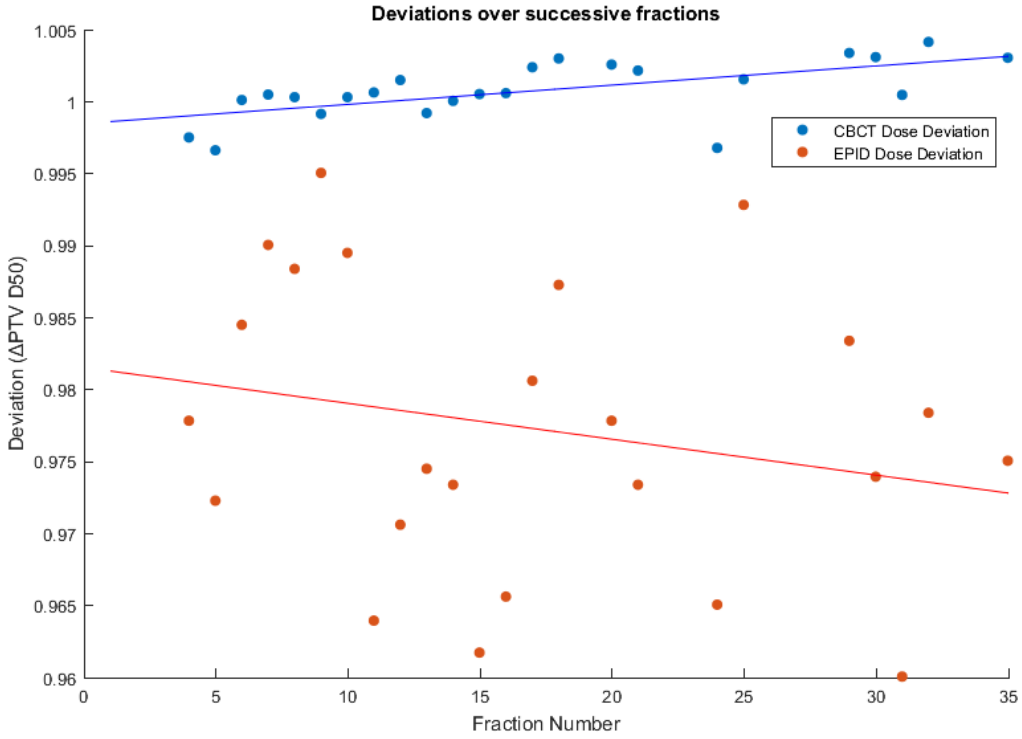

(b) Patient 3: CBCT and EPID ΔPTV D50 over successive fractions.

Figure B.3: Patient 3

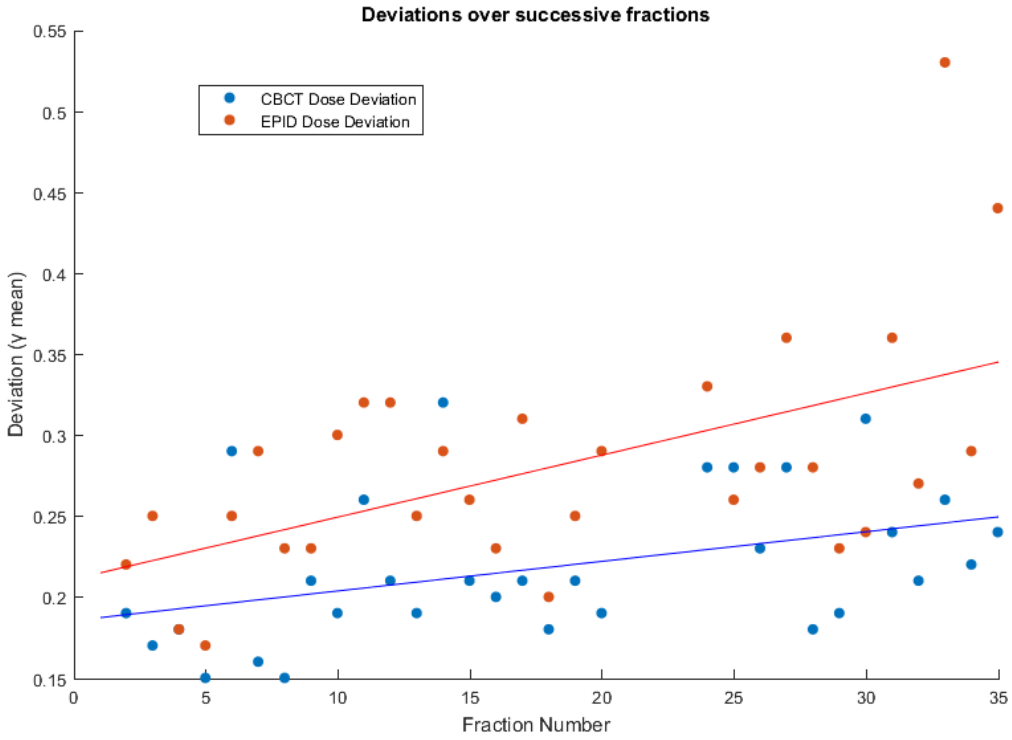

(a) Patient 4: CBCT and EPID γ mean over successive fractions.

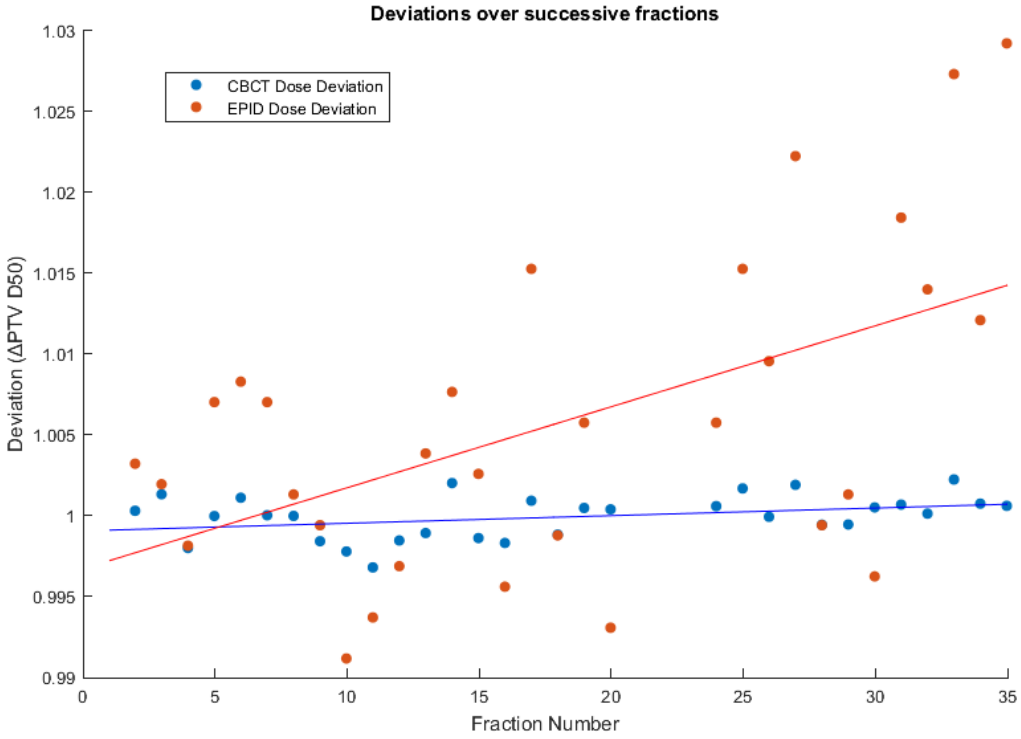

(b) Patient 4: CBCT and EPID ΔPTV D50 over successive fractions.

Figure B.4: Patient 4

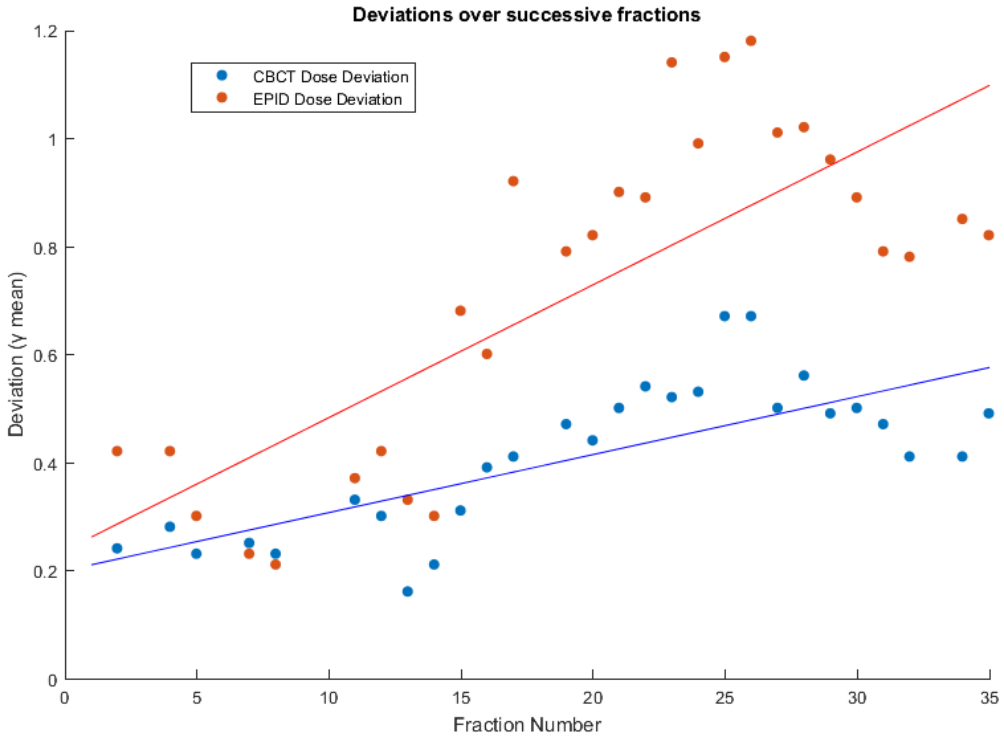

(a) Patient 5: CBCT and EPID γ mean over successive fractions.

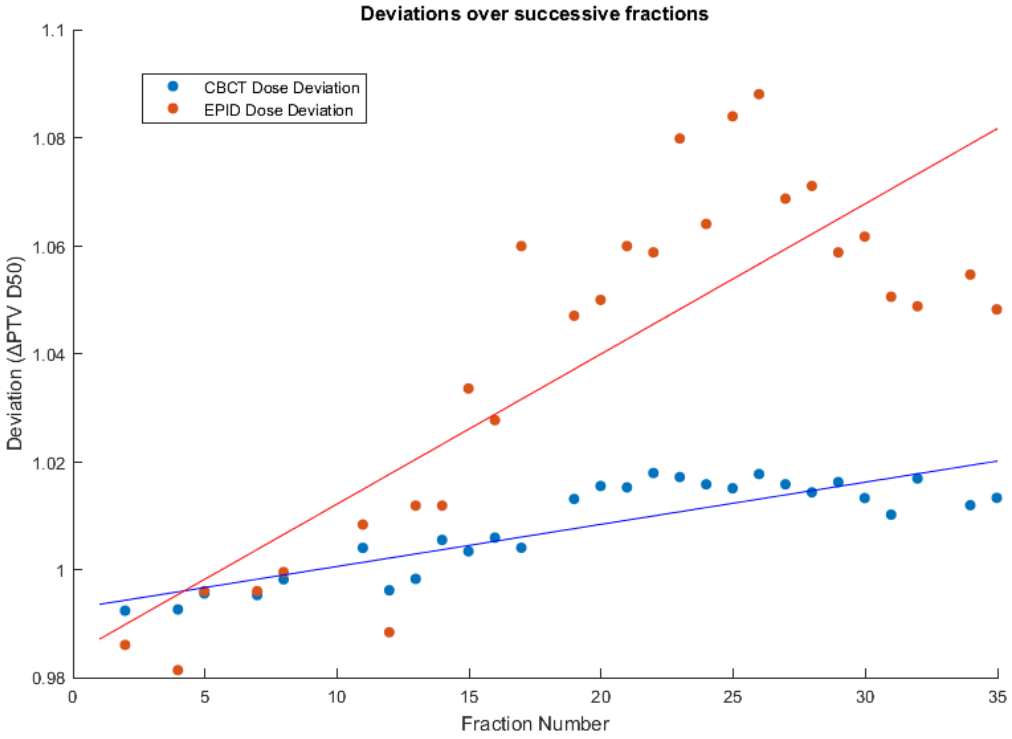

(b) Patient 5: CBCT and EPID ΔPTV D50 over successive fractions.

Figure B.5: Patient 5

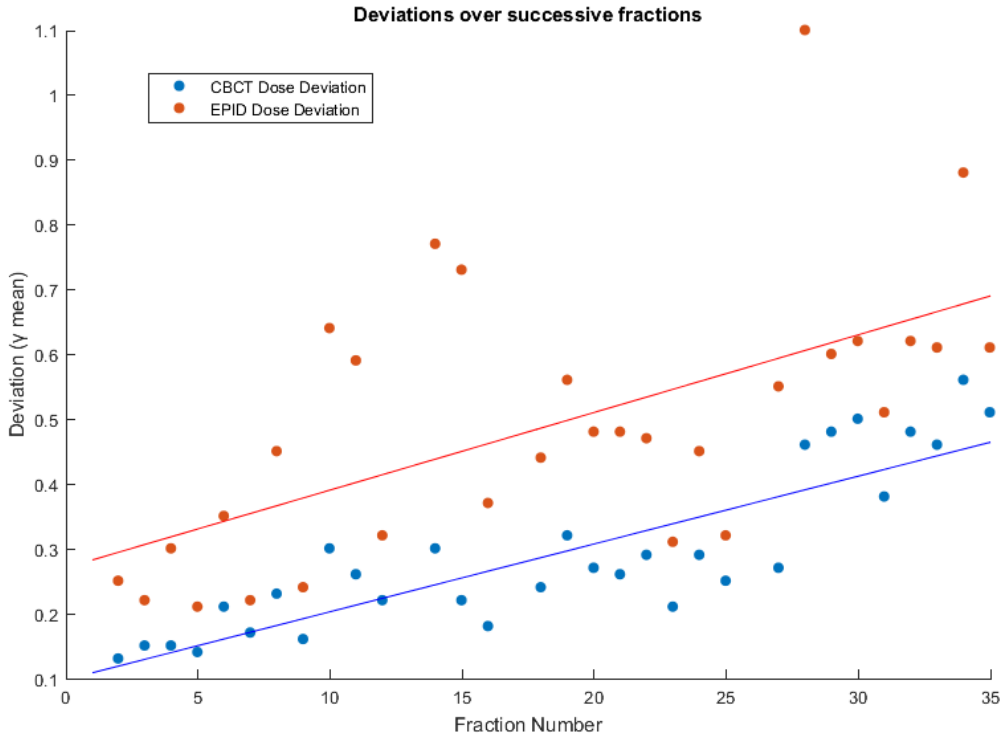

(a) Patient 6: CBCT and EPID γ mean over successive fractions.

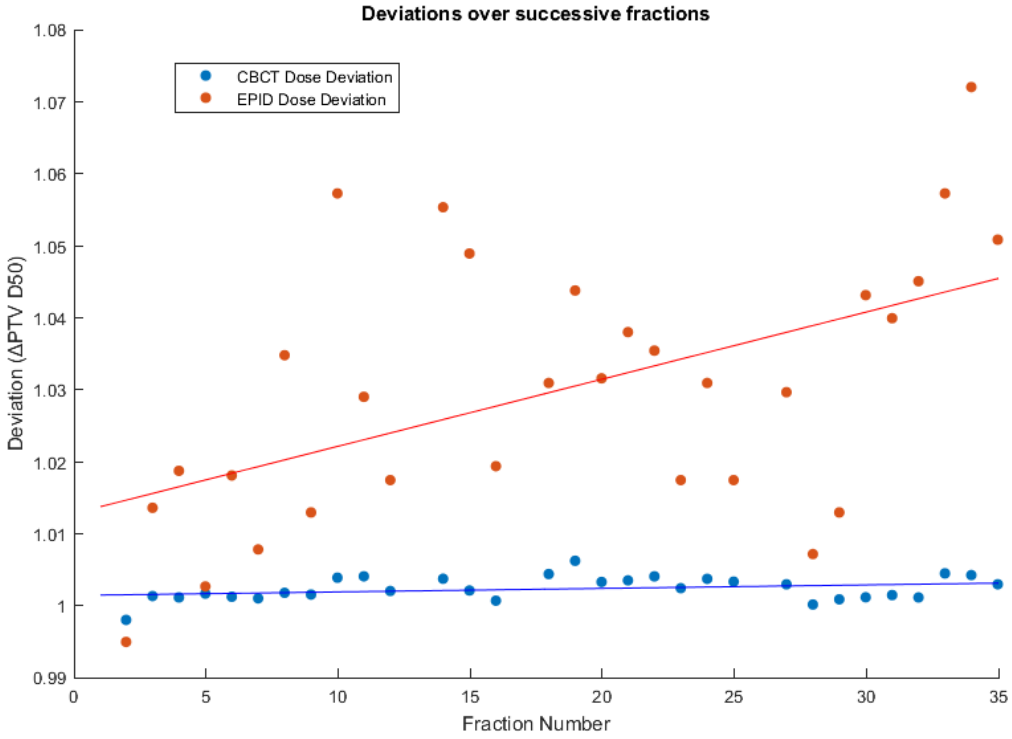

(b) Patient 6: CBCT and EPID ΔPTV D50 over successive fractions.

Figure B.6: Patient 6

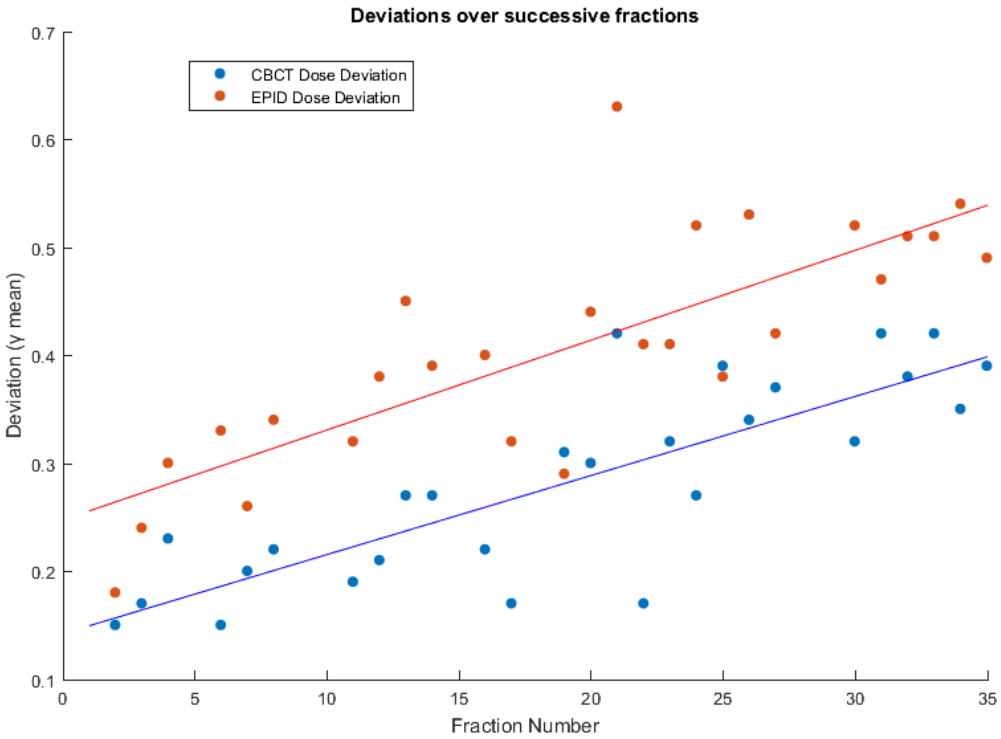

(a) Patient 7: CBCT and EPID γ mean over successive fractions.

Figure B.7: Patient 7

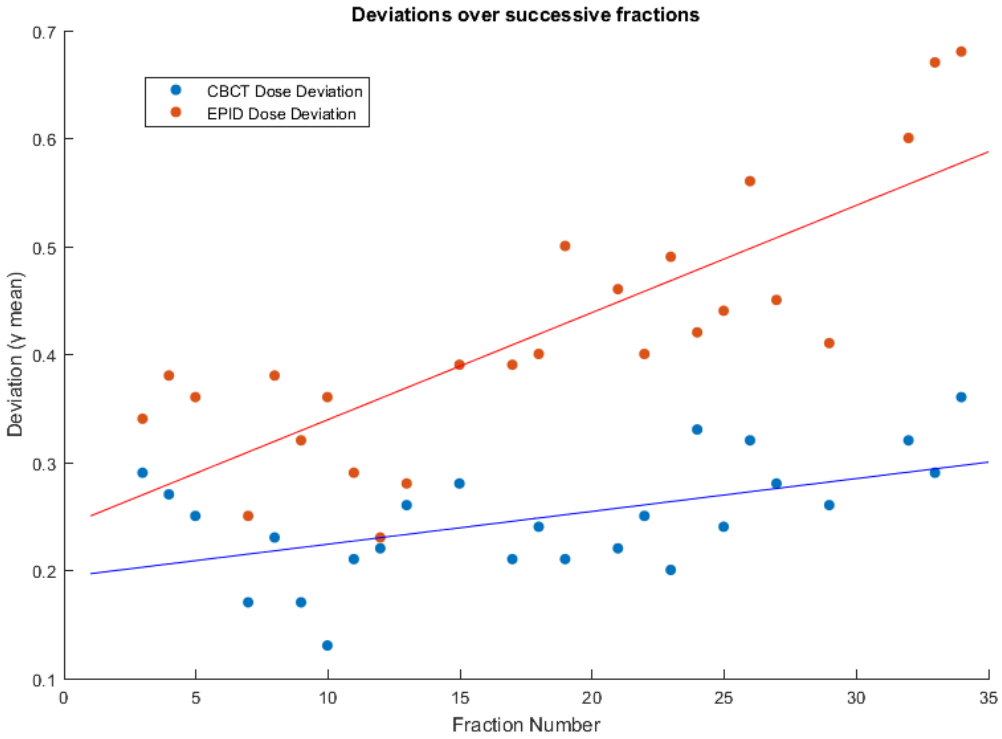

(a) Patient 8: CBCT and EPID γ mean over successive fractions.

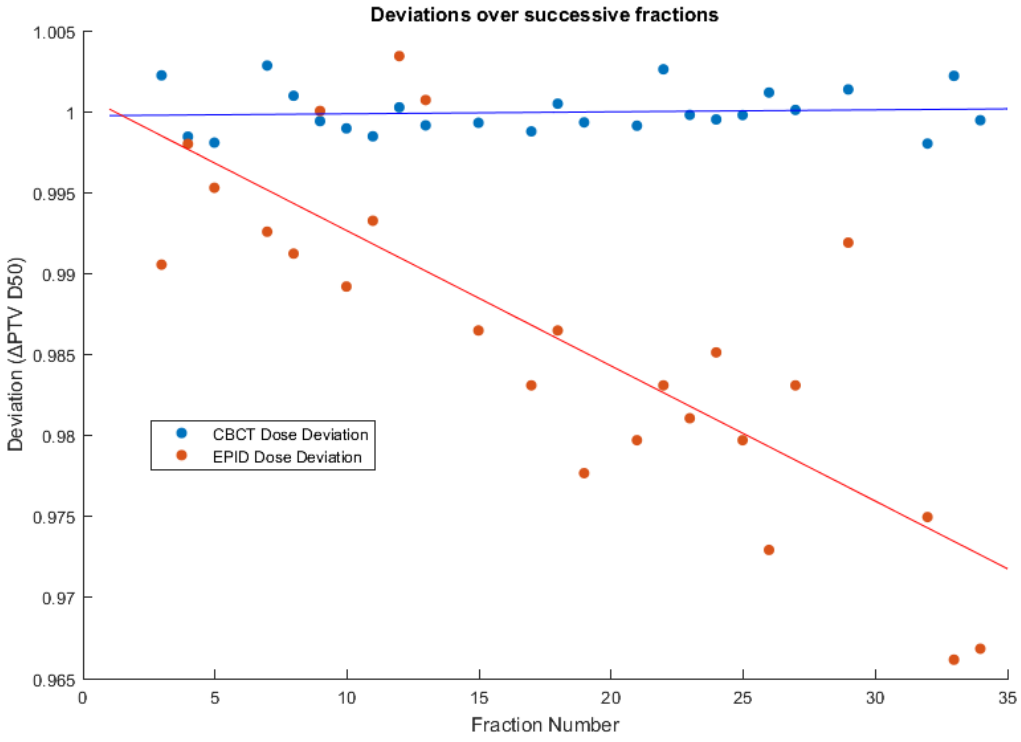

(b) Patient 8: CBCT and EPID ΔPTV D50 over successive fractions.

Figure B.8: Patient 8

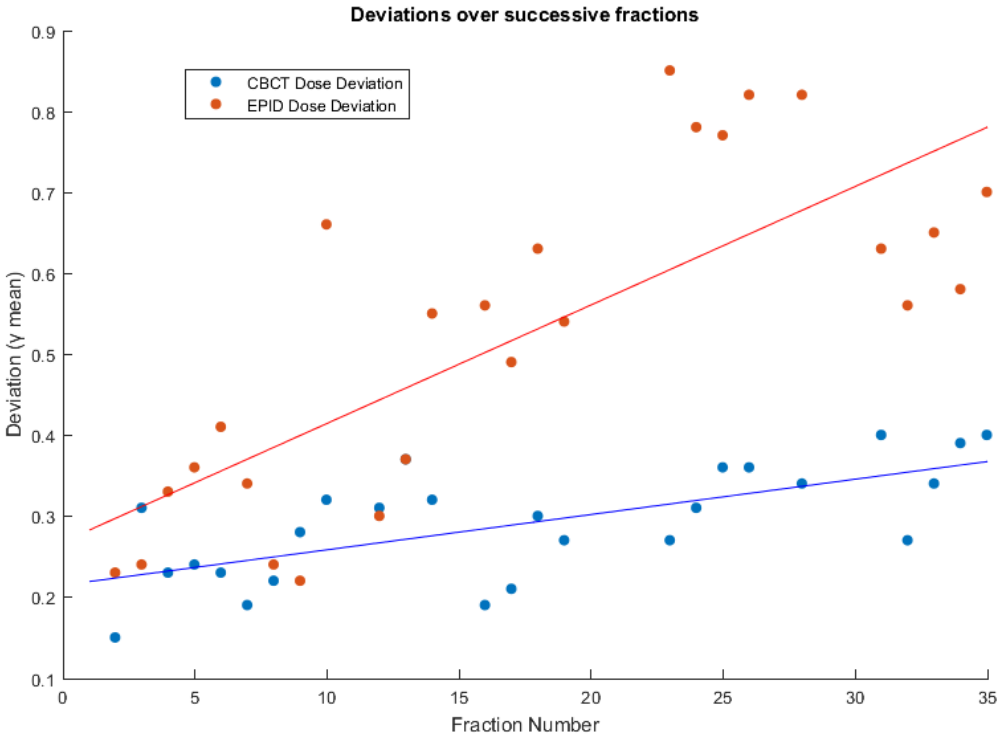

(a) Patient 9: CBCT and EPID γ mean over successive fractions.

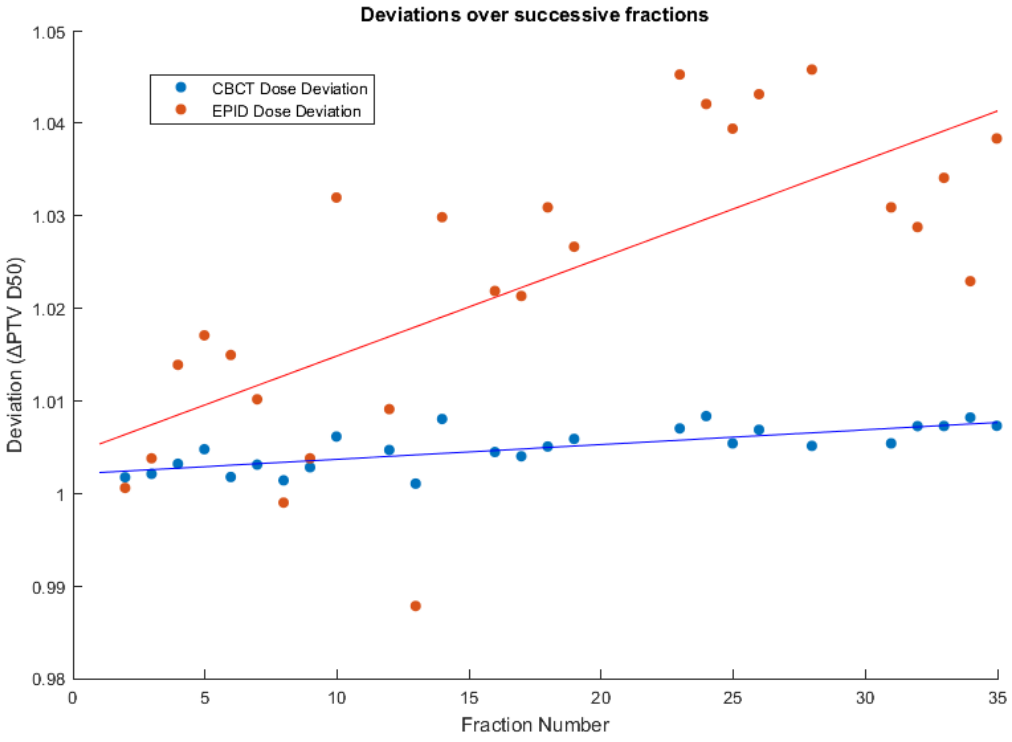

(b) Patient 9: CBCT and EPID ΔPTV D50 over successive fractions.

Figure B.9: Patient 9

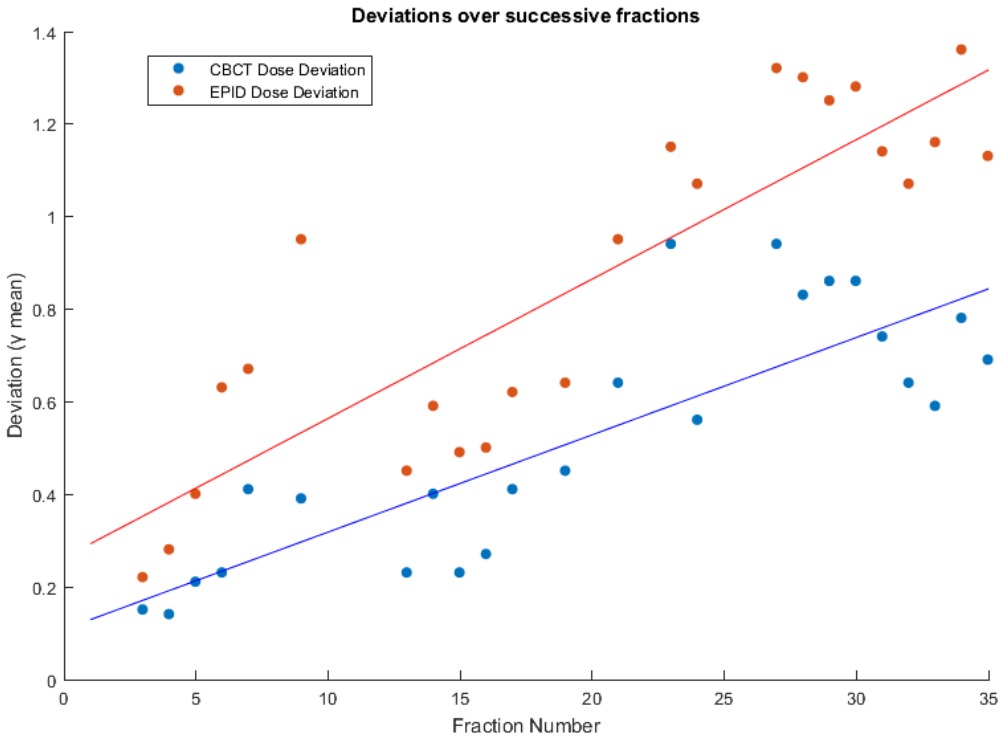

(a) Patient 10: CBCT and EPID γ mean over successive fractions.

Figure B.10: Patient 10

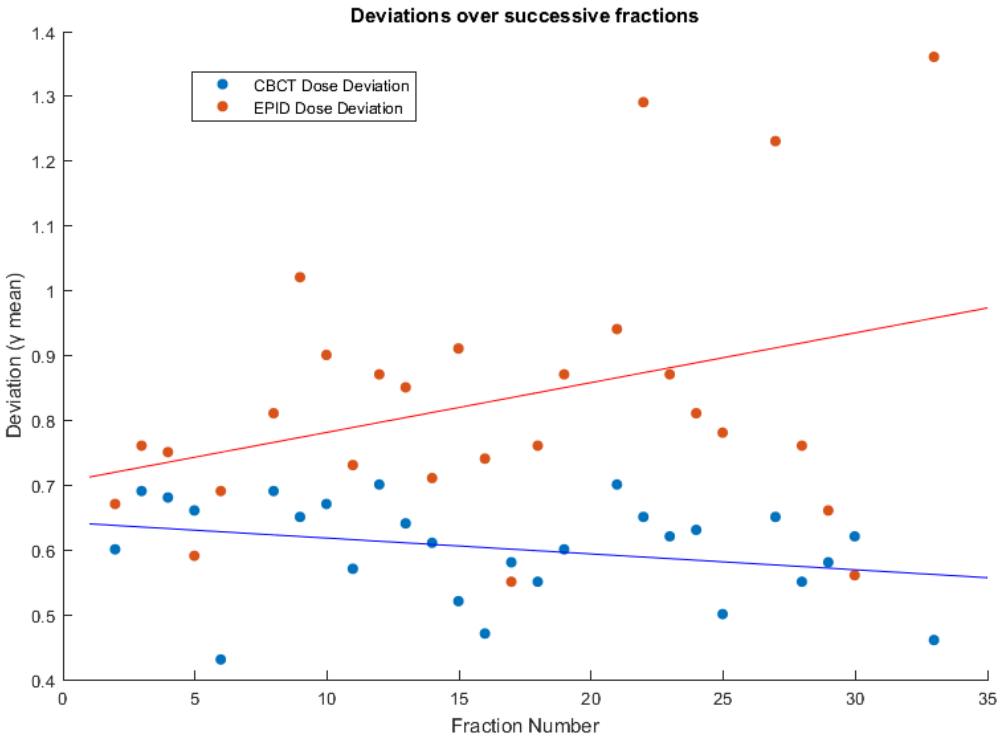

(a) Patient 11: CBCT and EPID γ mean over successive fractions.

Figure B.11: Patient 11

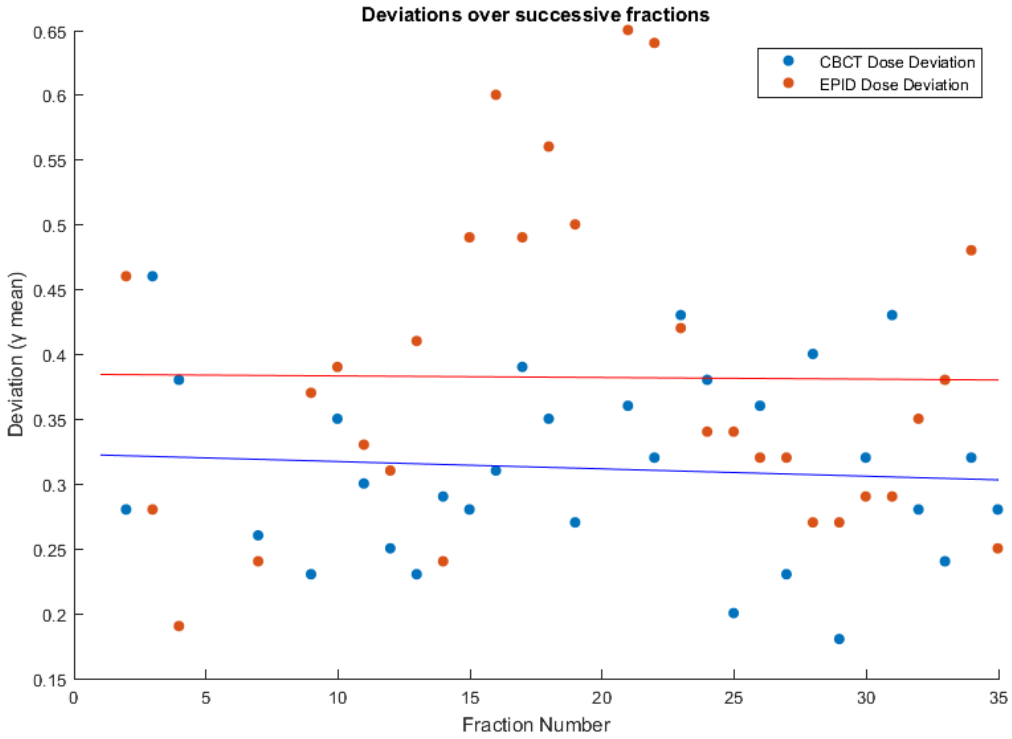

(a) Patient 12: CBCT and EPID γ mean over successive fractions.

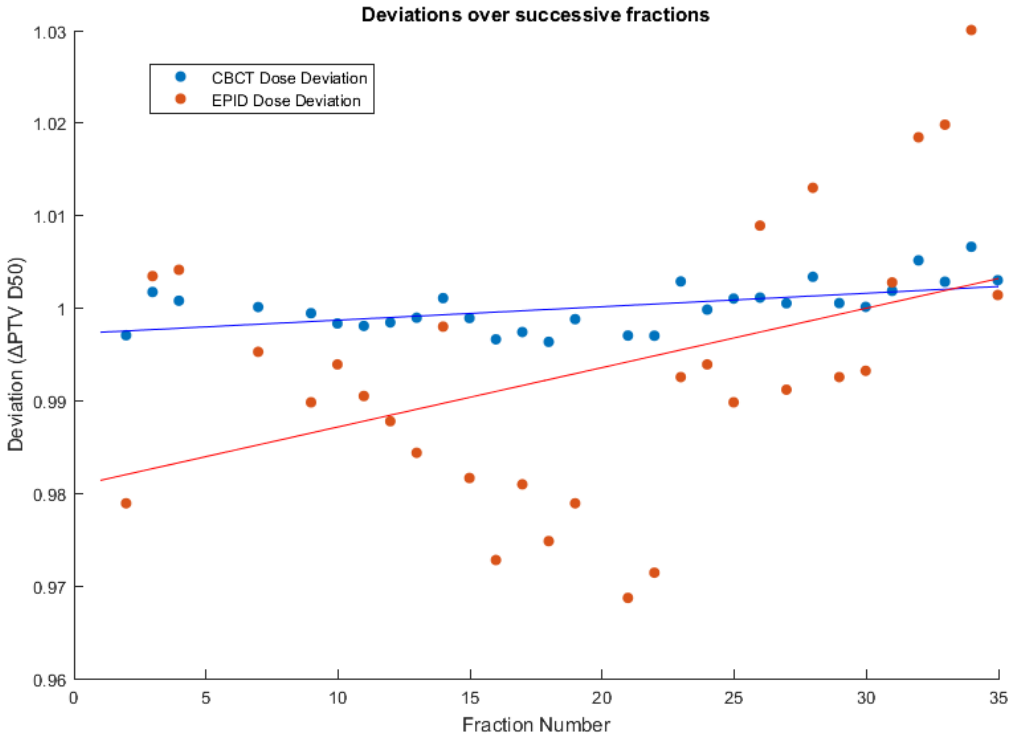

(b) Patient 12: CBCT and EPID ΔPTV D50 over successive fractions.

Figure B.12: Patient 12

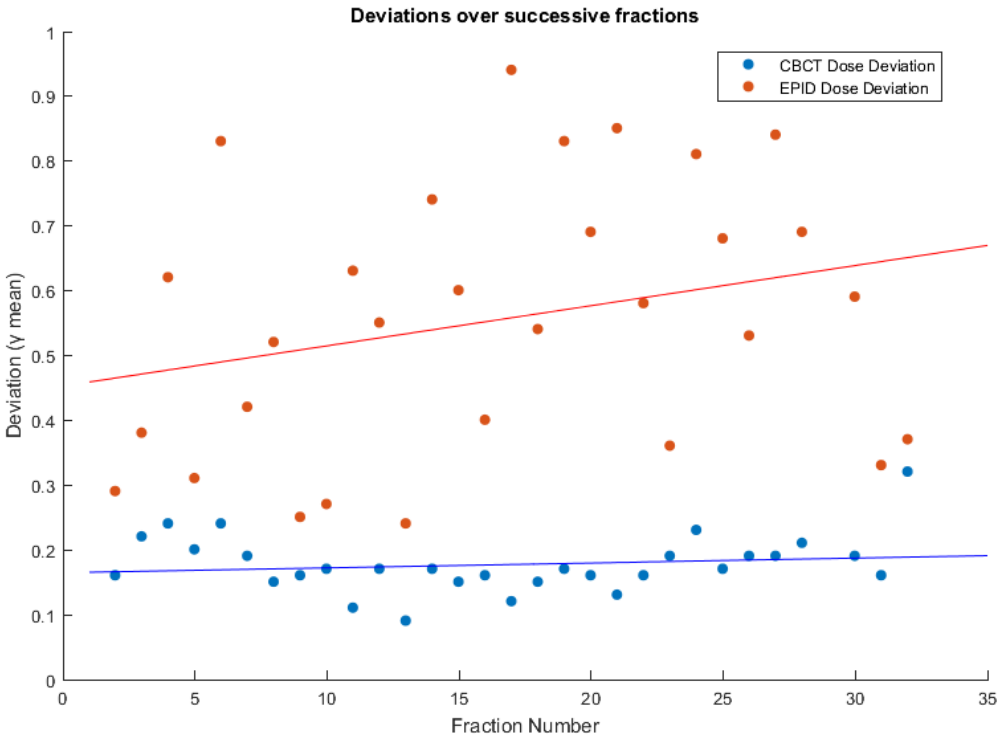

(a) Patient 13: CBCT and EPID γ mean over successive fractions.

Figure B.13: Patient 13

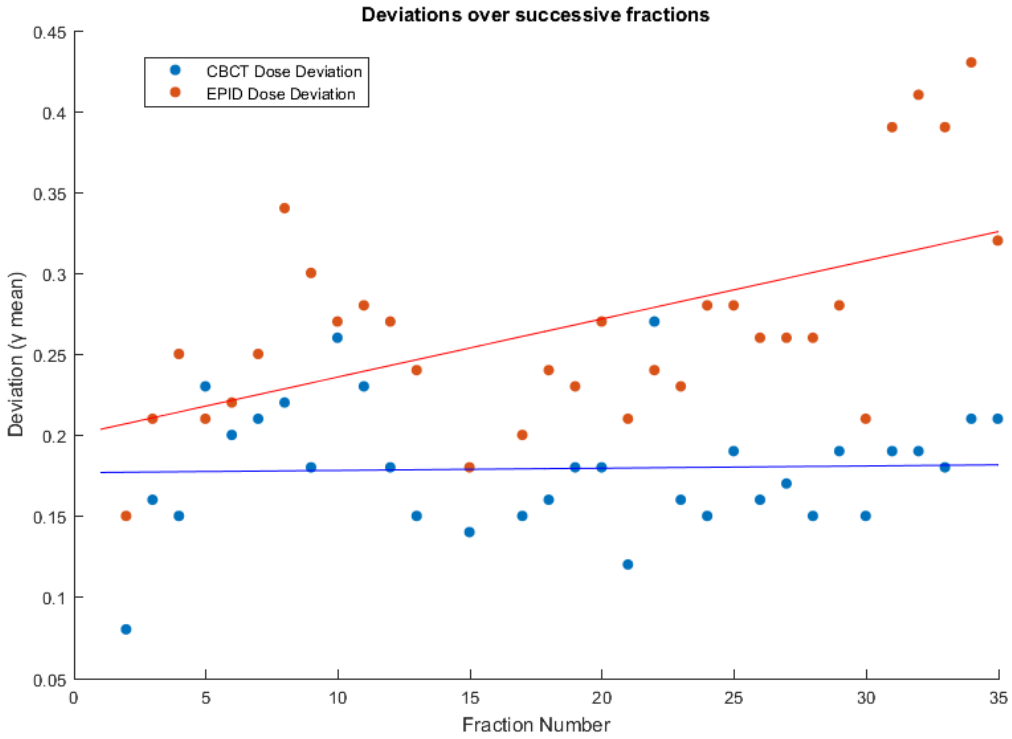

(a) Patient 14: CBCT and EPID γ mean over successive fractions.

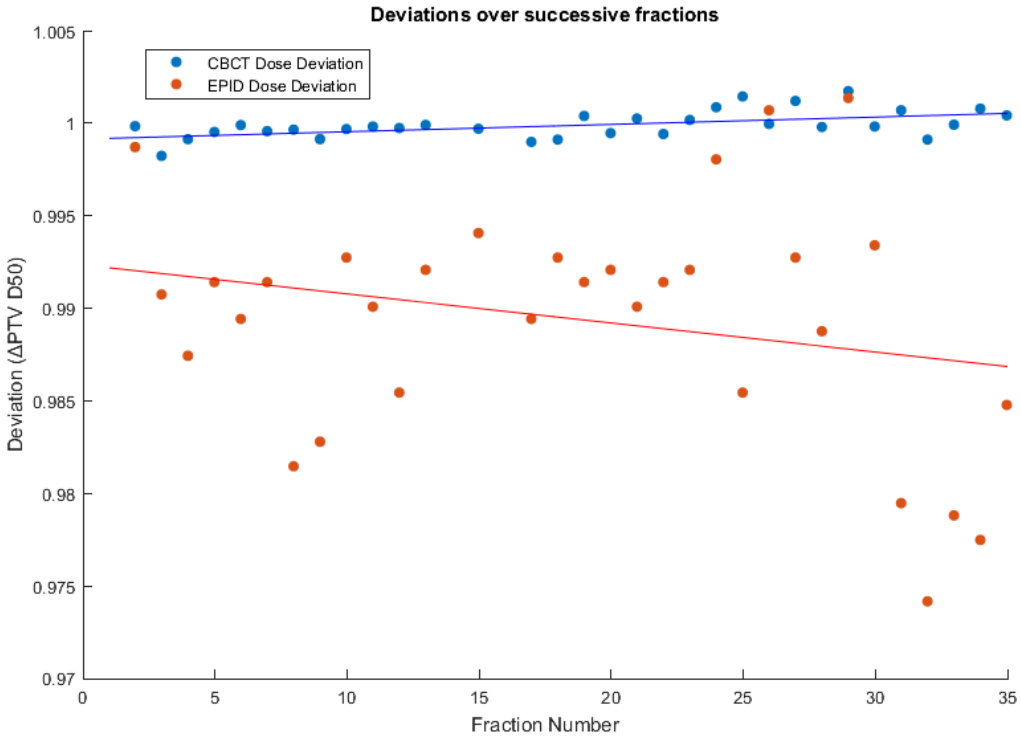

(b) Patient 14: CBCT and EPID ΔPTV D50 over successive fractions.

Figure B.14: Patient 14

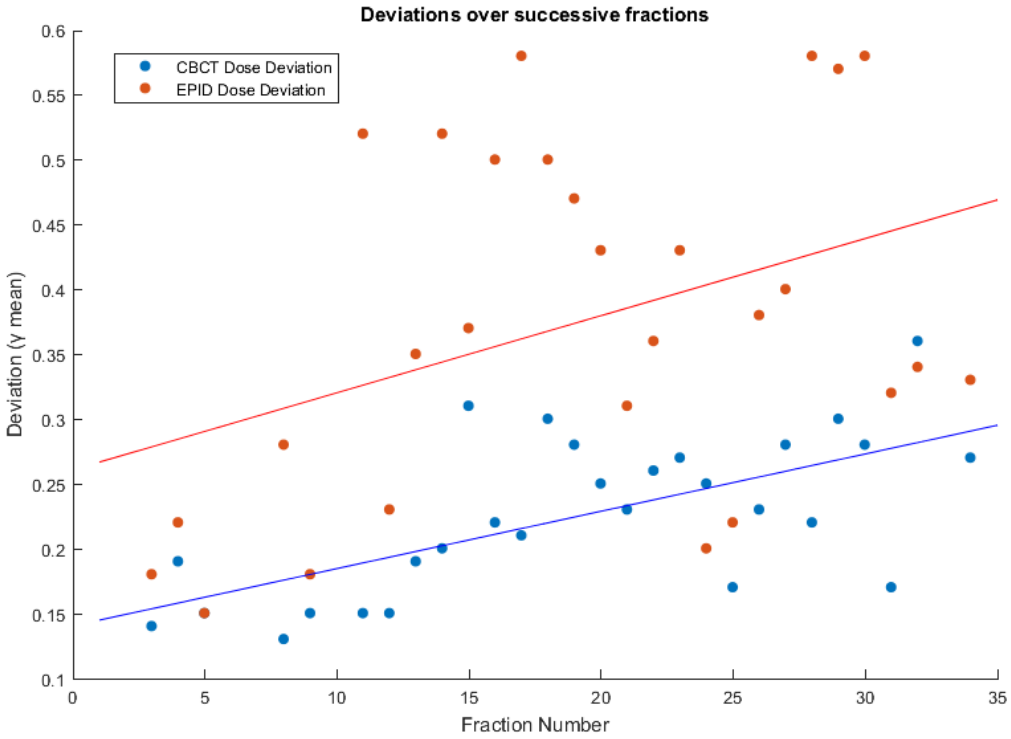

(a) Patient 15: CBCT and EPID γ mean over successive fractions.

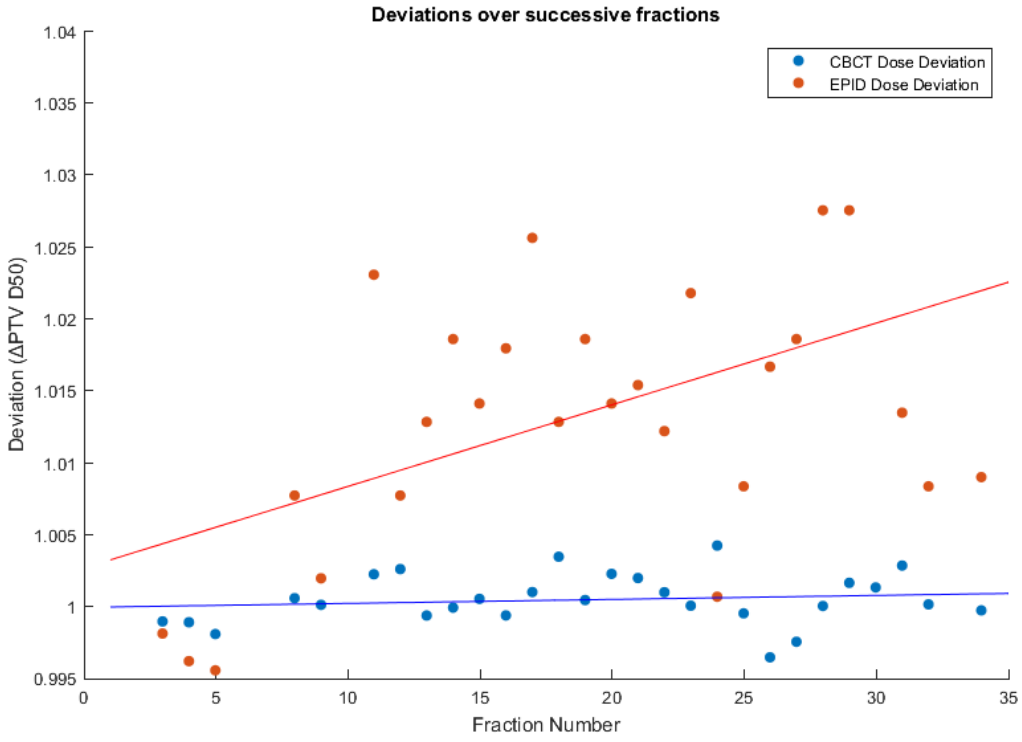

(b) Patient 15: CBCT and EPID ΔPTV D50 over successive fractions.

Figure B.15: Patient 15

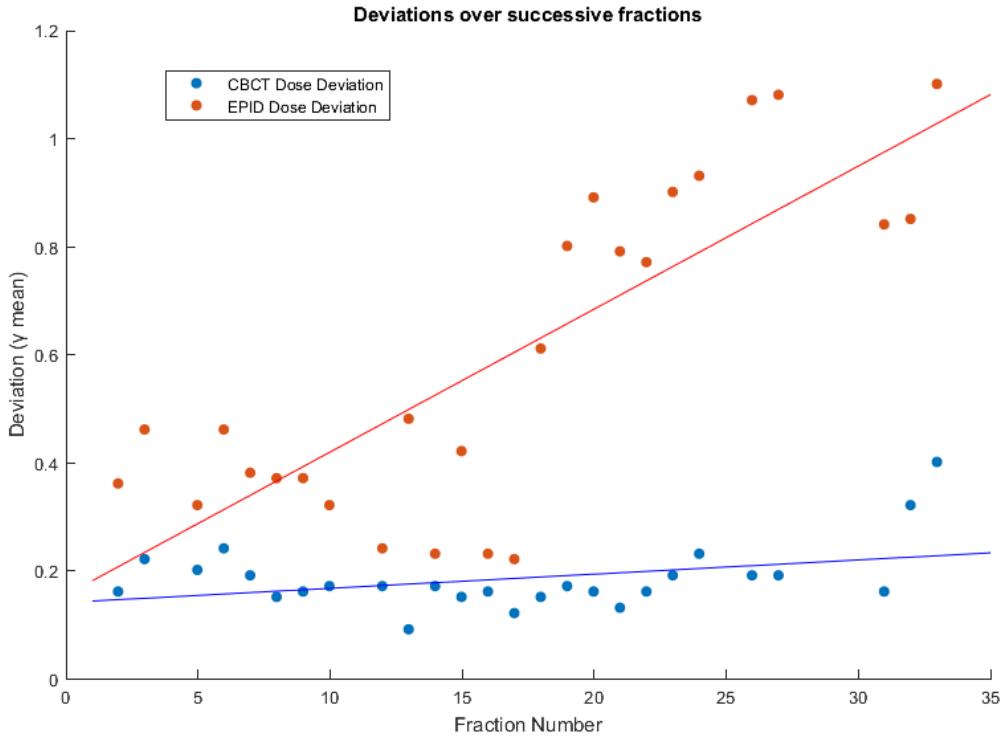

(a) Patient 16: CBCT and EPID γ mean over successive fractions.

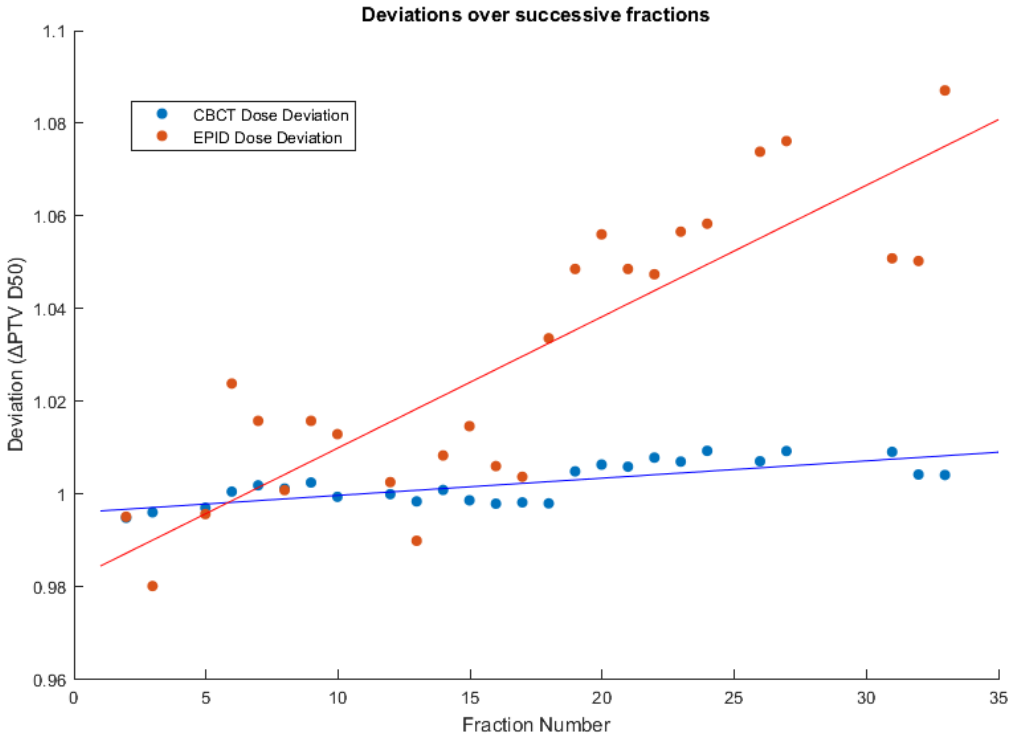

(b) Patient 16: CBCT and EPID ΔPTV D50 over successive fractions.

Figure B.16: Patient 16

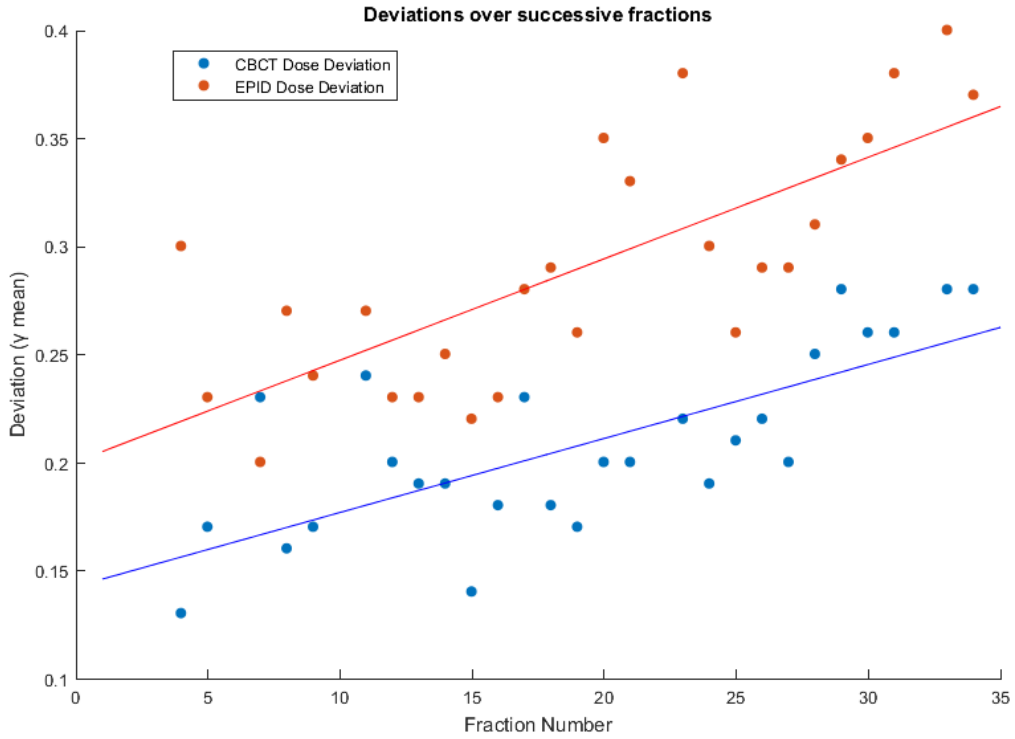

(a) Patient 17: CBCT and EPID γ mean over successive fractions.

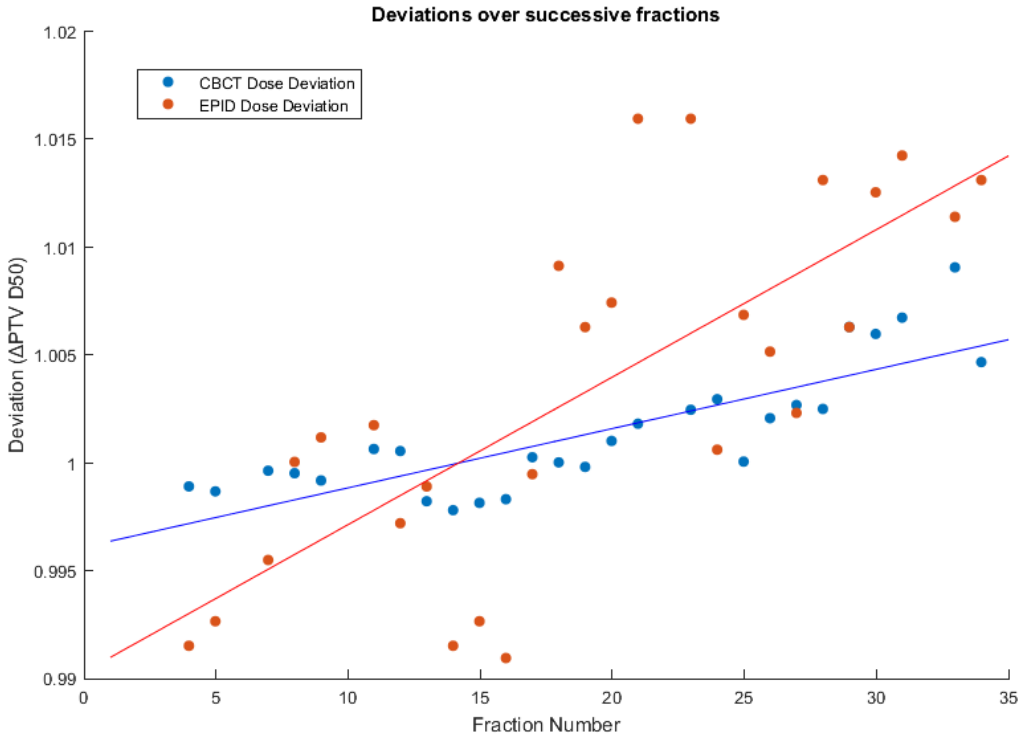

(b) Patient 17: CBCT and EPID ΔPTV D50 over successive fractions.

Figure B.17: Patient 17

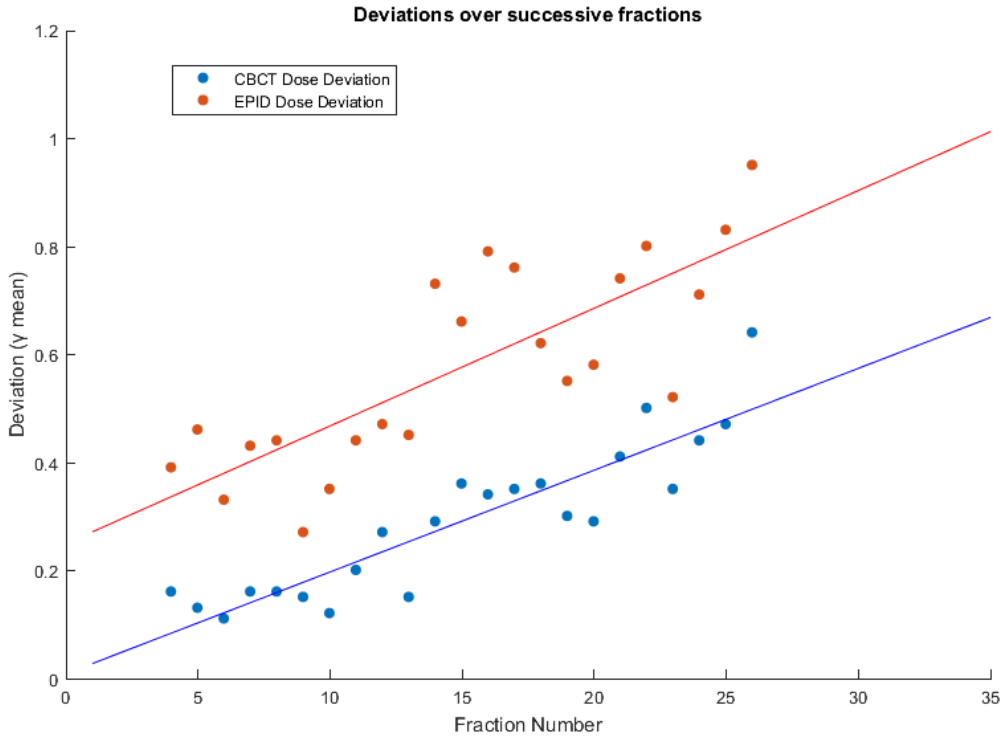

(a) Patient 18: CBCT and EPID γ mean over successive fractions.

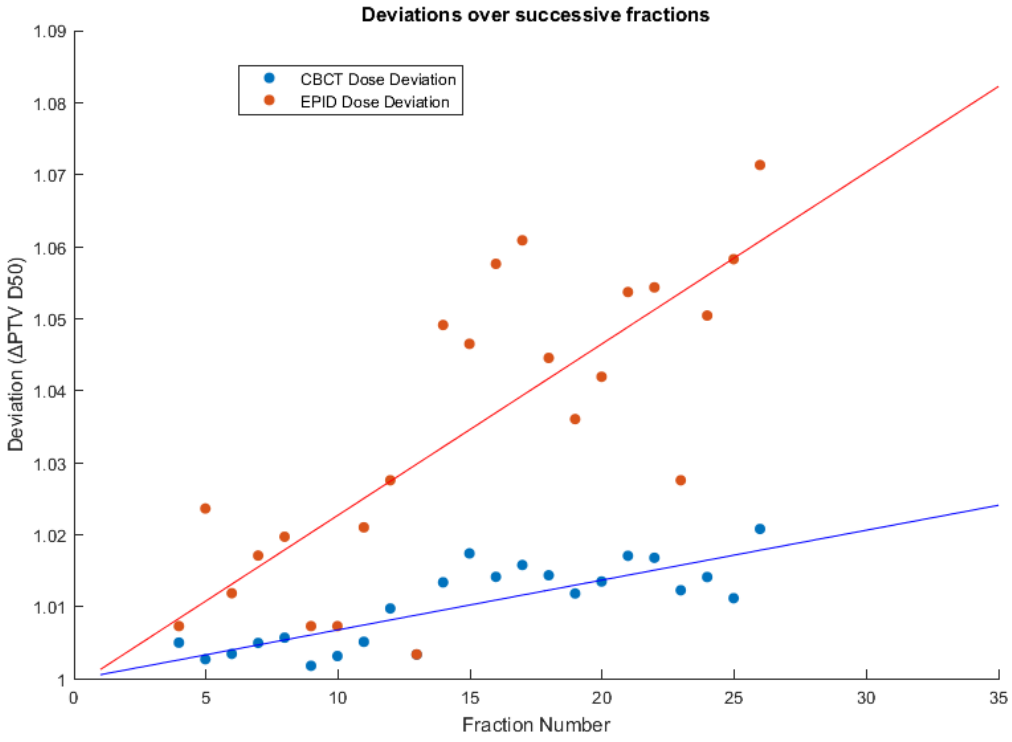

(b) Patient 18: CBCT and EPID ΔPTV D50 over successive fractions.

Figure B.18: Patient 18

Bibliography

[1] Ben J. Mijnheer, Patrick González, Igor Olaciregui-Ruiz, Roel A. Rozendaal, Marcel van Herk, and Anton Mans. Overview of 3-year experience with large-scale electronic portal imaging device–based 3-dimensional transit dosimetry. *Practical Radiation Oncology*, 5(6):e679–e687, nov 2015. ISSN 18798500. doi: 10.1016/j.prro.2015.07.001. URL http://linkinghub.elsevier.com/retrieve/pii/S1879850015002313.

[2] D. Sardari, R. Maleki, H. Samavat, and A. Esmaeeli. Measurement of depth-dose of linear accelerator and simulation by use of Geant4 computer code. *Reports of Practical Oncology and Radiotherapy*, 15(3):64–68, may 2010. ISSN 15071367. doi: 10.1016/j.rpor.2010.03.001. URL http://www.sciencedirect.com/science/article/pii/S1507136710000349.

[3] Rebecca Height, Vincent Khoo, Catherine Lawford, Jennifer Cox, Daryl Lim Joon, Aldo Rolfo, and Morikatsu Wada. The dosimetric consequences of anatomic changes in head and neck radiotherapy patients. *Journal of Medical Imaging and Radiation Oncology*, 54 (5):497–504, 2010. ISSN 17549477. doi: 10.1111/j.1754-9485.2010.02209.x.

[4] Roel A. Rozendaal, Ben J. Mijnheer, Olga Hamming-Vrieze, Anton Mans, and Marcel Van Herk. Impact of daily anatomical changes on EPID-based in vivo dosimetry of VMAT treatments of head-and-neck cancer. *Radiotherapy and Oncology*, 116(1):70–74, 2015. ISSN 18790887. doi: 10.1016/j.radonc.2015.05.020. URL http://dx.doi.org/10.1016/j.radonc.2015.05.020.

[5] Mariska de Smet, Danny Schuring, Sebastiaan Nijsten, and Frank Verhaegen. Accuracy of dose calculations on kV cone beam CT images of lung cancer patients. *Medical Physics*, 43(11):5934–5941, 2016. ISSN 00942405. doi: 10.1118/1.4964455. URL http://doi.wiley.com/10.1118/1.4964455.

[6] Antonetta C Houweling, Koen Crama, Jorrit Visser, Kyohei Fukata, Coen R N Rasch, Tatsuya Ohno, Arjan Bel, and Astrid van der Horst. Comparing the dosimetric impact of interfractional anatomical changes in photon, proton and carbon ion radiotherapy for pancreatic cancer patients. *Physics in Medicine and Biology*, 2017. ISSN 0031-9155. doi: 10.1088/1361-6560/aa6419.

[7] Anke van Mourik. Antoni van leeuwenhoek hospital/dutch cancer institute - internal online documentation. URL http://iprova-pod.

[8] Margriet Kwint, Sanne Conijn, Eva Schaake, Joost Knegjens, Maddalena Rossi, Peter Remeijer, Jan Jakob Sonke, and Jose Belderbos. Intra thoracic anatomical changes in lung cancer patients during the course of radiotherapy. *Radiotherapy and Oncology*, 113 (3):392–397, 2014. ISSN 18790887. doi: 10.1016/j.radonc.2014.10.009. URL http://dx.doi.org/10.1016/j.radonc.2014.10.009.

[9] S. Conijn, O. Hamming-Vrieze, L. Wiersema, and P. Remeijer. PD-0286: Anatomical changes in head and neck patients seen on CBCT, the traffic light protocol. *Radiotherapy and Oncology*, 111:S111, 2014. ISSN 01678140. doi: 10.1016/S0167-8140(15)30391-1. URL http://linkinghub.elsevier.com/retrieve/pii/S0167814015303911.

[10] Suzanne van Beek, Simon van Kranen, Angelo Mencarelli, Peter Remeijer, Coen Rasch, Marcel van Herk, and Jan Jakob Sonke. First clinical experience with a multiple region of interest registration and correction method in radiotherapy of head-and-neck cancer patients. *Radiotherapy and Oncology*, 94(2):213–217, 2010. ISSN 01678140. doi: 10.1016/j.radonc.2009.12.017.

[11] Ditte Sloth Møller, Azza Ahmed Khalil, Marianne Marquard Knap, and Lone Hoffmann. Adaptive radiotherapy of lung cancer patients with pleural effusion or atelectasis. *Radiotherapy and Oncology*, 110(3):517–522, 2014. ISSN 18790887. doi: 10.1016/j.radonc.2013.10.013.

[12] Markus Wendling, Robert J. W. Louwe, Leah N. McDermott, Jan-Jakob Sonke, Marcel van Herk, and Ben J. Mijnheer. Accurate two-dimensional IMRT verification using a back-projection EPID dosimetry method. *Medical Physics*, 33(2):259–273, 2006. ISSN 00942405. doi: 10.1118/1.2147744. URL http://doi.wiley.com/10.1118/1.2147744.

[13] Leah N. McDermott, R J W Louwe, J J Sonke, Marcel B. van Herk, and Ben J. Mijnheer. Dose-response and ghosting effects of an amorphous silicon electronic portal imaging device. *Medical physics*, 31(2):285–295, 2004. ISSN 00942405. doi: 10.1118/1.1637969.

[14] L. McDermott. On Radiotherapy Dose Verification With a Flat-Panel Image. *Radiotherapy and Oncology*, 92:S49, aug 2009. ISSN 01678140. doi: 10.1016/S0167-8140(12)72717-2. URL http://linkinghub.elsevier.com/retrieve/pii/S0167814012727172.

[15] Markus Wendling, Leah N. McDermott, Anton Mans, Jan-Jakob Sonke, Marcel van Herk, and Ben J. Mijnheer. A simple backprojection algorithm for 3D in vivo EPID dosimetry of IMRT treatments. *Medical Physics*, 36(7):3310–3321, 2009. ISSN 00942405. doi: 10.1118/1.3148482. URL http://doi.wiley.com/10.1118/1.3148482.

[16] Anton Mans, Peter Remeijer, Igor Olaciregui-Ruiz, Markus Wendling, Jan Jakob Sonke, Ben Mijnheer, Marcel van Herk, and Joep C. Stroom. 3D Dosimetric verification of volumetric-modulated arc therapy by portal dosimetry. *Radiotherapy and Oncology*, 94(2):181–187, 2010. ISSN 01678140. doi: 10.1016/j.radonc.2009.12.020. URL http://dx.doi.org/10.1016/j.radonc.2009.12.020.

[17] R. Pecharromán-Gallego, Anton Mans, Jan-Jakob Sonke, Joep C. Stroom, Ígor Olaciregui-Ruiz, Marcel van Herk, and Ben J. Mijnheer. Simplifying EPID dosimetry for IMRT treatment verification. *Medical Physics*, 38(2):983–992, 2011. ISSN 00942405. doi: 10.1118/1.3547714. URL http://doi.wiley.com/10.1118/1.3547714.

[18] Markus Wendling, Leah N. McDermott, Anton Mans, Ígor Olaciregui-Ruiz, Raul Pecharromán-Gallego, Jan-Jakob Sonke, Joep Stroom, Marcel van Herk, and Ben J. Mijnheer. In aqua vivo EPID dosimetry. *Medical Physics*, 2012. ISSN 00942405. doi: 10.1118/1.3665709.

[19] Igor Olaciregui-Ruiz, Roel Rozendaal, René F.M. van Oers, Ben Mijnheer, and Anton Mans. Virtual patient 3D dose reconstruction using in air EPID measurements and a back-projection algorithm for IMRT and VMAT treatments. *Physica Medica*, 37:49–57, 2017. ISSN 11201797. doi: 10.1016/j.ejmp.2017.04.016. URL http://linkinghub.elsevier.com/retrieve/pii/S1120179717301023.

[20] Jennifer De Los Santos, Richard Popple, Nzhde Agazaryan, John E. Bayouth, Jean-Pierre Bissonnette, Mary Kara Bucci, Sonja Dieterich, Lei Dong, Kenneth M. Forster, Daniel Indelicato, Katja Langen, Joerg Lehmann, Nina Mayr, Ishmael Parsai, William Salter, Michael Tomblyn, William T.C. Yuh, and Indrin J. Chetty. Image Guided Radiation Therapy (IGRT) Technologies for Radiation Therapy Localization and Delivery. *International Journal of Radiation Oncology*Biology*Physics*, 87(1):33–45, sep 2013. ISSN 03603016. doi: 10.1016/j.ijrobp.2013.02.021. URL http://linkinghub.elsevier.com/retrieve/pii/S0360301613002137.

[21] L. A. Feldkamp, L. C. Davis, and J. W. Kress. Practical cone-beam algorithm. *J. Opt. Soc. Am. A*, 1(6):612–619, Jun 1984. doi: 10.1364/JOSAA.1.000612. URL http://josaa.osa.org/abstract.cfm?URI=josaa-1-6-612.

[22] Uros Stankovic, Lennert S. Ploeger, Marcel van Herk, and Jan-Jakob Sonke. Optimal combination of anti-scatter grids and software correction for CBCT imaging. *Medical Physics*, 2017. ISSN 00942405. doi: 10.1002/mp.12385. URL http://doi.wiley.com/10.1002/mp.12385.

[23] Angelo Mencarelli, Simon Robert Van Kranen, Olga Hamming-Vrieze, Suzanne Van Beek, Coenraad Robert Nico Rasch, Marcel Van Herk, and Jan Jakob Sonke. Deformable image registration for adaptive radiation therapy of head and neck cancer: Accuracy and precision in the presence of tumor changes. *International Journal of Radiation Oncology Biology Physics*, 90(3):680–687, 2014. ISSN 1879355X. doi: 10.1016/j.ijrobp.2014.06.045. URL http://dx.doi.org/10.1016/j.ijrobp.2014.06.045.

[24] Christopher L. Guy, Elisabeth Weiss, Nuzhat Jan, Leonid B. Reshko, Gary E. Christensen, and Geoffrey D. Hugo. Effect of atelectasis changes on tissue mass and dose during lung radiotherapy. *Medical Physics*, 43(11):6109–6117, 2016. ISSN 00942405. doi: 10.1118/1.4965807. URL http://doi.wiley.com/10.1118/1.4965807.

[25] Brandon Disher, George Hajdok, An Wang, Jeff Craig, Stewart Gaede, and Jerry J Battista. Correction for 'artificial' electron disequilibrium due to cone-beam CT density errors: implications for on-line adaptive stereotactic body radiation therapy of lung. *Physics in medicine and biology*, 58:4157–74, 2013. ISSN 1361-6560. doi: 10.1088/0031-9155/58/12/4157. URL http://www.ncbi.nlm.nih.gov/pubmed/23689060.

[26] Christopher Kurz, George Dedes, Andreas Resch, Michael Reiner, Ute Ganswindt, Reinoud Nijhuis, Christian Thieke, Claus Belka, Katia Parodi, and Guillaume Landry. Comparing cone-beam CT intensity correction methods for dose recalculation in adaptive intensity-modulated photon and proton therapy for head and neck cancer. *Acta Oncologica*, 54(9):1651–1657, 2015. ISSN 0284-186X. doi: 10.3109/0284186X.2015.1061206. URL http://www.tandfonline.com/doi/full/10.3109/0284186X.2015.1061206.

[27] Daniel A. Low and James F. Dempsey. Evaluation of the gamma dose distribution comparison method. *Medical Physics*, 30(9):2455–2464, 2003. ISSN 00942405. doi: 10.1118/1.1598711. URL http://doi.wiley.com/10.1118/1.1598711.

[28] Markus Wendling, Lambert J. Zijp, Leah N. McDermott, Ewoud J. Smit, Jan-Jakob Sonke, Ben J. Mijnheer, and Marcel van Herk. A fast algorithm for gamma evaluation in 3D. *Medical Physics*, 2007. ISSN 00942405. doi: 10.1118/1.2721657.

[29] Leah N. McDermott, Markus Wendling, Jan Jakob Sonke, Marcel van Herk, and Ben J. Mijnheer. Anatomy changes in radiotherapy detected using portal imaging. *Radiotherapy and Oncology*, 79(2):211–217, 2006. ISSN 01678140. doi: 10.1016/j.radonc.2006.04.003.